D3.8 REPORT ON TERMINALS

Release: 1.0

Work package	WP 3
Task	Task 3.2
Due date	30/06/2025
Submission date	26/10/2025
Deliverable lead	University of Bologna
Version	1.0
Authors	Greenerwave, University of Bologna (Carla Amatetti, Alessandro Vanelli-Coralli), Ericsson (Eduardo Medeiros, Per-Erik Eriksson, Sebastian Euler), Ericsson France (Ioannis Xirouchakis), CTTC (Xavier Artiga), Thales France
Reviewers	Qualcomm (Mehmet Gurelli), DLR (Sandro Scalise), TH-SIX (Dorin Panaitopol)
Abstract	This deliverable focuses on the main evolutions and innovation areas of 6G NTN terminals. Innovative antenna design was identified to bear most technological potential for improved terminal characteristics for 6G NTN system. Based on the outcomes of D3.2, this deliverable provides a redefined antenna design (20x20), its fabrication process, and the performance evaluation conducted in laboratory. The antenna's performance has been characterized in terms of gain, scan loss, and radiation patterns, evaluating its compliance with the project system-level objectives.
Keywords	6G-NTN, terminals, antenna, antenna design

Grant Agreement No.: 101096479
Call: HORIZON-JU-SNS-2022

Topic: HORIZON-JU-SNS-2022-STREAM-B-01-03
Type of action: HORIZON-JU-RIA

Document Revision History

RELEASES	DATE	DESCRIPTION OF CHANGE	LIST OF CONTRIBUTOR(S)
R0.0	25/01/2025	Initial Report Structure	Carla Amatetti and Alessandro Vanelli-Coralli
R1.0	25/10/2025	Approval and Submission	Alessandro Vanelli-Coralli (UNIBO)

DISCLAIMER

Co-funded by the European Union

6GSNS

Project funded by
Schweizerische Eidgenossenschaft
Confédération suisse
Confederazione Svizzera
Confederaziun svizra
Swiss Confederation
Federal Department of Economic Affairs, Education and Research EAER
State Secretariat for Education, Research and Innovation SERI

6G-NTN (*6G Non Terrestrial Network*) project has received funding from the **Smart Networks and Services Joint Undertaking (SNS JU)** under the European Union's **Horizon Europe research and innovation programme** under Grant Agreement No 101096479. Views and opinions expressed are however those of the author(s) only and do not necessarily reflect those of the European Union. Neither the European Union nor the granting authority can be held responsible for them. This work has received funding from the Swiss State Secretariat for Education, Research and Innovation (SERI).

COPYRIGHT NOTICE

Project co-funded by the European Commission in the Horizon Europe Programme		
Nature of the deliverable:	**R**	
Dissemination Level		
PU	*Public, fully open, e.g., web (Deliverables flagged as public will be automatically published in CORDIS project's page)*	✓
SEN	*Sensitive, limited under the conditions of the Grant Agreement*	
Classified R-UE/ EU-R	*EU RESTRICTED under the Commission Decision No2015/ 444*	
Classified C-UE/ EU-C	*EU CONFIDENTIAL under the Commission Decision No2015/ 444*	
Classified S-UE/ EU-S	EU SECRET under the Commission Decision ***No2015/ 444***	

* R: Document, report (excluding the periodic and final reports)
DEM: Demonstrator, pilot, prototype, plan designs
DEC: Websites, patents filing, press & media actions, videos, etc.
DATA: Data sets, microdata, etc.
DMP: Data management plan
ETHICS: Deliverables related to ethics issues.
SECURITY: Deliverables related to security issues
OTHER: Software, technical diagram, algorithms, models, etc.

EXECUTIVE SUMMARY

Deliverable 3.8 (D3.8) constitutes the final report on terminal considerations and investigations, building upon the outcomes presented in deliverable D3.2. During the initial evaluation, user requirements and associated key performance indicators (KPIs), identified in deliverables D2.1, D2.2, and D2.3, were systematically mapped to various potential terminal types.

For the lower frequency ranges (sub 6GHz), narrowband communication being integrated into terminals seems to be a logical decision for price/bill of material, wide user acceptance and distribution reasons for 6G NTN capable terminals.

Conversely, wideband communication systems are envisioned for terminals operating in higher frequency bands (above 10 GHz). Upon evaluating relevant performance requirements, such as throughput and the form factor, it becomes evident that existing terminal designs optimized for 5G terrestrial networks in the FR2 band substantially fulfil the requirements. Although some frequency-specific adaptations for operation in the C or Q/V bands are necessary, contemporary terminal architectures largely encompass the essential components required for achieving the desired performance benchmarks.

Leveraging similarities with existing commercial terminal designs, notably from 5G terrestrial systems, significantly facilitates component reuse, thereby enhancing feasibility and cost-effectiveness.

The principal area identified as having significant potential for innovation and improvement in comparison with current terminal designs is the antenna. Innovative antenna designs are crucial, offering substantial improvements in gain that directly translate into enhanced throughput performance. Additionally, such designs are tailored to comply with the geometric constraints identified for specific use cases, including automotive applications and drones.

Consequently, D3.2 focused on the Q/V band antenna design (20x20) and assessment considering the user and use case requirements (geometry). Thus, based on these findings, D3.8 provides a redefined antenna design (20x20), its design and fabrication process, and the performance evaluation conducted in Greenerwave's laboratory. The antenna's performance has been thoroughly characterized in terms of gain, scan loss, and radiation patterns, evaluating its compliance with the overarching project system-level objectives.

In particular, these results demonstrated that the performance of the in-house designed and fabricated Q/V-band antenna closely aligns with the target specifications of the 6G-NTN project. Based on characterization results, the key outcomes are the following:

The antenna exhibits a good operation within the designed Q/V-band frequency range.

The measured gain and radiation patterns are in good agreement with the expected values for NTN communication use cases and project specifications.

The full integration of the metasurface, feeder, and mask shows strong potential for scalable manufacturing and system-level deployment and validates the efficiency of our cutting-edge technology.

These results confirm the feasibility of the proposed antenna design for high-frequency NTN applications and contribute positively to the technical validation phase of the 6G-NTN project.

In addition, an assessment of the 10x10 Q/V band antenna has been carried out.

TABLE OF CONTENTS

LIST OF FIGURES

LIST OF TABLES

ABBREVIATIONS

3D	3-Dimensional	**GEO**	Geostationary Earth Orbit
6G	Sixth Generation	**gNB**	Next-generation Node-B
3GPP	3rd Generation Partnership Project	**GND**	Ground
AI	Artificial Intelligence	**GNSS**	Global Navigation Satellite Systems
ACLR	Adjacent Channel Leakage power Ratio	**GPS**	Global Positioning System
ACU	Antenna Control Unit	**GSO**	Geosynchronous Orbit
AFS	Antenna Feeder System, Antenna Feeding System	**HAP**	High Altitude Platform
AI	Artificial Intelligence	**H-Pol**	Horizontal Polarization
ASIC	Application-Specific Integrated Circuit	**HV**	Host Vehicle
BOM	Bill Of Material	**HW**	Hardware
BS	Base station	**IC**	Integrated Circuit
BVLoS	Beyond Visual Line of Sight	**IF**	Intermediate Frequency
BW	Bandwidth	**IoT**	Internet of Things
BWP	Bandwidth Part	**ISL**	Inter-Satellite Link
C2	Command and Control	**KPI**	Key Performance Indicator
C2CSP	C2 Link communication service provider	**LC**	Liquid Crystal
CA	Carrier Aggregation	**LEO**	Low Earth Orbit
CC	Component Carrier	**LO**	Local Oscillator
CMOS	Complementary Metal-Oxide-Semiconductor	**LoS**	Line of Sight
COTS	Commercial off-the-shelf	**MBW**	Measurement Bandwidth
CoW	Cell on Wheels	**MEMS**	Micro-Electro-Mechanical Systems
C-SWaP	Cost Size Weight and Power	**MEO**	Medium Earth Orbit
CW	Continuous Wave	**MFCN**	Mobile/Fixed Communications Networks
DC	Direct Current	**mMTS**	Mini-Metasurface
DL	Downlink	**MNO**	Mobile Network Operator
DMA	Dynamic Metasurface	**MTS**	Metasurface
DS	Discrete Source	**NF**	Near-Field
EAB	External Advisory Board	**NGSO**	Non-Geostationary Orbit
E-tan	Tangential Electric Field	**NLoS**	Non-Line of Sight
EASA	European Union Aviation Safety Agency	**NR**	New Radio
EIRP	Equivalent Isotropic Radiated Power	**NTN**	Non-Terrestrial Network
EIS	Effective Isotropic Sensitivity	**OBW**	Occupied Bandwidth
E2E	End-to-end	**OCNG**	OFDMA Channel Noise Generator
FDD	Frequency-Division Duplexing	**OFDMA**	Orthogonal Frequency-Division Multiple-Access
FM/AM	Frequency Modulation/Amplitude Modulation	**OTA**	Over-The-Air
FPA	Fabry Perot Antenna	**OoB**	Out-of-Band
FR	First Responder	**OoBE**	Out-of-Band Emission
FR2	Frequency Range 2 according 3GPP	**PAPR**	Peak-to-Average Power Ratio

PCB	Printed Circuit Board	**UOF**	Uniformity of the field
PIN diode	Positive-Intrinsic-Negative diode	**USAT**	Ultra-Small-Aperture Terminal
PPDR	Public Protection and Disaster Relief	**VICTS**	Variable Inclination Continuous Transverse Stub
PPM	Parts per million	**vLEO**	Very Low Earth Orbit
PRB	Physical Resource Block	**VLoS**	Visual Line of Sight
PSD	Power Spectrum Density	**VNA**	Vector Network Analyzer
PTT	Push-To-Talk	**VNF**	Virtualized Network Function
QoE	Quality of Experience	**V-Pol**	Vertical Polarization
QoS	Quality of Service	**X-Pol**	Cross Polarization
RB	Resource Block	**VR**	Virtual Reality
Rel	Release	**VSAT**	Very-Small-Aperture Terminal
RF	Radio Frequency	**VTOL**	Vertical Take-Off and Landing
RIB	Radiated Interface Boundary	**WI**	Work Item
RIC	Radio Intelligent Controller	**WP**	Work Package
RIS	Reconfigurable Intelligent Surface		
RL	Return Loss		
RPE	Radiated Power Envelope		
Rx	Receiver		
SAN	Satellite Access Node		
SAR	Search and Rescue		
SCS	Subcarrier Spacing		
SE	Spurious Emission		
SI	Study Item		
SON	Self-organizing networks		
SOTM	Satellite-On-The-Move		
TE	Transverse Electric field		
TM	Transverse Magnetic Field		
TN	Terrestrial Network		
TR	Technical Report		
TRP	Total Radiated Power		
Tx	Transmit, transmitter		
TS	Technical Specifications		
UAM	Urban Air Mobility		
UAV	Uncrewed Aerial Vehicle		
UAV-C	UAV Controller		
UC	Use Case		
UE	User Equipment		
UL	Uplink		

1 INTRODUCTION

As highlighted in the previous version of this deliverable, *i.e.,* D3.2, antennas are identified as the main improvement area in the terminal design and hence, it will be one of the main contributions to 6G NTN performance.
While D3.2 focused on identifying new antenna design concepts having advantageous characteristics for broadband NTN usage, D3.8 focuses on the design, fabrication, and characterization of a 20x20 Q/V-band antenna intended for use in future non-terrestrial networks. In addition, an assessment of a 10x10 antenna is also considered. Moreover, the state of the art of very small antenna aperture (VSAT) requirements provided by the 3GPP has been updated as well as the survey of C band antennas for handheld and mounted devices.

1.1 SCOPE AND OBJECTIVES

The NTN frequency range can be divided into the lower frequency range i.e., sub 6GHz, consisting of S, L and also C band (which is in current consideration for NTN), and a higher frequency range above 6GHz, e.g., Q/V band.

Each of these frequency ranges has its own constraints with respect to the terminal design and is adopted in different use cases. Indeed, the sub-6GHz range for NTN is mainly intended for handhelds, being often dual design with terrestrial usage. Hence, the used components and antenna design are mainly the same as those used for the TN usage, as NTN in these devices only gets widely adopted if no further hardware (HW) constraints impacting terminal cost are placed. On the opposite, higher frequency bands (> 6 GHz) are used for broadband connectivity, and, for NTN, very small aperture terminal (VSAT) have been adopted in the past. However, to fulfil the user requirements in terms of size and achieve increased throughput compared to state-of-the-art NTN systems, new antenna designs for Q/V need to be investigated.

For the Q/V and C band most likely assumptions of technical realization with respect to amplifier in receiving and transmitting path are considered being based on state-of-the-art, as amplifiers have a slow innovation slope being already followed since years within other studies and projects.

Therefore, building on the finding of the previous deliverable, this deliverable provides a thorough description of the 20x20 Q/V-band antenna design and fabrication process and its performance evaluation conducted in Greenerwave's laboratory. The complete antenna system — including the metasurface, feeding structure, and mask — was entirely developed in-house. The analysis focuses on key parameters such as gain, scan loss and radiation pattern, aiming to assess compliance with the system-level objectives defined by the project consortium (reported for example in D3.6 and D3.10). To complete the analysis, also assessment of 10x10 antenna has been carried out.

1.2 STRUCTURE OF THE DOCUMENT

This deliverable is structured as follows:

- **Section 2** provides a detailed examination of UE types, their characteristics and potential implementation and band usage. In addition, the technical requirements for terminals operating in 3GPP-based non-terrestrial networks are reported.

- **Section 3** is dedicated to the state of the art on antenna technology for the C and Q/V band. Here a critical and detailed description of antenna technologies in C band is provided.
- **Section 4** describes the results of the antenna investigation following the objectives based on the considerations of Sections 2 and 3 of the D2.3 document. The investigation explores the usage of Metasurface for the antenna design. Simulations as well as measurements of the antenna samples are documented.
- **Section 5** describes the results of the antenna characterization in Q/V band considering a 20x20 cm antenna designed with PIN-diode as switching element.
- **Section 6** presents simulation results for both QRx and VTx $10\text{cm} \times 10\text{cm}$
- **Section 7** provides a comparison of the results for QRx and VTx (20cm x 20cm) antenna with the 6-GNTN project specifications and an estimate of the performances of the small (10cm x 10cm) antenna.
- **Section 8** concludes the deliverable.

2 SELECTED UE TYPES, CAPABILITIES AND SWAP CHARACTERISTICS

2.1 INTRODUCTION

Mobile communication terminals exist for various technologies and purposes, however a terminal for mobile communication typically consists of some commonly used building blocks. A terminal typically consists of a modem, a receiver and transmitter circuitry and corresponding antennas. For a better understanding a schematic representation is depicted in Figure 1.

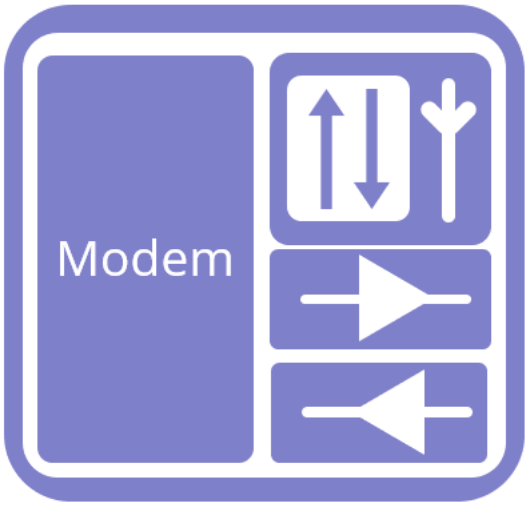

FIGURE 1: SCHEMATIC DRAWING OF A TERMINAL

The modem has the task to process the received data and even though modulation and coding for 6G-NTN may not be clear now, based on expected throughput for 6G-NTN today's modem processing capabilities for 5G terrestrial networks also including frequency range 2 (FR2) are able to cope with such high throughputs and even much higher data capabilities.

The receiving and transmitting circuitry mainly consists of receive and transmit amplifiers providing corresponding amplification and noise figure (receiver) being suitable for mobile communication. Transmitters and receivers of various sizes exist today, also in the considered frequency ranges. Hence, the state-of-the-art of such receivers and transmitters can be referred to. The selection for the respective terminal types used within a certain use case, also depends on additional aspects such as deployment, usage conditions or power consumption. Amplifier development is a separate general evolution topic and, hence in the context of 6G-NTN terminal considerations, reference will be made to available state-of-the art for the respective terminal types and use case scenario.

Receive and transmit antennas are a crucial topic with respect to use case KPIs and user acceptance given that their performance directly impacts achievable data throughput, and its dimension and weight directly impacts use case scenario and user experience.

Furthermore, the requirements for the antenna heavily depend on the use case, intended throughput, level of integration and further use case dependent aspects, hence playing a major role and for new or enhanced 6G NTN use cases being a key element for innovation.

In this section the outcome of T2.1 and T2.2 will be analysed and translated/classified into technical terminal requirements. It will be shown that several of the UE types identified in T2.1 andT2.2 will translate into the same technical terminal type and just will fulfil different use needs by different packaging. Especially a grouping of the terminals with respect to the usage as broadband or integrated narrowband communication terminal and their characteristics with respect to terminal antenna requirements will be made. Furthermore, the state-of-the-art terminal/UE requirements of 3GPP for existing NTN systems will be referenced to guide towards the innovative field of antenna analysis and show the increase in throughput and coverage that can be achieved with a 6G NTN system making use of such new antenna designs.

2.2 OVERVIEW ON UE TYPES AND THEIR REQUIREMENTS

In context of D2.2 following UE types were distinguished: handheld, drone and mounted devices. Each of the types is differentiated into two subclasses: commercial and professional handheld, respectively small or large drones and first responder stationary or mounted devices. The corresponding segmentation is depicted in Figure 2.

FIGURE 2: UE TYPES ACCORDING TO D2.2

When analysing the characteristics, it can be seen that only two basic terminal types need to be distinguished where one of these types can further be distinguished by a slight differentiation concerning acceptance for size and weight.

The commercial handheld refers to a design which has dual-use capabilities for TN and NTN networks intended for the sub-6GHz range i.e., being based on a classical integrated front end on handhelds. In that context, the used components (receive and transmit amplifiers as well as the antenna design) are bound to the typical values which are achievable for today's

commercial handhelds i.e., 23dBm output power, 9dB receiver noise figure and -5dBi antenna gain (assuming ETSI power class 3 UE, a max output power of 23dBm is considered). Such a terminal design making use of commercial handheld constraints allows for NTN narrowband communication by using the satellite bands in the sub-6GHz range (S and L band). As being bound in its components to commercial terrestrial handheld designs and being limited in antenna design due to dimension limitation of the UE type, a performance increase for this device type in 6G NTN will mainly come from other system elements besides the terminal, some examples are; increasing the satellite platform power capabilities, increasing the power amplification efficiency increasing the satellite antenna performances, both in the transmit and receive direction, to improve the antenna gain, as well as antenna isolation to reduce impact of internal interferences. Even though being an important type for 6G NTN, this UE type is of lower interest in the further terminal study due to its design limitations and the economy of scale pressure for this type of handheld devices.

Also, the professional handheld can be considered as being part of that category, being a slightly larger dimensioned handheld terminal allowing for slightly more weight than consumer handhelds and providing slightly increased RF performance with power amplifiers (26dBm) acceptable for use in proximity of a human head for a limited time and intensity.

Mounted devices (e.g., cars, trains) or stationary first responder devices refer in principle to the same terminal type being larger in dimension especially for the antenna design and heavier in weight. In this regard, it is worth highlighting that mounting antennas of mounted devices or stationary installations on a roof top can ensure better visibility to the satellite C band for vehicular, light drone, train and maritime backup can be considered with slightly improved antennas and larger power amplifiers (typically 26dBm), where the additional antenna gain is mainly due to improved efficiency.

Wideband and ultra-wideband communication mounted devices (e.g., trains, large drones and vessels) is a second terminal where achieving a high throughput is one of the major KPIs. This type of device can be heavier in weight and larger in dimension (which, in the context of Q/V band usage for wideband and ultra-wideband communication, can allow larger RF amplifier and antenna to overcome the higher attenuation). The mounted devices can be distinguished in an intermediate variant allowing for 20X20cm design and a smaller variant allowing for 10x10cm design. The dimension also refers to the acceptable antenna size being far larger than modem and respective device design (including amplifiers). These devices also need to support wideband communication, which includes at least C or even Q/V band i.e., realization of the support of higher frequency ranges and having superior antenna characteristics being directly related to the achievable throughput.

For wideband support in the Q/V band, even though larger power amplifiers can be used (up to 34 or even 37dBm) for certain use cases such as trains and vessels or large drones, i.e., allowing for mounting not in proximity of the human head because of healthcare considerations. The corresponding sustainability requirements are expressed in D2.3 page 55 (§4.4): STR-SUST-07 ("The 6G-NTN system shall be able to assess and minimize its impact regarding EMF exposure") and STR-SUST-08 ("The 6G-NTN system shall follow the existing international and national 6G EMF-awareness guidelines (e.g., those of ICNIRP [1]). It is obvious that a larger benefit for link level/throughput considerations, especially for these bands is related to the usage of corresponding high performing antennas.

Please see also D2.3 page 55 (§4.4): STR-SUST-07 ("The 6G-NTN system shall be able to assess and minimize its impact regarding EMF exposure") and STR-SUST-08 ("The 6G-NTN system shall follow the existing international and national 6G EMF-awareness guidelines (e.g., those of ICNIRP [1])."

A mapping of the UE types assessed in D2.2. to the terminal types described with their main characteristics is presented in the Table 1 (see also D2.3 section 3.4.1)

TABLE 1: MAPPING OF UE TYPES TO TERMINAL TYPES AND THEIR CHARACTERISTICS

UE type	Communication characteristics	Terminal type	RF characteristic	Frequency band
Handheld	narrowband	classical integrated front end on handheld	typ. NF=9 Gain : -5dBi, Tx=23 dBm	Sub 6GHz S and L band
Professional handheld	Narrowband medium	Enhanced RF front end	typ. NF=7 Gain : -3dBi, Tx=26 dBm	Sub 6GHz C band
Drone; car (small mounted UE)	medium	Enhanced Rf and antenna	typ. NF=7 Gain : 0 dBi, Tx =26 dBm	Sub 6GHz C band
Drone, train vessel (mounted UE)	wideband	Enhanced RF and improved noise figure performance	typ. NF=5; Tx =25,5 dBm	Q/V band
Drone, train vessel (mounted UE)	Ultra-wideband	Enhanced RF and extreme noise figure performance	typ. NF=4; Tx =28 dBm	Q/V band

As can be seen from the table above a from section 3.3.1 of this deliverable, for commercial handhelds, their tight restrictions are set on the components used for classical integrated frontends. However, even for other types of terminals, in terms of amplifiers/reception or transmission circuits, the state-of-the-art level achievable with commercially available devices has been reached. Relying solely on these devices significantly affects the terminal's bill of materials (BOM). However, it will be feasible to enhance existing handhelds through integration, enabling support for additional standalone or combined use cases with terminals available at a reasonable cost.

For wideband and ultra-wideband communications, which are not constrained by typical TN/NTN handheld or general design limitations, improved antenna performance can be achieved within the dimensional requirements defined in D2.2 and for the relevant UE types—specifically, sizes such as 10x10 cm or 20x20 cm. These dimensions are also critical for antenna design, as they directly influence the achievable maximum throughput.

Indeed, the antenna design is a key parameter to achieve higher throughput and increase coverage and hence maximize the usage of the 6G-NTN system.

Relevant terminal types are further investigated especially with respect to the antenna analysis for wideband Q/V designs, thus covering a broad enough space matching the assessed use cases where innovative antenna design can lead to improved terminal performance for 6G NTN.

The assessment and studies shall be conducted for the different acceptable dimensions i.e., 10x10cm and 20x20cm focusing first on Q/V band with maximum dimension.

Moreover, for the C band, handheld terminals are studied.

2.3 TRANSLATION INTO INVESTIGATION SCOPE

As shown by the analysis performed above, there are mainly 2 device types. The adaptation to the use case scenarios referenced in D2.2 and the UE types named in D2.3 is done via the way of implementation.

These 2 device types have the following characteristics:

- Terminal 1, narrowband sub-6GHz (S and L band partially C band), design is common with mobile terminals used for terrestrial communication or the terminal is often a dual-use having full alignment in the design. Using state-of-the-art design is key for distribution and availability for 6G-NTN communication terminals when being fully integrated into handhelds. Existing handheld terminals need small adaptations for frequency range for NTN but in general frequency range is feasible as being part of the sub-6GHz frequency range. The increased performance and throughput for 6G-NTN for these devices will mainly come, compared to state-of-the art systems, from other systems and design benefits of the 6G-NTN or from improved antenna performance in C band (which, as was already mentioned).
- Terminal 2, wideband and ultra-wideband communication needs achieving multiple 125/250MBits of throughput. Special reference is made here for the performance requirements in D2.3, especially STR-PERF-08 (§4.3.4) in which we very generally state "The 6G-NTN system SHALL be able to serve USAT UE with the performance specified in Table 10 via User Traffic Profile UTP2". Traffic Profile UTP2 exhibits experienced user data rate of 250/125 Mbps. Terminals will operate in mainly Q/V bands. In general, the used frequency range and, hence, related front-end is not that different from today's terrestrial terminals operating in 5G FR2. The higher pathloss and attenuation in 6G-NTN needs to be compensated/counteracted mainly by the antenna, as in the area of amplifier design only moderate improvements can be expected.

Especially terminal type 2, which can further be distinguished according to the amplifier and sensitive to the various use cases, is in the major evaluation field. The required amplifier and modem design concerning processing and throughput is considered to be available. Identified use cases and key performance characteristics as identified in D2.2 and D2.3 correspond to today's state –of-the-art terminal designs.

The main gain increase concerning throughput, especially when using Q/V or C band, should come from new and innovative/improved antenna designs respecting the geometry limitations, as analysed in the user requirements geometry constraints identified in D2.2.

Key performance indicators outlined in D2.3, such as data rate, network performance, and throughput, are closely linked to reception and transmission characteristics. Due to similarities and constraints in device components, only limited gains can be achieved through RX/TX modifications at the terminal. Therefore, significant performance improvements for 6G-NTN terminals must primarily come from advancements in antenna design, particularly in wideband scenarios. This is especially important when considering the dimensional constraints of UE types (e.g., small 10x10 cm and large 20x20 cm), as analyzed in the user requirements (D2.2) for the various use cases.

The focus of investigations and studies on antenna design and system integration for 6G-NTN terminals is well justified. In addition to being a critical factor for throughput and user experience—particularly due to constraints in size and weight—antenna design offers the highest potential for innovation. Meanwhile, relying on state-of-the-art designs and readily available components for other terminal parts is essential to enable classical, integrated handheld devices for consumers. At the same time, this approach supports the use of more specialized terminals for other use cases, ensuring sufficient availability and cost efficiency. This balance is key to enabling 6G-NTN to reach mass-market adoption.

2.4 EXISTING 3GPP REQUIREMENTS FOR NTN UE

In this section, we present a set of existing technical requirements for terminals operating in 3GPP-based non-terrestrial networks. The 3GPP requirements have been defined by 3GPP's RAN4 work group in [3] and refer mainly to the minimum radio frequency (RF) and performance requirements for a UE supporting satellite access operation.

In addition to the 3GPP UE related requirements, we also present requirements defined by ETSI for antennas in fixed radio services operating in frequencies overlapping with the Q/V bands [4].

One of the main advantages of 5G NTN and a target for 6G NTN is to provide service to normal smartphones (handheld) from flying nodes (e.g., LEO satellites). Given that their main use case is to be in coverage of the terrestrial network component, the requirements for smartphones are driven by a different set of documents than [1], namely [5][6][7][8]. Here, we then focus on the specific NTN requirements for terminals.

As mentioned in the previous subsections, handhelds, in the 6G-NTN project context are expected to be used in the C-band, while very small (VSAT) and ultra small aperture terminals (USAT) are expected to be used in the Q/V bands. In 3GPP, the term NTN-VSAT is used for a UE operating in FR2-NTN band.

For the mass-market, the form factor and power constraints in a smartphone are expected to be similar in the 6G timeframe. Given the intended use in the C-band, and form factor constraints, we expect that such aspects as the antenna design will resemble their counterparts in 5G. This is not true for (mounted) terminals in the Q/V band, as exemplified by the advanced antenna design described in chapter 4.

Therefore, we will focus on presenting the minimum requirements for terminals operating in Q/V bands, with the assumption that the terminal does not have a traditional smartphone form-factor. In other words, the focus is on terminals that can be mounted on vehicles or provide fixed-wireless access, including USAT.

One note about the content that follows is that the requirements are collected from the 3GPP requirements for 5G-NR, since equivalent ones for 6G will be defined later than the time-horizon for 6G-NTN's project conclusion. While possible, we focus on the requirements that

- may be relevant to VSAT/USAT terminals,
- are not dependent on a specific band (e.g., 3GPP band n256),
- are influenced by the choice of antenna design.

This approach is chosen so that for the remainder of the project, we can perform feasibility evaluations that are realistic, with a set of requirements that are likely to resemble their upcoming 6G NTN counterparts.

In a few instances, we list requirements that refer to operation in the FR2-NTN band. While not including the target Q/V bands, these are the highest frequencies considered for 3GPP NTN services so far. In these cases, the requirements are included here as an indication or illustration of what performance or receiver/transmitter characteristics could be expected.

Unless noted, the requirements presented next originate from [3]. The radiated transmitter characteristics is for a NTN UE only operating in FR2-NTN and the term NTN VSAT is used for those terminals.

2.4.1 Bands of interest for the 6G-NTN project

The frequency bands below are considered for research activities in the 6G-NTN project [10], a detailed study on the 6G NTN frequency bands is conducted within D2.5.

2.4.1.1 Q/V bands

The Q/V-bands have been identified as candidate for use in the service link as part of 6G NTN, with the following frequency ranges for both NGSO and GSO satellite services:

- Downlink: 37.5 – 42.5 GHz (Q-band).
- Uplink: 47.2 – 50.2 GHz and 50.4 – 51.4 GHz (V-band).

2.4.1.2 C band

The C-band is a new NTN frequency band opportunity for direct connectivity to smartphones and cars to be considered for the 6G-NTN project

- Downlink NTN satellite communications could potentially use TN TDD (Time Division Duplex) frequency bands n77 (3,300 – 4,200 MHz) / n78 (3,300 – 3,800 MHz).
- Uplink NTN satellite communications could potentially use the upper frequency spectrum (around 6 GHz) or lower frequency spectrum (e.g., UL n255 or UL n256).

2.4.2 Operating bands and channel arrangement

The channel arrangements presented in this section are based on the operating bands and channel bandwidths defined in [3].

Requirements throughout the RF specifications are in many cases defined separately for different frequency ranges (FR). The frequency ranges in which NTN satellite can operate according to 3GPP release 18 specifications are identified as described in Table 2.

As specified in [3], the bands in Table 2 only support frequency division duplexing (FDD) operation.

TABLE 2: DEFINITION OF NTN FREQUENCY RANGES

Frequency range designation	Corresponding frequency range
FR1-NTN[1]	410 MHz – 14500 MHz
FR2-NTN[2]	10700 MHz – 30000 MHz
NOTE 1: [NTN bands within this frequency range are regarded as a FR1 band when referenced from other 3GPP specifications.] NOTE 2: [NTN bands within this frequency range are regarded as a FR2 band when referenced from other 3GPP specifications.]	

2.4.2.1 Non-Terrestrial Network operating bands

Table 3 and Table 4 report current bands that have been designated for FR1-NTN and FR2-NTN.

TABLE 3: NTN SATELLITE BANDS IN FR1-NTN

Satellite *operating band*[1]	Uplink (UL) *operating band* SAN receive / UE transmit $F_{UL,low}$ – $F_{UL,high}$	Downlink (DL) *operating band* SAN transmit / UE receive $F_{DL,low}$ – $F_{DL,high}$	Duplex mode
n256	1980 MHz – 2010 MHz	2170 MHz – 2200 MHz	FDD
n255	1626.5 MHz – 1660.5 MHz	1525 MHz – 1559 MHz	FDD
n254	1610 MHz – 1626.5 MHz	2483.5 MHz – 2500 MHz	FDD
n253	1668 MHz – 1675 MHz	1518 MHz – 1525 MHz	FDD
n252	2000 MHz – 2020 MHz	2180 MHz – 2200 MHz	FDD
n251	1626.5 MHz – 1660.5 MHz	1518 MHz – 1559 MHz	FDD
n250	1668 MHz – 1675 MHz	1518 MHz – 1559 MHz	FDD
n248	14000 MHz - 14500 MHz	10700 MHz – 12750[2,3] MHz	FDD
n247	13750 MHz - 14000 MHz	10700 MHz – 12750[2,3] MHz	FDD
NOTE 1:Satellite bands are numbered in descending order from n256. **NOTE 2:For Region 2, the downlink is limited to 10700 – 12700 MHz.** **NOTE 3:For the US, the downlink is limited to 10700 – 12200 MHz for Mobile VSAT**			

TABLE 4: SATELLITE OPERATING BANDS IN FR2-NTN

Satellite operating band	Uplink (UL) operating band SAN receive / UE transmit $F_{UL,low}$ – $F_{UL,high}$	Downlink (DL) operating band SAN transmit / UE receive $F_{DL,low}$ – $F_{DL,high}$	Duplex mode
n512(Note 1)	27500 MHz - 30000 MHz	17300 MHz - 20200 MHz	FDD
n511(Note 2)	28350 MHz - 30000 MHz	17300 MHz - 20200 MHz	FDD
n510(Note 3)	27500 MHz - 28350 MHz	17300 MHz - 20200 MHz	FDD
n509(Note4)	14000 MHz - 14500 MHz	10700 MHz – 12750[4,5] MHz	FDD
n508(Note5)	13750 MHz - 14000 MHz	10700 MHz – 12750[4,5] MHz	FDD
NOTE 1:This band is applicable in the countries subject to or referring to CEPT ECC Decision(05)01 and ECC Decision (13)01. **NOTE 2:This band is applicable in the countries subject to or referring to FCC 47 CFR part 25.** **NOTE 3:This band is applicable for Earth Station operations in the USA subject to FCC 47 CFR part 25. FCC rules currently do not include ESIM operations in this band (47 CFR 25.202).** **NOTE 4:For Region 2, the downlink is limited to 10700 – 12700 MHz.** **NOTE 5:For the US, the downlink is limited to 10700 – 12200 MHz for Mobile VSAT.**			

Figure 3 describes the designation of the 3GPP specified NTN bands together with the bands that are studied in 6G-NTN.

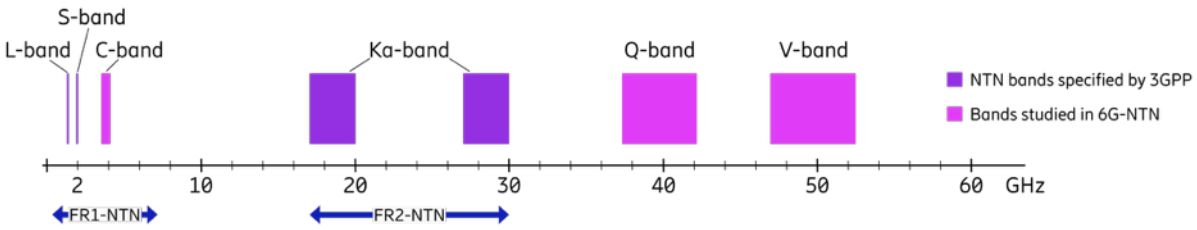

FIGURE 3. 3GPP SPECIFIED NTN BAND TOGETHER WITH THE BANDS STUDIED IN 6G-NTN

2.4.2.2 Terrestrial Network operating bands

The designation of operating bands for the terrestrial network (TN), defined in [6] is different and listed below for reference. For terrestrial networks, the FR1 frequency supports both FDD and TDD usage.

TABLE 5: FREQUENCY RANGE DESIGNATION FOR TN

Frequency range designation		Corresponding frequency range
FR1		410 MHz – 7125 MHz
FR2	FR2-1	24250 MHz – 52600 MHz
	FR2-2	52600 MHz – 71000 MHz

Details for the definition of bands in the FR2-1 range [6] are listed in Table 6.

While the frequencies of interest for 6G-NTN (see Section 2.4.1) are not covered by Table 5, they overlap with the definition for TN FR2 according to Table 6. Some of the requirements defined in [6] may be applicable to UEs in the Q/V bands, with the caveat that they are specified for TN TDD systems in addition to the parameters in [3] which are specifically tailored toward the satellite use case.

TABLE 6: BAND DESIGNATION FOR FR2-1 (TN)

Operating Band	Uplink (UL) operating band BS receive UE transmit	Downlink (DL) operating band BS transmit UE receive	Duplex Mode
	F_{UL_low}[2] – F_{UL_high}[3]	F_{DL_low} – F_{DL_high}	
n257	26500 MHz – 29500 MHz	26500 MHz – 29500 MHz	TDD
n258	24250 MHz – 27500 MHz	24250 MHz – 27500 MHz	TDD
n259	39500 MHz – 43500 MHz	39500 MHz – 43500 MHz	TDD
n260	37000 MHz – 40000 MHz	37000 MHz – 40000 MHz	TDD
n261	27500 MHz – 28350 MHz	27500 MHz – 28350 MHz	TDD
n262	47200 MHz – 48200 MHz	47200 MHz – 48200 MHz	TDD
n263	57000 MHz – 71000 MHz	57000 MHz – 71000 MHz	TDD[1]

NOTE 1: This band is for unlicensed operation and subject to regional and/or country specific regulatory requirements.

NOTE 2: F_{UL_low}, F_{DL_low} indicate the lower limit for the uplink and downlink bands respectively

NOTE 3: F_{UL_high}, F_{DL_high} indicate the upper limit for the uplink and downlink bands respectively

2.4.2.3 UE channel bandwidth

2.4.2.3.1 General

The UE channel bandwidth (BW) supports a single radio frequency (RF) carrier in the uplink or downlink at the UE. From a Satellite Access Node (SAN) perspective, different UE channel bandwidths may be supported within the same spectrum for transmitting to and receiving from UEs connected to the SAN.

From a UE perspective, the UE is configured with one or more bandwidth parts (BWP) / carriers, each with its own UE channel bandwidth. The UE does not need to be aware of the SAN channel bandwidth or how the SAN allocates bandwidth to different UEs.

The placement of the UE channel bandwidth for each UE carrier is flexible but can only be done completely within the SAN channel bandwidth.

The relationship between the channel bandwidth, the guardband and the maximum transmission bandwidth configuration is shown in Figure 4.

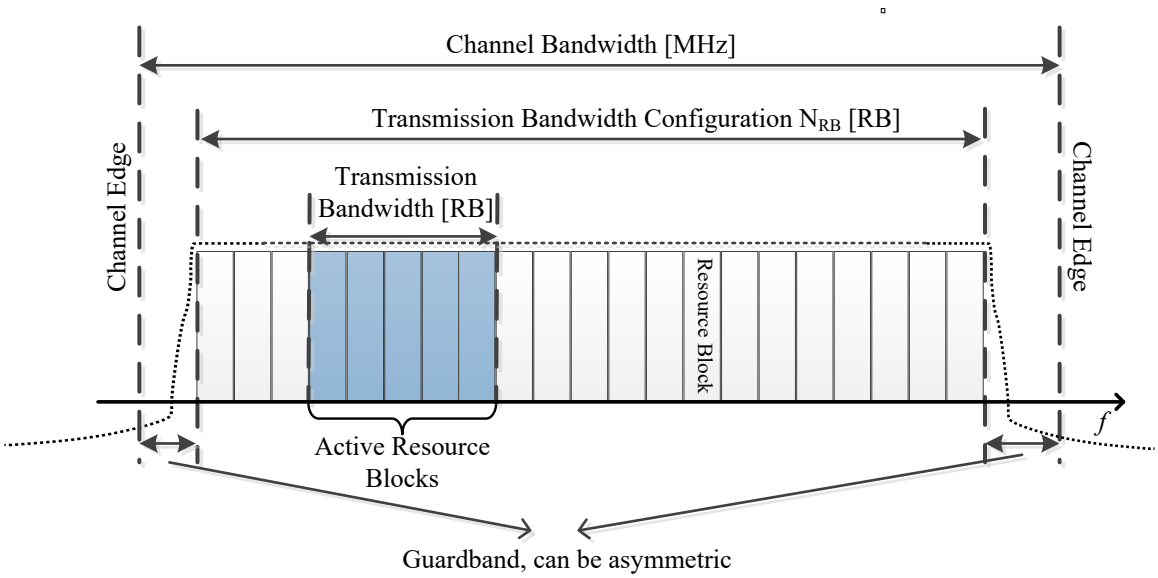

FIGURE 4: DEFINITION OF THE CHANNEL BANDWIDTH AND THE MAXIMUM TRANSMISSION BANDWIDTH CONFIGURATION FOR ONE CHANNEL

2.4.2.3.2 Maximum transmission bandwidth configuration

The maximum transmission bandwidth configuration is defined in resource blocks (N_{RB}) for each UE channel bandwidth and subcarrier spacing (SCS) in Table 7 for FR1-NTN and Table 8 for FR2-NTN. A resource block is a group of 12 subcarriers with the given subcarrier spacing.

TABLE 7: MAXIMUM TRANSMISSION BANDWIDTH CONFIGURATION NRB FOR FR1-NTN

SCS (kHz)	5 MHz	10 MHz	15 MHz	20 MHz	25 MHz	30 MHz	35 MHz	50 MHz	70 MHz	100 MHz
	N_{RB}	N_{RB}	N_{RB}	N_{RB}	N_{RB}	N_{RB}	N_{RB}	N_{RB}	N_{RB}	N_{RB}
15	25	52	79	106	133	160	188	270	N/A	N/A
30	11	24	38	51	65	78	92	133	189	273
60	N/A	11	18	24	31	38	44	65	93	135

TABLE 8: MAXIMUM TRANSMISSION BANDWIDTH CONFIGURATION NRB FOR FR2-NTN

SCS (kHz)	50 MHz	100 MHz	200 MHz	400 MHz
	N_{RB}	N_{RB}	N_{RB}	N_{RB}
60	66	132	264	N/A
120	32	66	132	264

2.4.3 Radiated Transmitter Characteristics

2.4.3.1 General

Unless otherwise stated, the transmitter characteristics are specified over the air (OTA) with a single or multiple transmit chains under either LHCP (Left Hand Circular Polarization) or RHCP (Right Hand Circular Polarization) or Linear Polarization.

2.4.3.2 Transmitter power

2.4.3.2.1 NTN VSAT maximum output power

2.4.3.2.1.1 General

The NTN VSAT classes are specified based on the assumptions of certain NTN VSAT types with specific device architectures including antenna beam steering types. The requirements are specified for different NTN VSAT types. For the hybrid beam steering capable NTN VSAT, which can adjust its antenna(s) or beam(s) in both electronic steering and mechanical steering ways, the applicable requirements shall follow either electronic or mechanical beam steering requirements depending on the NTN VSAT type it declared. The NTN VSAT types are specified in Table 9 below.

TABLE 9: DEFINITIONS OF NTN VSAT TYPES

NTN VSAT class	NTN VSAT type	Type description
Fixed VSAT	1	Fixed VSAT communicating with GSO and LEO with mechanical steering antenna.
	2[2]	Fixed VSAT communicating with GSO and LEO with electronic steering antenna.
	3	Fixed VSAT communicating with LEO only with electronic steering antenna.
Mobile VSAT	4[3]	Mobile VSAT communicating with GSO and LEO with mechanical steering antenna.
	5[2, 3]	Mobile VSAT communicating with GSO and LEO with electronic steering antenna.
	6[4]	Mobile VSAT communicating with LEO only with electronic steering antenna.
NOTE 1:The NTN VSAT types are assuming NTN VSAT has only one antenna beam towards one satellite at a given time in this release. **NOTE 2:NTN VSAT may need power reduction to comply with OFF-axis EIRP requirement defined in clause 9.2.2. There is no requirement for the potential power reduction.** **NOTE 3:GSO support is applicable to bands n512, n511, n510, n509, n508 and n248, n247; LEO support is only applicable to bands n509, n508 and n248, n247.** **NOTE 4:The NTN VSAT type 6 is only applicable to bands n509, n508 and n248, n247.**		

2.4.3.2.1.2 Minimum requirements for Fixed VSAT

The following requirements define the maximum output power radiated by the Fixed VSAT for any transmission bandwidth within the channel bandwidth for non-CA configuration, unless otherwise stated. The period of measurement shall be at least one sub-frame (1ms). The

minimum output power values for EIRP are specified in Table 10. The requirement should be verified with test metrics of EIRP (Link=Tx beam peak direction, Meas=Link angle).

The peak EIRP of Tx beam peak direction should be verified within the declared minimum elevation angle supported for transmitting. The steered beam peak directions can be achieved by mechanical steering and/or electronic steering according to VSAT Type. Where the supported minimum elevation angle shall be declared by manufacturer and within the range of $3° \leq \text{minimum elevation angle} \leq 75°$, and it can be expressed as (90-θ) if the coordinate systems in Figure 5 below is taken as an example.

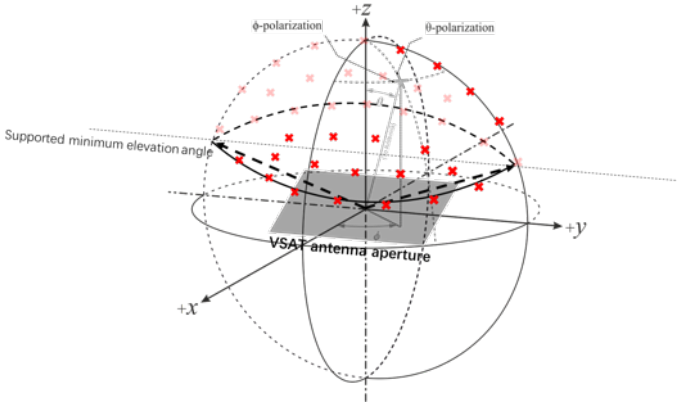

FIGURE 5 EXAMPLE MEASUREMENT GRID FOR MIN PEAK EIRP WITH THE DECLARED SUPPORTED MINIMUM ELEVATION ANGLE

TABLE 10: MINIMUM PEAK EIRP FOR FIXED VSAT

Operating band	UE Type	Min peak EIRP (dBm)
n512, n511, n510	1	70
	2	70
	3	61
Note: Minimum peak EIRP is defined as the lower limit without tolerance.		

The maximum output power values for EIRP are reported in Table 11.

TABLE 11: UE MAXIMUM OUTPUT POWER LIMITS FOR FIXED VSAT

Operating band	UE Type	TRPMAX (dBm)	EIRPmax (dBm)
n512, n511, n510	1	35	76.2
	2, 3	43	76.2
NOTE: Maximum EIRP is defined using 13RBs allocation with 120kHz SCS.			

2.4.3.2.1.3 Minimum requirements for Mobile VSAT

The following requirements define the maximum output power radiated by the UE for any transmission bandwidth within the channel bandwidth for non-CA configuration, unless otherwise stated. The period of measurement shall be at least one sub frame (1ms). The minimum output power values for EIRP are found in Table 12. The requirement is verified with the test metric of EIRP (Link=TX beam peak direction, Meas=Link angle).

The peak EIRP of Tx beam peak direction should be verified within the declared minimum elevation angle supported for transmitting. The steered beam peak directions can be achieved by mechanical steering and/or electronic steering according to VSAT Type. Where the supported minimum elevation angle shall be declared by manufacturer and within the range of $3° \leq \text{minimum elevation angle} \leq 75°$, and it can be expressed as (90-θ) if the coordinate systems Figure 6 below is taken as an example.

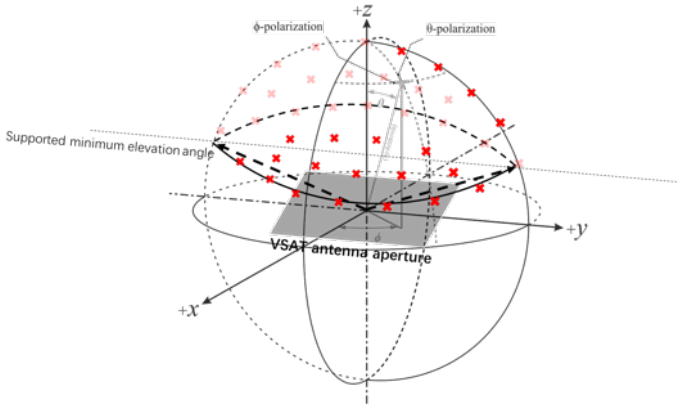

FIGURE 6 EXAMPLE MEASUREMENT GRID FOR MIN PEAK EIRP WITH THE DECLARED SUPPORTED MINIMUM ELEVATION ANGLE

TABLE 12: MINIMUM PEAK EIRP FOR MOBILE VSAT

Operating band	UE Type	Min peak EIRP (dBm)
n512, n511	4	70
	5	70
n509, n508	4	70
	5	70
	6	60
n248, n247	4	70
	5	70
	6	60
NOTE: Minimum peak EIRP is defined as the lower limit without tolerance.		

The maximum output power values for TRP and EIRP for mobile VSAT are specified in Table 13.

TABLE 13: MAXIMUM OUTPUT POWER LIMITS FOR MOBILE VSAT

Operating band	UE Type	TRP_{MAX} (dBm)	$EIRP_{max}$ (dBm)
n512, n511, n510	4	35	76.2^{1}
	5	43	76.2^{1}
n509, n508	4	47	$88.2^{2,4}$
	5	47	$88.2^{2,4}$
	6	40	$76.6^{2,4}$
n248, n247	4	47	$88.2^{3,4}$
	5	47	$88.2^{3,4}$
	6	40	$76.6^{3,4}$

NOTE 1: Maximum EIRP is defined using 13RBs allocation with 120kHz SCS.
NOTE 2: Maximum EIRP is defined using 6RBs allocation with 120kHz SCS.
NOTE 3: Maximum EIRP is defined using 27RBs allocation with 30kHz SCS or using 54RBs allocation with 15kHz SCS.
NOTE 4: For land ESIM operating in CEPT regions, the upper limits of $EIRP_{max}$ is 84.5 dBm.

2.4.3.3 Transmitter signal quality

2.4.3.3.1 Frequency Error

The NTN VSAT UE basic measurement interval of modulated carrier frequency is 1 uplink (UL) slot. The NTN VSAT UE pre-compensates the uplink modulated carrier frequency by the estimated Doppler shift according to 3GPP TS 38.300 [11] clause 16.14.2. The mean value of basic measurements of VSAT UE modulated carrier frequency shall be accurate to within ± 0.1 parts per million (PPM) observed over a period of 1 ms of cumulated measurement intervals compared to ideally pre-compensated reference uplink carrier frequency.

[NOTE: The ideally pre-compensated reference uplink carrier frequency consists of the UL carrier frequency signaled to the NTN VSAT UE by SAN and UL pre-compensated Doppler frequency shift. For the test case, the location of the NTN VSAT UE is explicitly provided to the NTN VSAT UE from the test equipment.]

Requirement will be verified for at least two cases of which one has zero Doppler conditions.

The frequency error is defined as a directional requirement. The requirement is verified in beam locked mode with the test metric of Frequency (Link=TX beam peak direction, Meas=Link angle).

2.4.3.3.2 Transmit modulation quality

Transmit modulation quality defines the modulation quality for expected in-channel RF transmissions from the NTN VSAT. The transmit modulation quality is specified in terms of: error vector magnitude (EVM) for the allocated resource blocks (RBs)

All the parameters defined in sub-clause 2.4.3.3.2 are defined using the measurement methodology specified in Annex F of [3].

All the requirements in sub-clause 2.4.3.3.2 are defined as directional requirement. The requirements are verified in beam locked mode on beam peak direction, with parameter *maxRank* (as defined in TS 38.331) set to 1. The requirements are applicable to UL transmission from each configurable antenna port (as defined in TS 38.331) of UE, enabled one at a time.

2.4.3.3.2.1 Error vector magnitude

The Error Vector Magnitude is a measure of the difference between the reference waveform and the measured waveform. This difference is called the error vector. Before calculating the EVM, the measured waveform is corrected by the sample timing offset and RF frequency offset. Then the carrier leakage shall be removed from the measured waveform before calculating the EVM.

For DFT-s-OFDM waveforms, the EVM result is defined after the front-end FFT and IDFT as the square root of the ratio of the mean error vector power to the mean reference power expressed as a percentage value (%). For CP-OFDM waveforms, the EVM result is defined after the front-end FFT as the square root of the ratio of the mean error vector power to the mean reference power expressed as a percentage value (%).

The basic EVM measurement interval in the time domain is one preamble sequence for the PRACH and one slot for PUCCH and PUSCH in the time domain. The EVM measurement interval is reduced by any symbols that contains an allowable power transient in the measurement interval as as defined in sub-clause 9.3.3 in [3].

The RMS average of the basic EVM measurements over 10 subframes for the average EVM case, and over 60 subframes for the reference signal EVM case, for the different modulation schemes shall not exceed the values specified in Table 14 for the parameters defined in Table 15. For EVM evaluation purposes, all 13 PRACH preamble formats and all 5 PUCCH formats are considered to have the same EVM requirement as QPSK modulated.

The requirement is verified with the test metric of EVM (Link=TX beam peak direction, Meas=Link angle).

TABLE 14. MINIMUM REQUIREMENTS FOR ERROR VECTOR MAGNITUDE

Parameter	Unit	Average EVM level	Reference signal EVM level
Pi/2 BPSK	%	30.0	30.0
QPSK	%	17.5	17.5
16QAM	%	12.5	12.5
64QAM	%	8.0	8.0

TABLE 15 PARAMETERS FOR ERROR VECTOR MAGNITUDE

Parameter	Unit	Level
NTN VSAT EIRP	dBm	≥ [Min peak EIRP]
NTN VSAT EIRP for UL 16QAM	dBm	≥ [Min peak EIRP]
NTN VSAT EIRP for UL 64QAM	dBm	≥ [Min peak EIRP]
Operating conditions		Normal conditions

2.4.3.4 Output RF spectrum emissions

2.4.3.4.1 Occupied bandwidth

Occupied bandwidth (OBW) is defined as the bandwidth containing 99 % of the total integrated mean power of the transmitted spectrum on the assigned channel. The occupied bandwidth for all transmission bandwidth configurations (Resources Blocks) shall be less than the channel bandwidth specified in Table 16.

The occupied bandwidth is defined as a directional requirement. The requirement is verified in beam locked mode with the test metric of OBW (Link=TX beam peak direction, Meas=Link angle).

TABLE 16: OCCUPIED CHANNEL BANDWIDTH

	Occupied channel bandwidth / Channel bandwidth for FR2-NTN			
	50 MHz	**100 MHz**	**200 MHz**	**400 MHz**
Channel bandwidth (MHz)	50	100	200	400

	Occupied channel bandwidth / Channel bandwidth for FR1-NTN above 10 GHz							
	10 MHz	15 MHz	20 MHz	25 MHz	35 MHz	50 MHz	70 MHz	100 MHz
Channel bandwidth (MHz)	10	15	20	25	35	50	70	100

2.4.3.4.2 Out of Band Emissions

2.4.3.4.2.1 General

The out of band (OoB) emissions are unwanted emissions immediately outside the assigned channel bandwidth resulting from the modulation process and non-linearity in the transmitter but excluding spurious emissions (SE). This OoB emission limit is specified in terms of a spectrum emission mask and an adjacent channel leakage power ratio. Additional requirements to protect specific bands are also considered.

The requirements in subsection 2.4.3.4.2.2 only apply when both UL and DL of an NTN VSAT are configured for single component carrier (CC) operation, and they are of the same bandwidth.

All out of band emissions for FR2-NTN are specified as TRP.

The spectrum emission mask of the NTN VSAT applies to frequencies starting from the ± edge of the assigned NR channel bandwidth.

2.4.3.4.2.2 Spectrum emission mask

2.4.3.4.2.2.1 General NR spectrum emission mask

The power of any NTN VSAT emission shall not exceed the Basic limits specified in Table 17 for the specified channel bandwidth. The requirement is verified in beam locked mode with the test metric of TRP (Link=TX beam peak direction, Meas=TRP grid). Where:

- Δf is the separation between the Transmission BW *channel edge* frequency and the nominal -3dB point of the measuring filter closest to the carrier frequency.
- f_offset is the separation between the *channel edge* frequency and the centre of the measuring filter.

TABLE 17: GENERAL NR SPECTRUM EMISSION MASK FOR NTN-FR2

Frequency offset of measurement filter -3dB point, Df	Frequency offset of measurement filter centre frequency, f_offset	Basic limits (dBm)	Measurement bandwidth
0 MHz ≤ Δf < 2× BW	0.5 MHz ≤ f_offset < 2× BW + 0.5 MHz	$max\left(11, TRP_{rated} - 10\log10(\text{BW}) - 40 \times log10\left(\frac{f\_offset - 0.5}{BW} \times 2 + 1\right)\right) dBm$	1 MHz
NOTE 1: TRP_{rated} is the declared rated output power lower than or equal to TRP_{max} specified in sub-clause 9.2.1; NOTE 2: Transmission BW is in the unit of MHz; NOTE 3: The 11dBm/1MHz value corresponds to the spurious emission limit specified in spurious emission sub-clause 9.5.3, and is converted from the SE limit requirement defined on 4 kHz to a value defined over 1 MHz; NOTE 4: PSD attenuation as in ITU-R SM.1541-6 [6], Annex 5 OoB domain emission limits for earth stations.			

2.4.3.4.3 Adjacent channel leakage ratio

Adjacent Channel Leakage power Ratio (ACLR) is the ratio of the filtered mean power centred on the assigned channel frequency to the filtered mean power centred on an adjacent channel frequency. ACLR requirement is specified for a scenario in which adjacent carrier is another NR channel.

NR Adjacent Channel Leakage power Ratio (NR_{ACLR}) is the ratio of the filtered mean power centred on the assigned channel frequency to the filtered mean power centred on an adjacent channel frequency at nominal channel spacing. The assigned NR channel power and adjacent NR channel power are measured with rectangular filters with measurement bandwidths specified in Table 18 for FR2-NTN and Table 19 for FR1-NTN above 10 GHz.

If the measured adjacent channel power is greater than –35 dBm then the NR_{ACLR} shall be higher than the value specified in Table 18. The requirement is verified in beam locked mode with the test metric of TRP (Link=TX beam peak direction, Meas=TRP grid).

TABLE 18: GENERAL REQUIREMENTS FOR NR ACLR FOR FR2-NTN

	Channel bandwidth / NR_{ACLR} / Measurement bandwidth			
	50 MHz	**100 MHz**	**200 MHz**	**400 MHz**
NR_{ACLR} for band n512, n511, n510	14 dB	14 dB	14 dB	14 dB
NR channel measurement bandwidth (MHz)	47.58	95.16	190.20	380.28
NR_{ACLR} for band n509, n508	18.5 dB	18.5 dB	18.5 dB	18.5 dB
Adjacent channel centre frequency offset (MHz)	+50 / -50	+100 / -100	+200 / -200	+400 / -400

TABLE 19: GENERAL REQUIREMENTS FOR NR ACLR FOR FR1-NTN ABOVE 10 GHZ

	Channel bandwidth / NR_{ACLR} / Measurement bandwidth							
	10	**15**	**20**	**25**	**35**	**50**	**70**	**100**
NR_{ACLR} for band n248, n247	18.5 dB							
NR channel measurement bandwidth (MHz)	9.375	14.235	19.095	23.955	33.855	48.615	68.07	98.31
Adjacent channel centre frequency offset (MHz)	+10 / -10	+15 / -15	+20 / -20	+25 / -25	+35 / -35	+50 / -50	+70 / -70	+100 / -100

2.4.3.4.4 Spurious Emissions

2.4.3.4.4.1 General

Spurious emissions are emissions which are caused by unwanted transmitter effects such as harmonics emission, parasitic emissions, intermodulation products and frequency conversion products, but exclude OoB emissions unless otherwise stated. The spurious emission limits are specified in terms of general requirements in line with SM.329 [12]. and NR operating band requirement to address UE co-existence. Spurious emissions are measured as TRP.

To improve measurement accuracy, sensitivity and efficiency, the resolution bandwidth may be smaller than the measurement bandwidth. When the resolution bandwidth is smaller than

the measurement bandwidth, the result should be integrated over the measurement bandwidth in order to obtain the equivalent noise bandwidth of the measurement bandwidth.

Unless otherwise stated, the spurious emission limits apply for the frequency ranges that are more than F_{OOB} (MHz) in Table 20 starting from the edge of the assigned NR channel bandwidth. The spurious emission limits in Table 21 apply for all transmitter band configurations (NRB) and channel bandwidths. The requirement is verified in beam locked mode with the test metric of TRP (Link=TX beam peak direction, Meas=TRP grid).

NOTE: For measurement conditions at the edge of each frequency range, the lowest frequency of the measurement position in each frequency range should be set at the lowest boundary of the frequency range plus MBW/2. The highest frequency of the measurement position in each frequency range should be set at the highest boundary of the frequency range minus MBW/2. MBW denotes the measurement bandwidth defined for the protected band.

TABLE 20: BOUNDARY BETWEEN NR OOB AND SPURIOUS EMISSION DOMAIN

Channel bandwidth	50 MHz	100 MHz	200 MHz	400 MHz
OOB boundary FOOB (MHz)	100	200	400	800

TABLE 21: SPURIOUS EMISSIONS LIMITS

Frequency Range	**Maximum Level**	**Measurement bandwidth**
30 MHz ≤ f ≤ 2nd harmonic of the upper frequency edge of the UL operating band in GHz	-13 dBm	4 kHz

2.4.4 Radiated Receiver Characteristics

2.4.4.1 General

Unless otherwise stated, the receiver characteristics are specified over the air (OTA) at the RIB for Ka bands fixed and mobile VSAT. The power level for all DL wanted signals and interference is defined assuming a 0 dBi reference antenna located at the center of the quiet zone.

2.4.4.2 Polarization characteristics

The minimum requirements on the receiver characteristics apply under either LHCP (Left Hand Circular Polarization) or RHCP (Right Hand Circular Polarization) or Linear Polarization.

2.4.4.3 OTA reference sensitivity level

2.4.4.3.1 General

The OTA reference sensitivity (REFSENS) requirement is a *directional requirement* and is intended to ensure the minimum OTA reference sensitivity level at the centre of the quiet zone in the receive (RX) beam peak direction. The OTA reference sensitivity power level $EIS_{REFSENS}$ is the minimum mean power received over the air at the RIB, at which the throughput shall meet or exceed the requirements for a specified reference measurement channel.

2.4.4.3.2 Minimum requirement

The throughput shall be ≥ 95 % of the maximum throughput of the reference measurement channels as [specified in Annexes A.3.2.1.2 and A.3.2.1.3 of [3] (with one sided dynamic orthogonal frequency-division multiple-access (OFDMA) Channel Noise Generator (OCNG) Pattern OP.1 Frequency Division Duplexing (FDD) for the downlink (DL)-signal as described in Annex A.5.1.1) with peak reference sensitivity specified in Table 22. $EIS_{REFSENS\_50M}$ declared by the vendor is an integer value in the range specified in Table 23 for different types of NTN VSAT. The requirement is verified with the test metric of EIS (Link=RX beam peak direction, Meas=Link Angle).

The EIS of Rx beam peak direction should be verified within the declared minimum elevation angle supported for receiving. The steered beam peak directions can be achieved by mechanical steering and/or electronic steering according to VSAT Type. Where the supported minimum elevation angle shall be declared by manufacturer and within the range of $3° \leq \text{minimum elevation angle} \leq 75°$ and it can be expressed as (90-θ) if the coordinate systems in Figure 7 below is taken as an example

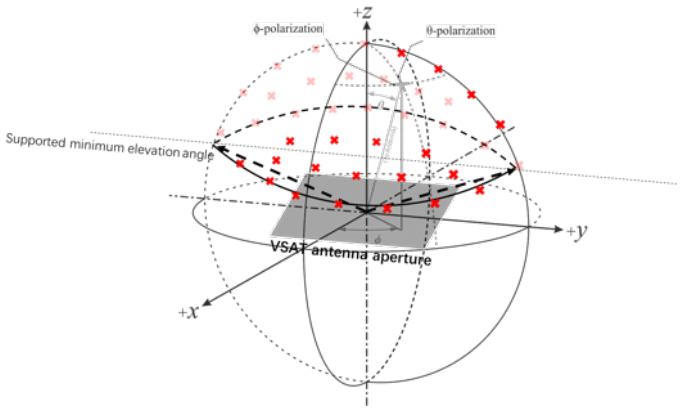

FIGURE 7 EXAMPLE MEASUREMENT GRID FOR EIS WITH THE DECLARED SUPPORTED MINIMUM ELEVATION ANGLE

TABLE 22: OTA REFERENCE SENSITIVITY REQUIREMENT FOR NTN VSAT

NTN VSAT channel bandwidth (MHz)	UL/DL RB allocation	OTA reference sensitivity level, EISREFSENS (dBm)
50, 100, 200, 400	Full RB allocation N_{RB} as specified in sub-clause 5.3.2	$EIS_{REFSENS\_50MHz} + 10\log_{10}(N_{RB} \times SCS \times 12 / factor)$ (NOTE 1)
NOTE 1: The "factor" represents the normalized factor to scale EIS for different (Channel bandwidth, SCS) configurations. The value of factor is 66 RBs x 60 kHz SCS x 12, i.e. 47520 kHz.		

TABLE 23 THE RANGE OF $EIS_{REFSENS\_50MHz}$ DECLARED BY VENDOR PER NTN VSAT

Operating band	*NTN VSAT class*	*NTN VSAT type*	The range of $EIS_{REFSENS\_50MHz}$ (dBm)
n512, n511	Fixed VSAT	1, 2	≤ -122
		3	≤ -115.6
n512, n511, n510	Mobile VSAT	4, 5	≤ -122

For Mobile VSAT communication with GSO, $EIS_{REFSENS\_50MHz}$ is [-126.8] dBm.

2.4.5 Fixed radio service requirements applicable for antennas in the Q/V band

Another source of requirements applicable to terminals operating in the Q/V bands is the ETSI specification EN 302 217-4 [4]. It covers fixed radio services for frequencies in the Q/V band and describes requirements for antennas in frequency ranges between 1 GHz and 86 GHz.

For co-existence and general spectrum compliancy, the radiation pattern envelope (RPE) for an antenna is an important parameter. It provides, e.g., the requirement on the allowed side lobe level in azimuth degrees from the main lobe. The RPE for frequencies between 30 and 47 GHz is illustrated in Figure 8 below, adapted from [4].

The fixed radio services use FDD, so the duplexing distances that are specified in [4] for the bands coinciding with the 6G-NTN Q/V could also be used as an input for future analysis of the UE antenna requirement specification (See chapter 4).

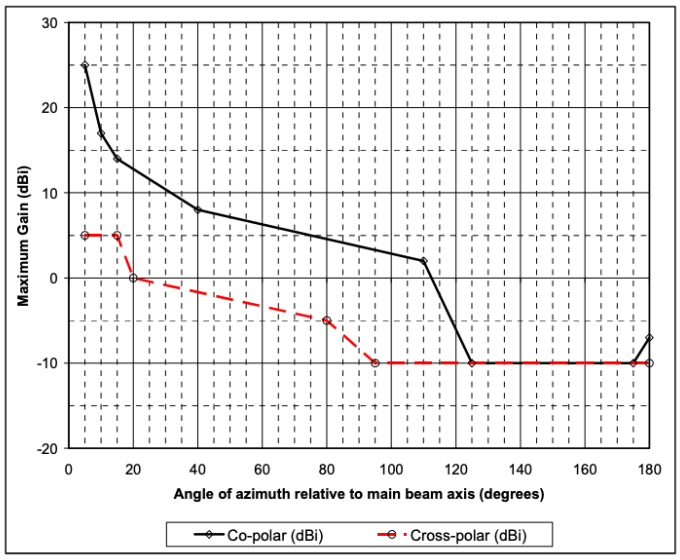

Angle (°)	Co-polar (dBi)	Angle (°)	Cross-polar (dBi)
5	25	5	5
10	17	15	5
15	14	20	0
40	8	80	-5
110	2	95	-10
125	-10	180	-10
175	-10		
180	-7		

FIGURE 8: RPES FOR CLASS 1 ANTENNAS IN THE FREQUENCY RANGE FROM 30 TO 47 GHZ

It should also be observed that in the 6G-NTN deliverable 4.4 [10] there are assumptions given for the radiation pattern when simulating interferences into other systems. The requirement put on antennas based on new technologies for the radiation pattern could as a first approach, be required to stay within the limits for the antenna radiation pattern used in the co-existence simulations in [10].

3 ANTENNA TECHNOLOGY SURVEY IN C AND Q/V BAND

3.1 INTRODUCTION AND INVESTIGATION SCOPE FOR ANTENNAS

The aim of this chapter is to provide a survey on Q/V and C-Band antenna technologies, with special focus on moving terminal applications, nicknamed as Satellite On-The-Move (SOTM), Earth Station in Motion (ESIM) and/or Earth Station on Moving Platform (ESOMP),and considering the requirements already derived in previous section for mounted devices, which are the main object of study in 6G-NTN project. For the C-band case, handheld antennas are also analyzed. The critical joint analysis of the State-of-the-Art technologies and the terminal requirements allows identifying promising solutions, determining short and mid-term research paths. Therefore, the next two sections provide an antenna technology survey and a critical analysis of potential solutions for both Q/V and C-band, taking into account the specific requirements of identified 6G-NTN terminal types.

Let us remark that for satellites terminals, the term “antenna” is often not limited to the device radiating/receiving the intended signals but it includes everything between the modem output/input, typically at L-band, and the radiating elements themselves. Since satellite systems typically operate in frequency division duplex (FDD) scheme, these may include two different antenna apertures containing the radiating mechanisms for Tx and Rx as well as their corresponding up and down conversion circuits. In addition, an Antenna Control Unit (ACU) featuring a more or less sophisticated inertial system is responsible for controlling the antenna pointing in close collaboration with the modem. This modem-antenna interface is often standardized using OpenAMIP [13] solution. The analysis performed here will be focused on the radiating apertures, since for the rest of components, the use of the Q/V band or the specific 6G-NTN requirements does not imply significant changes.

3.2 ANTENNA TECHNOLOGY SURVEY IN Q/V BAND

A quick analysis of the state-of-the-art reveals that there is only one pre-commercial SOTM terminal in Q/V band provided by ThinKom. Remarkably, it implements a passive mechanical steering solution, based on the ThinKom patented Variable Inclination Continuous Transverse Stub (VICTS) technology [14]. As depicted in Figure 9, it consists of two panels placed one on top of the other supporting a parallel plate waveguide transmission. The lower panel implements parallel plate mode feeding lines, and the upper transverse stubs that create a leaky wave that is responsible of the radiation of a narrow pencil beam. By controlling the relative rotation between both panels, the beam can be steered in both azimuth and elevation angles.

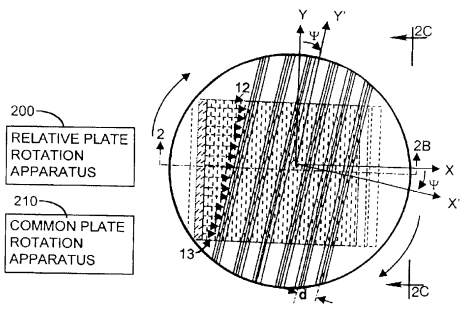

FIGURE 9: THINKOM PRE-COMMERCIAL Q/V- BAND TERMINAL. LEFT: TERMINAL PICTURE FROM [14]; RIGHT: VICTS TECHNOLOGY FROM [15].

The fact that the first pre-commercial product is based on mechanical steering may be just a coincidence, obeying the ThinKom strategy to be the first announcing a product in the market, but it exemplifies the challenges of developing a cost and power efficient low-profile antenna with electronic steering at millimetre wave ranges. It is foreseen that once the market demands them (note that nowadays Q/V are mostly considered for the feeder link), more players will develop antenna terminals in different technologies, as is the case today for Ka and Ku bands. Indeed, the jump between Ka and Q/V is not that high, so it could be envisaged that the same technologies will be used and adapted to the Q/V range. Therefore, we analyse next the evolution of SOTM antenna terminals in commercial Ku/Ka bands.

Firstly, let us remark that the antenna has been traditionally the main barrier for the massive spread of SOTM terminals. It represents 90% of the terminal cost [15], and their size, power consumption and weight represent also challenges for their deployment on smaller platforms like cars. The move to LEO orbits opens new opportunities since lower pathloss require reduced antenna sizes, so reduced costs. Indeed, Starlink terminals can be seen as a massive deployment of beam scanning antennas, though in this case they are fixed terminal, not SOTM ones. Wide reviews on antenna technologies for SOTM [16], LEO terminals [17], beam steering solution for satellite communications (SATCOM) and 5G [18] or just for 5G [19] have been already published.

Initial SOTM terminals relied on mechanically steered parabolic reflectors, resulting in heavy and bulky systems not suitable for smaller platforms. Nowadays they still have applications in large platforms like vessels. The need for more aerodynamic low-profile solutions went through the use of modified reflectors to the implementation of single or multiple rectangular panels. Passive mechanical steering, as already explained for the VICTS case, is still a suitable technology when considering cost and power efficiency. A review on recent passive steering solutions is presented in [15], which includes the discussion of low profile near-field meta-steering antenna systems. They can be seen as an extension of the VICTS concept in which a low layer excites an upper layer consisting of a metasurface creating a radiating leaky wave mode. The mechanical interaction between the two layers controls the beam steering. In that regard, Figure 10 shows the evolution of mechanically steered antennas.

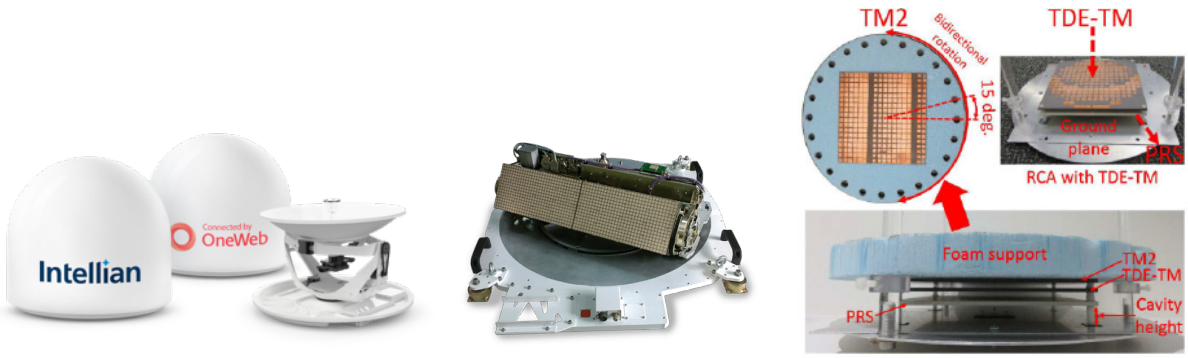

FIGURE 10: MECHANICALLY STEERED TECHNOLOGY EXAMPLES. LEFT: PARABOLIC REFLECTOR [21]; CENTER: FLAT RECTANGULAR PANEL (FROM [22]); AND RIGHT: NEAR-FIELD META-STEERING (FROM [16])

Beam steering reconfiguration rates in mechanically steered parabolic reflectors were in the order of seconds, so the need for fast steering motivated the use of electronic steering solutions. Although initially hybrid systems providing electronic elevation steering and mechanical azimuth steering were issued, nowadays full electronic steering is a reality. Indeed, it experienced a huge progression in the last decade, driven by the needs of both SATCOM and 5G applications, and relying in technological improvements in integrated circuits (IC) and metasurface technologies. Three main steering solutions have been developed: array-based, reflector/lens-based and leaky-wave (metasurface) based. They are further discussed next.

Array-based electronic steering

Electronic steering with array-based antennas has been demonstrated with multiple configurations: tile and brick, digital, analogue and hybrid beamforming, for analogue it has been implemented in RF, intermediate frequency (IF) or local oscillator (LO). For hybrid, partially connected and fully connected solutions have been investigated [18]. For SOTM terminals, the major trend is the tile configuration with analog beamforming at RF. Phasor, now Hanwha-Phasor [21], was one of the pioneering companies demonstrating this technology in a commercial product, as shown in Figure 11. Nowadays, there is a large set of companies using this technology in Ku and Ka bands (e.g., ViaSat, Rockwell Collins, Qest, OneWeb, SpaceX, Boeing, Coxsat, etc.). The main enablers for this solution are the multi-channel beamformer IC and the printed circuit board (PCB) advancements. Specifically, beamformer ICs typically implement amplification (low noise amplifier or power amplifier) and phase and magnitude control for beam steering, for dual polarization and for multiple elements from 4 to 16. This provides the required level of integration for the tile configuration, placing the IC underneath the set 4 or 16 array module. The combination of multiple modules permits realizing large antenna apertures. Several companies like Renesas, Analog Devices or Anokiwave offer Commercial off-the-shelf (COTS) beamformer IC that can be used by system integrators to realize their own antenna solutions. The drawbacks of analog beamforming include the large feeding networks required that imply significant losses, the single-beam operation, and the beam squint in large apertures. All of them can be addressed by using digital or hybrid beamforming. Digital beamforming has been demonstrated by Satixfy [22], which developed their own application-specific integrated circuit (ASIC) suitable for given antenna configurations. In the case of hybrid-beamforming, the partially connected solution in which each antenna element is only connected to the RF chain is the preferred choice due to the large apertures. Note that a full-connected solution would require having large combining networks for each antenna element, significantly increasing losses. Losses in feeding networks can be overcome by amplifiers, but it not only worsens the thermal management of the antenna but also the power consumption, which is already a limiting factor in some moving platforms.

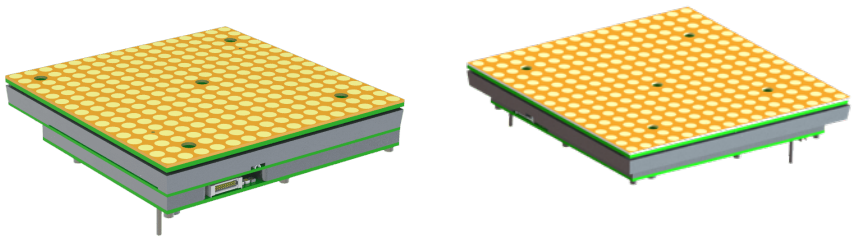

Figure 11: Tx (left) and Rx (right) apertures for Hanwha-Phasor analog RF beamformer antenna

The move to Q/V bands would increase the integration level required, and complicate the thermal management due to the denser element distribution. Still, arrays at 40 GHz have been designed for 5G [18], and it is expected that solution for SATCOM will come if the market demands them.

Reflector/lens-based electronic steering

A potential alternative in order to get rid of the large losses in array feeding networks is the use of spatial feeding configurations of transmit/reflectarrays [23] . In this case, a single feed or a very small array illuminates a reflector or lens surface made of phase shifting reflecting/transmitting elements. Therefore, the beam steering is performed in the spatially illuminated lens/reflector surface and there is no need for feeding networks. However, this solution requires having a quite large distance between the feed and the lens/reflector surface

similar to the lens/reflector diameter resulting in high profile antennas. They can be reduced by the use of folded reflect array configurations, but still the profile is not low enough to be considered as a planar antenna (e.g., [24]).

Leaky-wave/metasurface-based electronic steering

To get rid of large feeding networks and keep low profile configurations, the alternative is to illuminate a metasurface through a parallel plate waveguide mode or a surface wave (metasurface antennas) or a Fabry-Perot cavity (Fabry Perot antennas (FPA)). The metasurface illumination excites a leaky-wave forming the radiation beam at the antenna far-field. This process can be also explained by holographic theory [25]. Leaky-wave antennas inherently scan their beams with the change in frequency, so fixed frequency scanning requires changing the surface impedance of each metasurface unit cell. For metasurface antennas, typically the reconfiguration has been obtained through varactor diodes of liquid-crystal (LC). It must be noted that the size of the metasurface unit cells need to be well below the wavelength, increasing the number of unit cells with respect to array-based systems where half-wavelength is enough. However, the use of simple varactors or LC still provides important power and cost improvements with respect to active arrays. Metasurface antennas has been demonstrated for SOTM applications using LC by Kymeta [26] or for 5G applications using varactor diodes by Pivotal [27], depicted in Figure 12 . Remarkably, Kymeta solution interleaved transmits and receive unit cells on the same metasurface realizing a shared Tx/Rx aperture [18]. For FPA, beam steering at mm-wave has been demonstrated using beam switching with a focal -plane array instead of a single feed element [28][29]. In lower frequencies varactor, and PIN diodes, LC or liquid-metal has been used but the achieved beam steering was limited and not covering 360º in azimuth and 50º in elevation.

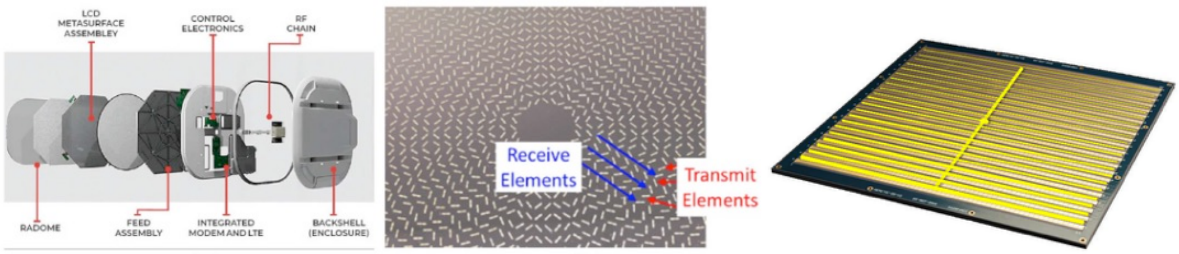

FIGURE 12: COMMERCIAL METASURFACE ANTENNAS. LEFT: KYMETA FROM [18]; RIGHT: PIVOTAL FROM [18];

In this case, moving to Q/V band would again imply a denser grid of unit cells, increasing the number of reconfigurable elements.

Hybrid solutions

Other companies developed terminal antennas using a combination of the aforementioned technologies. This is the case of Isotropic systems, now All.Space (Figure 13), which uses an array of lenses illuminated by focal-plane arrays. The beam steering is achieved by exciting different elements in each focal-plane array. Shared Tx-Rx and multibeam operation is supported by exciting more than one element in each focal-plane array at the same time. Alcan systems is another example, realizing a phased array antenna with LC distributed phase shifters underneath of the radiating elements, providing improvements in terms of power consumption, thermal managements and cost with respect to IC-based phased arrays.

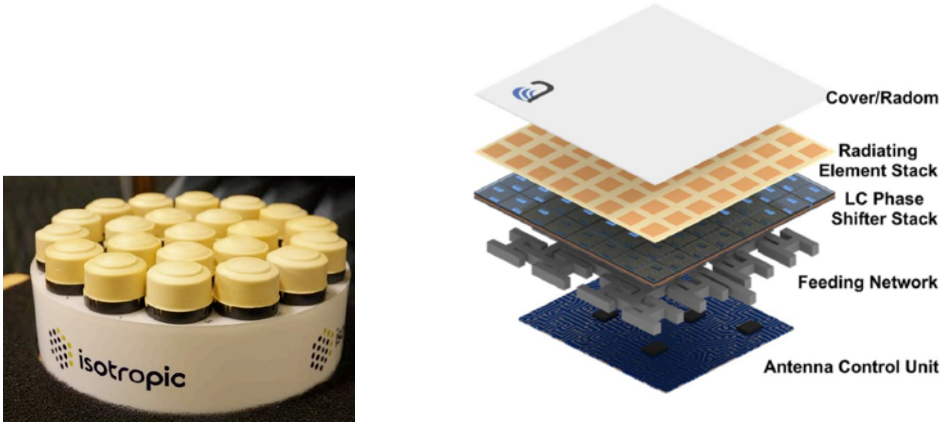

FIGURE 13: HYBRID COMMERCIAL METASURFACE ANTENNAS. LEFT: ALL.SPACE ARRAY OF LENSES; RIGHT: ALCAN SYSTEMS PHASED ARRAY WITH DISTRIBUTED LC PHASE SHIFTERS

3.2.1 Critical analysis of Q/V band solutions

The main requirement imposed by the 6G-NTN considered terminals is to have a maximum size of 20x20cm or even 10cmx10cm for the smaller variant. Fixing the antenna size, the antenna design must ensure a minimum aperture efficiency in order to reach a given antenna gain, which was considered to be 32 dBi (20x20cm case) and 28 dBi (10x10cm case) in D3.5. Figure 14 plots the required aperture efficiency for different antenna sizes at 40 GHz. It can be observed that for a 20cmx20cm aperture, the required gain is achieved even for efficiencies as low as 20%. However, considering that the available size needs to be shared by Tx and Rx apertures, the required efficiency increases to 35%. Moreover, if two beams need to be realized in order to implement make-before-break hand overs, the efficiency becomes as high as 70%. The numbers get worse if the smaller variant of 10cm x 10cm is used as a baseline. In this case, only the use of the full aperture allows efficiencies below 50%, whereas with TX - RX and two beams, the required gain is not realizable. Beam steering antennas at Q band may provide rather low aperture efficiencies below 50% so there is a need to exploit efficiently the available area. It can be done through using the same aperture for both Tx and Rx, or even for dual-beam transmission in each direction. As described before, Kymeta or ALL.Space solutions already support shared Tx/Rx aperture, whereas other examples with leaky wave and array solutions can be found in [30] and references therein. Otherwise, link budgets need to be re-analysed if the available area needs to be shared by Tx and Rx and two beams per direction.

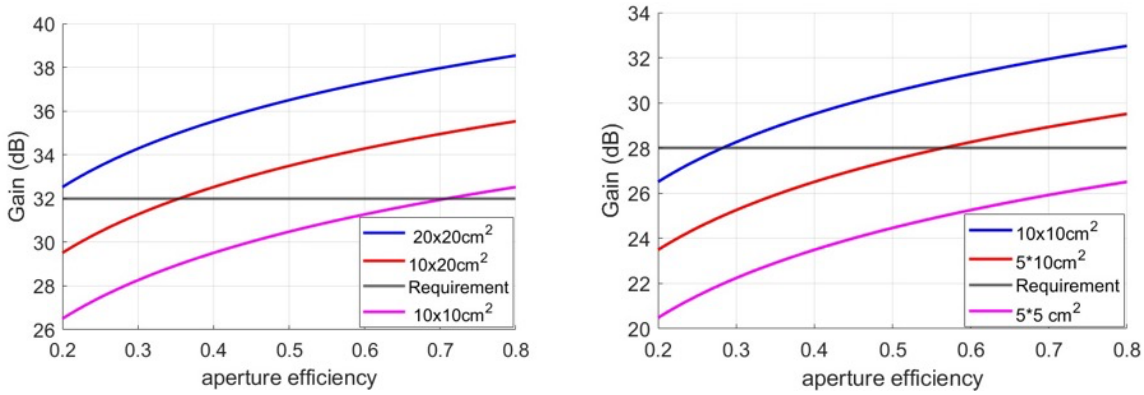

FIGURE 14: REQUIRED APERTURE EFFICIENCIES FOR DIFFERENT ANTENNA SIZES: LEFT 20CMX20CM BASELINE; RIGHT 10CM X10 CM BASELINE [24]

Array solutions provide accurate control on the phase and amplitude of each array element, and so the best radiation pattern control. However, at this technological stage, their implementation at Q/V present almost unaffordable challenges. First, they need to rely on beamformer IC driving multiple elements and performing both amplification and phase-amplitude variation. These IC will most likely be available in the next future when the use of Q/V band for user link is targeted by the market, but right now there is no availability. Therefore, the implementation of array-based antennas is mostly shifted to the development of highly integrated beamformer ICs. In addition, for an array of 20cmx20cm, more than 2000 elements would be required considering a separation between elements slightly larger than half-wavelength, to avoid the appearance of grating lobes. Hence, large feeding networks would represent another issue to deal with.

Bearing this in mind, leaky-wave antennas are identified as a more suitable solution. Besides the low profile, they provide lower costs and low power consumptions at the price of reduced radiation pattern control, since unit cells are fed from travelling waves that do not permit an exact amplitude control. In the case of metasurface antennas, these unit cells typically have subwavelength sizes ranging between λ/6-λ/8 [31]. As a result, a 20cmx20xm aperture would require tens of thousands of reconfigurable unit cells, which may be only feasible considering LC technology as in LCD TV monitors. Fabry-Perot architectures may allow alleviating this issue by using larger unit cells, enabling the use of varactor diodes for reconfigurations, which constitute not only a more mature solution but also provide faster beam-steering reconfiguration.

In conclusion, leaky-wave beam steering antennas based on Fabry-Perot excitation and varactor diodes for beam steering reconfiguration seem to be a priori a suitable solution to be further developed in 6G-NTN. In the long term, the implementation of shared Tx-Rx apertures and dual-beam operation will also be of high interest to make the most efficient use of the available area.

3.3 ANTENNA TECHNOLOGIES FOR C BAND SOLUTIONS

C-band has been traditionally used for satellite broadcast or communications and still have special significance in certain regions due to its lower losses in case of rain and bad weather conditions. In these cases, the considered terminals where VSATS equipped with rather bulky parabolic reflectors. 6G-NTN targets a different use case based on the transmission to/from a vLEO satellite to a handheld terminal or a mobile platform terminal like a drone or a car. Neither antennas for handheld terminals nor antennas for mobile platforms require major advances with respect to state-of-the art solutions, according to the main antenna requirements in terms of gain, bandwidth and frequency of operation. However, on the handheld side, the use of c-band for satellite communications is a new topic that requires further assessment. On the mobile platform side, operational requirements such as the size constraints, the placement location on the platforms and the targeted type of connectivity (only NTN or dual TN-NTN) may introduce new design challenges too. Antenna solutions for the two types of terminals are further discussed next.

3.3.1 Handheld terminals

Integrated antennas in handheld terminals are a mature technology, with flagship smartphones featuring tens of antennas covering different bands and services as sketched in Figure 15, extracted from [32]. Indeed, reference [32] provides a recent comprehensive survey on the topic. In both TN and NTN cases, the antennas evolved from external configurations to internal integrated solutions, being the current trend the integration in the phone metal bezel. In this case, most of the proposed solutions are optimized versions of four basic antenna

configurations: inverted-F antenna (IFA), slot antennas, loop antennas and planar inverted-F antennas (PIFA). The resonant frequencies are controlled by the length of critical design dimensions: the large arm of the F structure in the IFA, the slot length, the loop length or the large dimension of the patch in the PIFA. Due to the limited space available, miniaturization techniques and multiband solutions are used to efficiently cover all required bands.

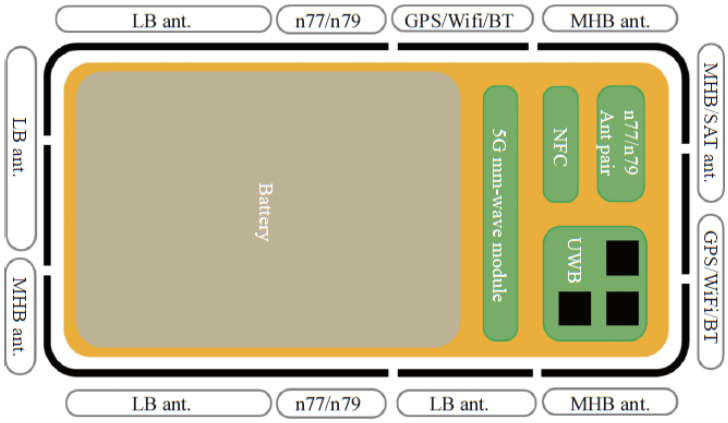

FIGURE 15: INTEGRATED ANTENNAS IN NOWADAYS SMARTPHONES

Focusing on integrated antennas for satellite communications, there is a growing interest in the last 2 or 3 years. Most of the works target L and S band operating ranges, some of them directly addressing 3GPP NTN bands n256 and n255. So far, C-band attracted less researchers though some studies are still available (*e.g.* [33]). Besides, all of them focus on circular polarization (CP), which can be achieved either in broadside or end-fire configurations (see Figure 16).

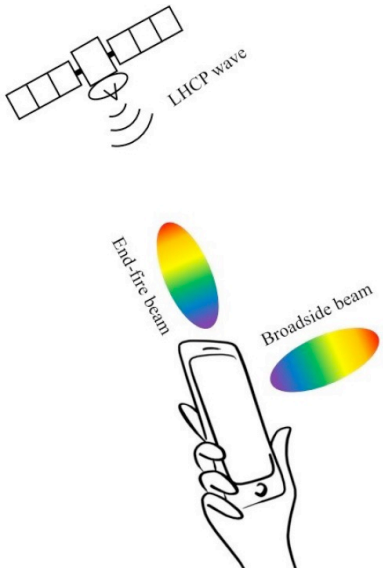

FIGURE 16: BROADSIDE VS END-FIRE CIRCULAR POLARIZATION RADIATION

End-fire seems to be the preferred option according to the typical posture in which users hold their phone [34]. However, it is clear that the antenna performance and so the link budget will depend on the phone position, thus requiring kind of manual pointing of the user towards the satellite. To get rid of this, one alternative would be to deploy multiple satellite antennas with different orientations, thus benefiting from antenna diversity to ensure good antenna properties

despite the phone orientation. This is in line with TN solutions which use multiple antennas in a MIMO configuration. Note however, that due to the aforementioned space constraints and the large number of antennas to be deployed, implementing diversity with NTN antennas will become very challenging, unless a high integration with NTN solutions is realized. In this sense, an open research question is how we can benefit from the fact that TN bands n77 and n78 may overlap with foreseen C-band NTN. One option would be the direct use of n77-n78 antennas for satellite communications. Although they are linearly polarized, part of the depolarization loss can be overcome by the diversity combination of multiple antenna elements.

The solution to realize the circular polarization is the combination of two radiating structures with orthogonal modes. For instance, two dipole elements placed in orthogonal planes benefiting from a foldable phone [35], a magnetic-electric dipole pair [36], a loop and a parasitic branch [34], etc. A wide set of solutions are identified in [32]-[34] and references therein. As introduced before, multiband solutions are also proposed to cover some TN and NTN bands with more integrated structures.

An a priori objective of this analysis was the derivation of achievable performance in terms mainly of antenna gain, which can be used to evaluate link budgets. Unfortunately, it is almost impossible to identify a specific achievable gain value. First , because there is a lack of works addressing the specific bands considered in 6G-NTN project; and second, because different works consider different design requirements in terms of specific NTN band to be covered, additional cellular bands, beamwidths, etc. Table 24 shows the performances obtained by a selected set of designs. Observed peak gains are in the range of 0.9 to 5 dBi, 0.8 dBi for a low S-band design and 4.8dBi for a high S-band with very low Bw. Note that C-band designs may present better performance than S or L bands solutions due to the shorter wavelengths. This is somehow observed for [33], though the larger bandwidth here may impact on the achievable gain. In any case, a range of peak CP gains around 2-4dBi can be envisaged.

TABLE 24: PERFORMANCE OF CP INTEGRATED SATELLITE ANTENNAS

Reference	Center frequency (GHz)	Peak gains (dBi)	beamwidth	Impedance. Bw %	Axial ratio (AR) Bw %
Error! Reference source not found.	3.8	2.42	112º/92º	17.8	3.7
Error! Reference source not found.	2.49	4.8	94º/69º	10	0.76
Error! Reference source not found.	1.985/2.185	0.9/1.92	NA	6.5/3	4.5/5
Error! Reference source not found.	2.49	1.9	143 º /117 º	1.6	1.4

Interestingly, integrated TN antennas covering multiple bands (n77-n79) like [37]-[38] provide linearly polarized gains around 4 dBi, so in the high range of CP designs. Therefore, they still represent a potential solution if diversity is used to overcome depolarization.

Note that the gain figures reported so far correspond to peak gains. For practical conditions, extra miss pointing losses, as discussed before, as well as attenuation due to hand shadowing effects need to be accounted for. Miss pointing loss can be in the order of 3dB if we consider that the user holds the phone in a rather vertical position (in the end-fire case), though larger margins would be required for other assumptions if a proper antenna diversity is not implemented. Hand effects can provide losses in the order of 1-2dB [38]. As a result, a gain range around -3 dB to -1 dB can be envisaged assuming a vertical phone position.

3.3.2 Mobile platform terminals

As introduced before, the set of identified requirements for the mobile platform case, namely a frequency of operation of 3.4 GHz (Rx) and 3.9 GHz (Tx), gain of 0 dBi and bandwidth of 100 MHz (see D3.5), do not require any specific advance over the state-of-the-art. However, depending on the size constraints, the placement location on the platforms and the targeted type of connectivity (only NTN or dual TN-NTN), not so standardized antenna solution would be required. We next discuss three different use cases:

Case 1: Available area for C-band of 20 cm x 20 cm (10 cm x 10 cm) and NTN only connectivity

For this case we consider that the available areas discussed previously for the Q/V band are here available only for C-band. In addition, the antenna, needs to connect only with NTN platforms with a minimum elevation of 40º, as considered in D3.5. In these conditions a simple microstrip patch antenna would satisfy all requirements. It may occupy less than 4 cm x 4 cm and require a ground plane around 13.6 cm x 13. 6 cm. So two elements, one for transmission and the other for reception can be easily deployed for both 20 cm x 20 cm and 10 cm x 10 cm cases. They would provide gains in the range from 5 dBi to 8 dBi and 3dBi to 0dBi at low elevation angle, representing a large improvement on the link budget margin with respect to the requirement of 0 dBi at low elevation angle. They are considered to be placed in a horizontal surface such as the roof of a car, covering the upper half hemisphere with a -3 dB beamwidth around 90º. For the 20 cm x 20 cm case, it may be even possible to include two arrays of 2x2 elements, increasing the gain in 4-5 dB (taking into account implementation losses), but requiring a beam steering solution due to a lower beamwidth. Note that for the 10 cm x 10 cm case, the ground plane size is not an issue, the car rooftop can be used as a ground plane or in the drone case, a reduced ground plane of 10 cm x 10 cm would just imply a slight gain reduction but also would bring a wider beamwidth for a better coverage. In any case, circular polarization can be easily used by exciting two ports with 90º phase difference or by cutting diagonal corners or slits in each patch. A review of compact microstrip patches can be found in [41].

Case 2: Available area shared with Q/V band of 20 cm x 20 cm (10 cm x 10 cm) and NTN only connectivity

In this case, we consider that the available areas for deploying the antennas need to be shared by both Q/V and C- band solutions, providing dual-connectivity. Since the analysis of Q/V band solutions revealed that there is a need of fully using the whole available area, the only suitable solution here is to consider multi-functional shared aperture solutions. They represent a research goal that further requires advancements beyond the state-of-the-art. A recent review of multifunctional apertures was provided in [30]. They are of special relevance the included references on dual-frequency shared apertures with high frequency ratios. Some basic solutions are based on using a large structure acting both as a patch for the lower band and as a support for the radiating elements at the higher band like a slot array [40] or a partially reflecting surface forming part of a Fabry-Perot cavity [42]. Interestingly, there are different references proposing solutions including Fabry-Perot cavities, which can be more straightforward used to combine the target C-Band with the already identified Q/V band solution. Note however, that keeping large aperture efficiencies with beam steering functionality at Q/V band and at the same time sharing the aperture with a large C-band patch becomes a research challenge.

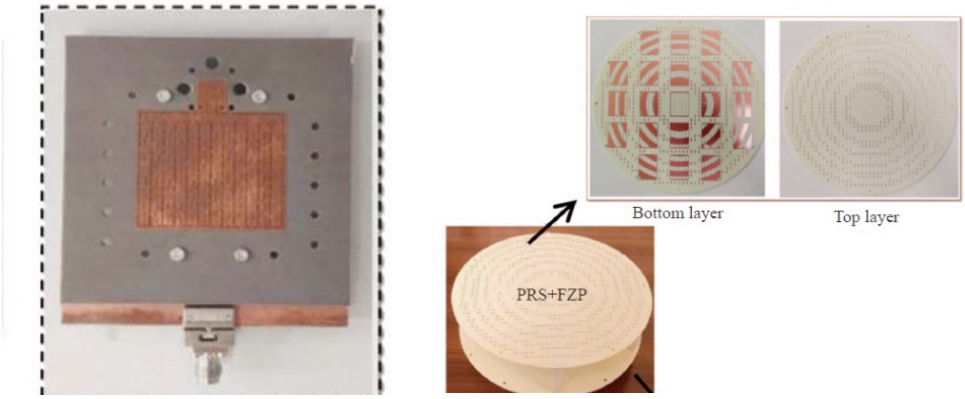

FIGURE 17: EXAMPLES OF MM-WAVE/SUB 6GHZ DUAL FREQUENCY SHARED APERTURES

In the case of terminals in cars, a potential alternative to shared aperture antennas is to co-locate the C-Band antenna with the antennas of other systems (e.g., Global Positionning System (GPS), frequency/amplitude modulation (FM/AM) radio), which usually are all integrated in a shark fin radome (e.g., Figure 18). The option here would be to resort to miniaturized patch solutions or dielectric-loaded helical antenna [43] with a low number of turns [44]. The compatibility with the other antennas within the radome would again represent a research challenge.

FIGURE 18: SHARK FIN ANTENNA SYSTEM

Case 3: Dual NTN-TN connectivity

In the case of dual NTN-TN connectivity, the antenna not only needs to point towards the sky supporting a minimum elevation of 40º, but also needs to be able to connect to terrestrial infrastructure. If simultaneous dual-connectivity is targeted, quasi omni-directional patterns are required, which result in reduced directivities and gains, thus not providing link budget margin improvements with respect to the specified 0 dBi gain antennas. For cars, monopole-like structures would permit covering the required half hemisphere while drones need to rely on dipole-like solutions to cover upper and lower hemispheres. Note that both monopoles and dipoles have radiation nulls in their main axis, so using architectures with slanted 45º crossed dipoles would avoid placing a radiation null towards 90 º elevation and at the same time, providing some polarization diversity.

If sequential dual-connectivity is targeted, pattern reconfigurable antennas can be envisaged. For instance, for cars, microstrip patches capable of switching from patch-like to monopole-like patterns can be of interest (e.g. [45]). Note however, that pattern reconfiguration may include some extra losses due to reconfiguration mechanisms, and need to be combined with the size constraints discussed in the previous two points, becoming another open research challenge.

In conclusion, for C-Band, suitable antenna architectures depend on the considered use case. Three open research challenges have been identified: (i) dual frequency Q/V- C-band shared apertures; (ii) Integration of C-band antennas (e.g. patch or helix) in shark fin radomes for cars; and (iii) reconfigurable pattern solutions combined with dual-frequency shared aperture solutions.

4 ANTENNA INVESTIGATION

4.1 INTRODUCTION

The continuous advancement of digitization and technology, including wireless communications and service infrastructure, is reshaping every sector of our economy and society. Expectations are high for 6G to supersede 5G-Advance (5G-A) and usher in a new era of enhanced connectivity, pushing the boundaries of communication networks even further [46].

NTN is expected to play a key role in many applications of 6G [47], facilitating further enhancement of connectivity in rural areas. This is fuelling the need for cutting-edge components for NTNs that can deliver high throughput and low latency services seamlessly integrating with future 6G terrestrial telecommunication networks. These components are expected to enhance system capacity, flexibility, and adaptability to address uncertainties and market changes while also improving system availability, scalability, and resilience. Moreover, they aim to reduce costs and energy consumption [48].

High throughput, increased coverage, and ecological trends require designing a low SWaP-C (size, weight, power and cost) components of mobile network like electronically steerable antenna (such as dynamic Metasurface (MTS) antenna-DMA), reflectarray/ transmitarray antennas and reconfigurable intelligent surfaces (RIS)[49]-[52], operating in the new spectrum of the mmWave bands, namely Q-band (37.5 GHz to 42.5 GHz) for receive signals (Rx) and V-band (47.2 GHz to 50.2 GHz) for transmit signals (Tx).

A promising solution for a low-cost and low power consumption DMA antenna is the antenna based on leaky cavity concept [53], [54].

This antenna relies on wave control inside a cavity rather than wave emission from the antenna array. The antenna beamformer control is performed inside the cavity and doesn't require calculation of complex distribution of phase/amplitude weights, as it happens in phases array antenna technology. Antenna cavity beamformer is fed from a single RF input. Hence, it becomes standard and protocol agnostic, and can be compatible with any back-end, and is easily scalable to the required frequency band.

The beamforming of the antenna does not result from the synchronization of many elementary sources such as in phased-array, but rather from the shaping of a wavefield inside a cavity. That is, the same antenna can work for 5G mmWaves or Ka-band satellite communications without the need to adapt the radiating elements or the feeding. Moreover, it doesn't require the phase-shifting elements, individual amplifiers, and hence complex and expensive electronics. The beamforming is realized in a passive way (the Metasurface is direct current (DC) active but RF passive). The antenna consumes very little energy to beamform.

Compared to phased arrays, this design approach is much more energy efficient since there are no dissipative circuits or materials to guide the waves, and it can switch beams at the speed of electronics just like active phased arrays. Furthermore, the cavity of the antenna can be made of any shape, meaning that the antenna is perfectly conformable to the surface of an object (vehicle, drone, plane). The Metasurface resembles the main part of the DMA leaky cavity antenna and RIS. The technology requires low dissipation in reflection and independent control of the reflected phase for both vertical and horizontal polarizations. The control of the reflected phase is provided by the switching element. In this deliverable, we introduce the

design of the Metasurface for Q- and V-bands exhibiting low dissipation and providing the binary control of the phase of the reflected wave for two polarisations.

4.2 OBJECTIVE

Table 25 summarizes the KPI's characterization of Q and V band Antenna System for future 6G NTN systems.

TABLE 25: THE KPI'S SPECIFICATION OF THE QV BAND ANTENNA SYSTEM

		Q-Rx size 20cm x 20cm	V-Tx size 20cm x 20cm
Frequency Range		37.5-42.5 GHz	47.2-50.2 GHz
Beamformer dimension		20cm x 20cmx 3cm ~27x27λ @ 40 GHz	20cm x 20cmx 3cm ~33 x 33 λ @ 50 GHz
Total Efficiency		-14 dB	-14 dB
Gain (Elev 90°)		25.5 dBi	27 dBi
EIRP with BUC 10 Watt		N/A	27 + BUC power i.e. 30 dBW @ 2W BUC
G/T with LNB noise figure of 1.5 dB		~5 dB/K at 90° Elev target: -0.5 dB/K @ 2dB LNB NoiseFigure best: +1 dB/K	N/A
Bandwidth	**Total**	5 GHz	3 GHz
	Instantaneous (from 0°-60°)	150 MHz	150 MHz
Side Lobe Level		First sidelobe -15 dB typical	First sidelobe -15 dB typical
Scan Angle		ScanLoss (power cos): target: TBD ±70°, 1.4 ±50° best: 1@ ±50	ScanLoss (power cos): target: TBD ±70°, 1.4 ±50° best: 1@ ±50

4.3 ANTENNA COMPONENTS

The full antenna system consists of four main components:

1. Metasurface

2. Antenna Feeder System
3. Antenna Mask
4. Antenna Cavity

4.3.1 Metasurface

The concept of the Metasurface is based on the original design, proposed in [8]. As illustrated by Figure 19, the design can be broken down into three separate parts: a microstrip patch resonator (outlined in a red rectangle), a parasitic resonator (outlined in a green rectangle) and the interconnection region with the active switching component (outlined in a blue rectangle). The phase shift for each pixel of the MTS is controlled by the coupling between the patch and the parasitic element. The resonance frequencies of patch and parasitic elements are defined correspondingly by their electrical length (proportional to physical size) and initially tuned to lie close to each other. The resonance frequency of the parasitic element is fine-tuned by its length. Due to the coupling of the closely positioned resonance frequencies, the resonance frequency of the patch resonator depends on and is affected by the resonance of the parasitic element.

To control the operating states of the 1-bit reconfigurable MTS, the parasitic element and the patch are connected through a low-cost active switching component. This component operating as a switch has two states, ON-state and OFF-state. It either allows the current to pass through or isolates its passage, essentially making an electrical connection between the patch and the parasitic or isolating the two. In the general case, different components can be used as active switching element such as PIN diode, micro-electro-mechanical systems (MEMS), photo-diode, VO2, liquid crystal or any other active component which has a switching functionality, meaning it can be put in a conductive or isolating state, ON and OFF state respectively. The selection of the element is dictated by the cost, switching speed, power handling, dissipation, and other requirements. In case of the binary 1-bit control, we deal with OFF and ON states only of the switching component. In the OFF state, the switching component is opened and the phase of the pixel will only be that of the resonating patch. In the ON state the switch is closed and the phase of the pixel will change due to the introduction of the parasitic element of a certain electrical length. During the design process, we are aiming to maximize the reflecting property of the MTS i.e., providing the maximum amplitude of the reflected wave in both states. Perfect binary MTS should provide 0 dB reflection loss, and the 180° phase shift between the two operating states.

The proposed design ensures the necessary amplitude levels and phase shifts for both TE (horizontal) and TM (vertical) polarizations. As the operational mechanism remains identical for each polarization, the pixel was initially developed to function solely in one polarization. Subsequently, the parasitic element and the active switching component were mirrored along the diagonal axis of the pixel, and optimized to accommodate both polarizations. The subsequent optimization of the design is necessary to minimize the cross-polarization effect, when reflected wave partially converted to the orthogonal polarization. For this reason the patch have truncated corners (see Fig. 19). This also prevents direct shorting to ground via contact with grounding vias. To provide efficient control of the reflected wave and avoid the appearance of the grating lobes, the density of the elements at the Metasurface should not overcome half of the operating wavelength. The size of the designed pixel is 0.5λ × 0.5λ. The pixel was designed using a low-loss substrate, METEROWAVE 8300 from AGC εr = 3, tan δ = 0.0025). The rest of the substrate layers are placed behind the radiofrequency ground and can be fabricated with a conventional FR-4 substrate. The 3D electromagnetic model with floquet boundary conditions was simulated and optimized using a Frequency Domain solver in

CST Studio Suite software. The main challenge of the pixel design is to provide a low cost layout suitable for a conventional PCB manufacturing technology.

4.3.1.1 Design and Schematic of the V-Tx Metasurface

1. The designed unit cell consists of 3 main important elements which could generate the response mentioned in the objectives:
    I. Patch – Main radiating element
    II. Parasitic element – helps generate the phase shift between the two states
    III. Diode – To switch between the two states
2. The phase shift between the two pixel states is obtained by introducing a longer electrical length element, a parasitic element, in the ON state.
3. The parasitic element is shorted directly to a GND via.
4. The main reflector patch, couples to a coupler which is connected to the complementary metal-oxide semiconductor (CMOS) footprint and the parasitic element. The length of the coupler can be adjusted to either increase or decrease the coupling strength.
5. The main reflector patch also has truncated corners, this is done for 2 reasons. Firstly, to make sure that the patch doesn't short directly to ground by touching the vias and second, is to reduce cross coupling.
6. Each switch has 4 GND vias and 1 enable via. The two switches share 1 GND via to save space on the unit cell.
7. Bigger vias were used to reduce the cost per pixel.
8. The detailed dimensions of the whole structure vary depending on the desired frequency band. It will be presented in the following sections.
9. Parameter details:
    I. Substrate heigh = 0.5 mm
    II. Via diameter = 0.25 mm
    III. Via pad diameter = 0.5 mm

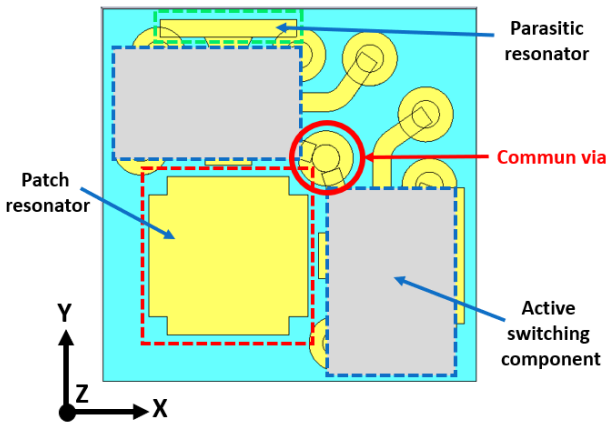

FIGURE 19: DESIGN OF A SINGLE UNIT CELL DIVIDED INTO THREE PARTS, PATCH RESONATOR (RED), PARASITIC RESONATOR (GREEN) AND ACTIVE SWITCHING COMPONENT (BLUE)

4.3.1.2 Simulation Result of V-Tx Unit cell

During the design of a dual polarized pixel, the switch is mirrored with respect to the center of the patch to keep the symmetry for each polarization. During the mirroring process two of the via pads, highlighted in Fig 19 (red circle), overlap. Since it wouldn't be feasible to fabricate a design with two vias so close to each other, the design had to be modified to include only one common via.

RESULTS – DISSIPATION AND PHASE DIFFERENCE

CO-POL Dissipation level (S11 Vs Frequency) – 47.2 to 50.2 GHZ: The highest dissipation level is -2.9dB seen at 50.2GHz as shown in Figure 19.

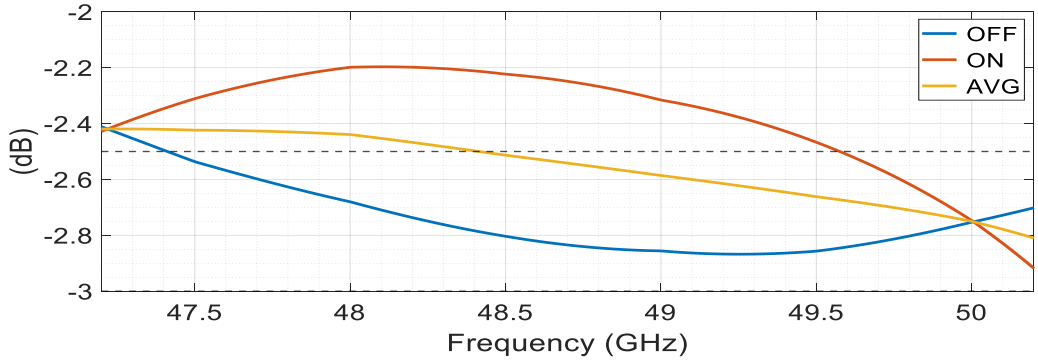

FIGURE 19: SIMULATED REFLECTION COEFFICIENT VERSUS FREQUENCY. THE HIGHEST DISSIPATION LEVEL IS -3 DB SEEN AT 50.2 GHZ.

CO-POL Phase difference level – 47.2 to 50.2 GHZ: The phase difference is over 160° across the band as illustrated in Figure 20.

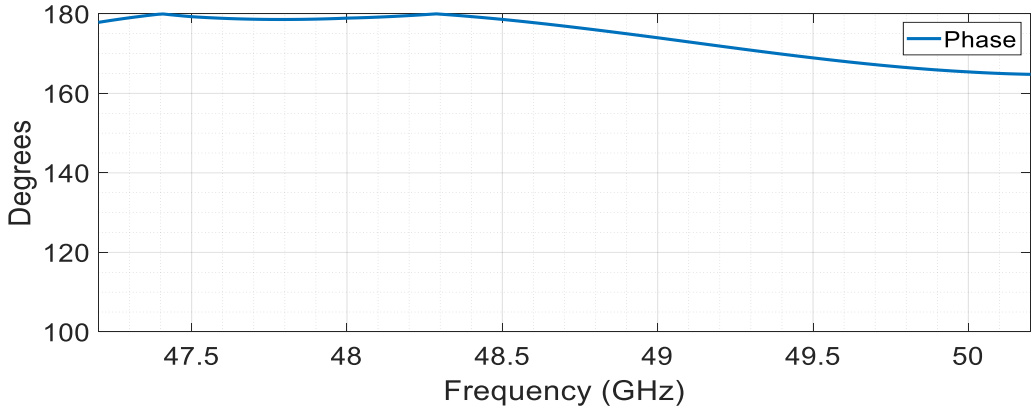

FIGURE 20 SIMULATED PHASE DIFFERENCE VERSUS FREQUENCY ACROSS THE FREQUENCY BAND OF INTEREST

Same curve within extended frequency band allow to clearly analyse the antenna total bandwidth. Also more precise analysis of the resonance behaviour is possible when resonances are plot within large frequency band.

CO-POL Dissipation level (S11 Vs Frequency) – 40 to 56 GHZ: The highest dissipation level is -2.9dB seen at 50.2GHz for the band 47.2 to 50.2 dB (see Figure 21).

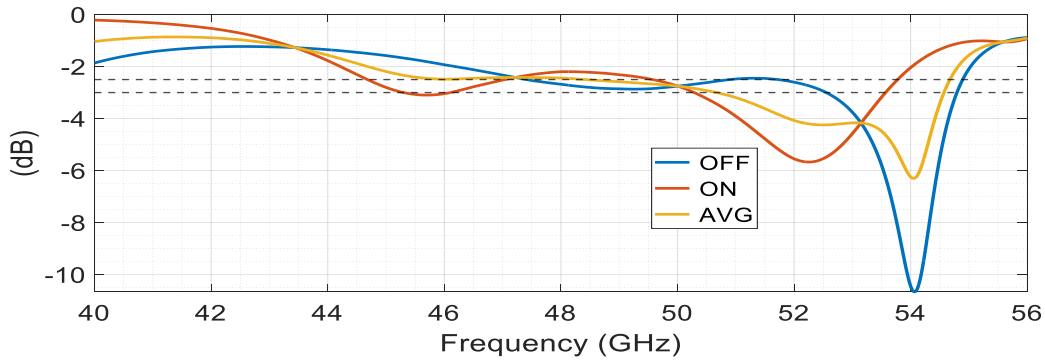

FIGURE 21: DISSIPATION VERSUS. FREQUENCY FOR WIDE FREQUENCY RANGE

CO-POL Phase difference level – 40 to 56 GHZ: The phase difference is over 160° across the band 47.2 to 50.2 dB, as reported in Figure 22.

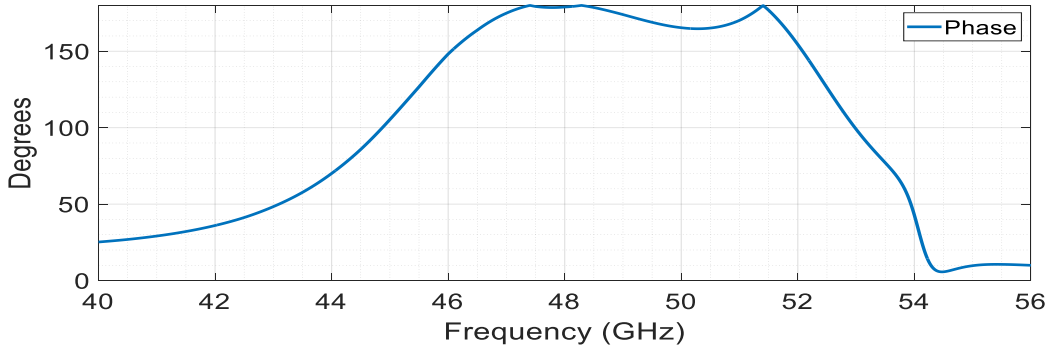

FIGURE 22: PHASE DIFFERENCE VERSUS FREQUENCY

Cross-POL Dissipation level (S11 Vs Frequency) – 40 to 56 GHZ: as shown in Figure 23, the X-pol levels in most of the frequency range is below -10 dB across the band 47.2 to 50.2 dB.

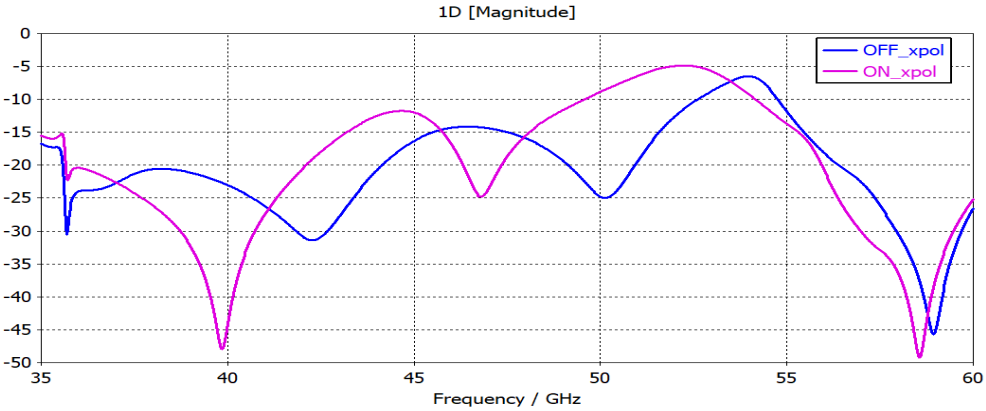

FIGURE 23: SIMULATED CROSS POLARIZATION DISSIPATION VERSUS FREQUENCY

The simulation results show better than −3 dB and more than 160◦ phase difference in the band of interest (47.2− 50.2 GHz). The average dissipation is above −2.6 dB in the middle of the operational band.

4.3.1.3 Design and Schematic of the Q-Rx Unit Cell

Based on the V-Tx pixel design presented in the previous sections, the unit cell was modified (patch and resonators size, distance between the patch, the resonators and the switch, vias placement...) in order to meet the specifications of the Q-Rx antenna

4.3.1.4 Simulation Result of Q-Rx Unit cell

CO-POL Dissipation level (S11 Vs Frequency) – 37.5 to 42.5 GHZ: The highest dissipation level is -2.5dB seen at 38 GHz, as illustrated in Figure 24.

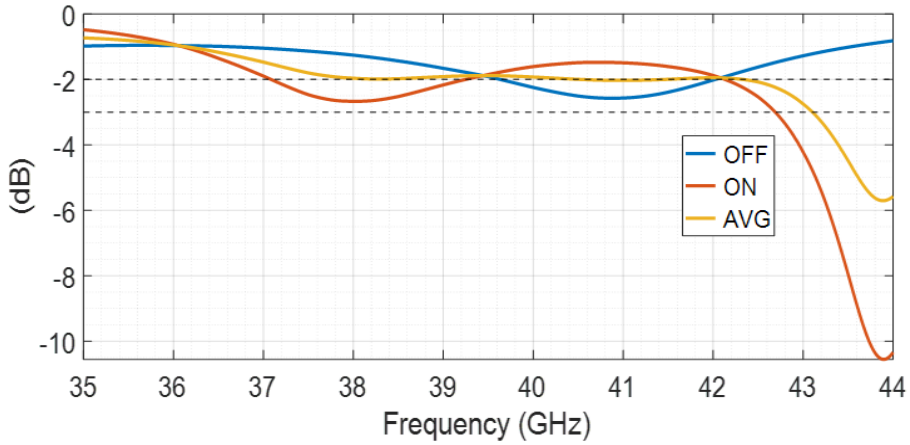

FIGURE 24: SIMULATED REFLECTION COEFFICIENT VERSUS FREQUENCY

CO-POL Phase difference level – 37.5 to 42.5 GHZ: The phase difference is over 140° across the band (Figure 25).

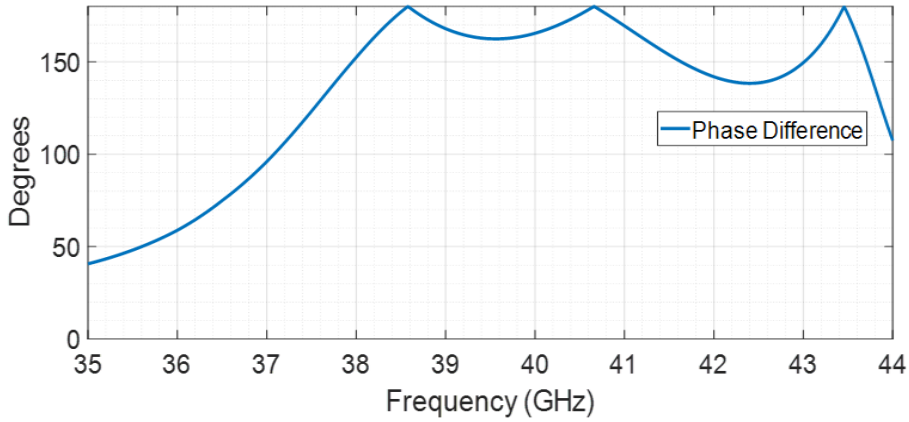

FIGURE 25: SIMULATED PHASE DIFFERENCE VERSUS FREQUENCY ACROSS THE FREQUENCY BAND OF INTEREST

Cross-POL Dissipation level (S11 Vs Frequency) – 37.5 to 42.5 GHZ : The X-pol levels for over the all the frequency band is below -20 dB, as shown in Figure 26. It meets the project KPI's Specification of below -15 dB.

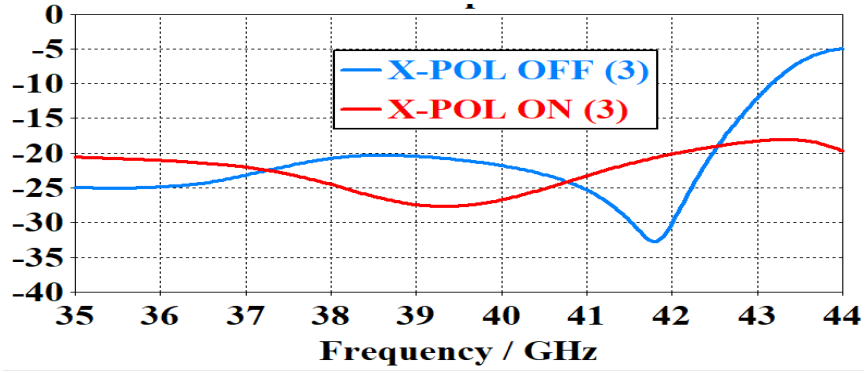

FIGURE 26: SIMULATED CROSS POLARIZATION DISSIPATION VERSUS FREQUENCY

The simulation results show better than −2.5 dB and more than 140◦ phase difference in the band of interest (37.5− 42.5 GHz). The average dissipation is above −2 dB in the middle of the operational band.

METASURFACE AND MINI-METASURFACE LAYOUT DESIGN

In a standard MTS, one shift register controls 4 pixels. However, due to the small dimension of the unit cell in the Q/V band (3.4mm), placing the pixels in their standard layout orientation would result in the enable vias going directly through the shift register on the other side of the PCB. To prevent that, an alternative layout option was proposed, see Figure 27. In this orientation, the distance between the patches is uneven. In this case, the periodic pattern contains 4 pixels rather than one pixel, but the same control as standard MTS is used in this case (one shift register for 4 pixels). Despite the non-periodic pixel arrangement and symmetry violation, the technology of the antenna allows to compensate all the possible negative effects of the non-uniform arrangement of the antenna unit cells. Below the optimization procedure is described which is normally used to generate the proper beamforming configuration of the metasurface inside the antenna.

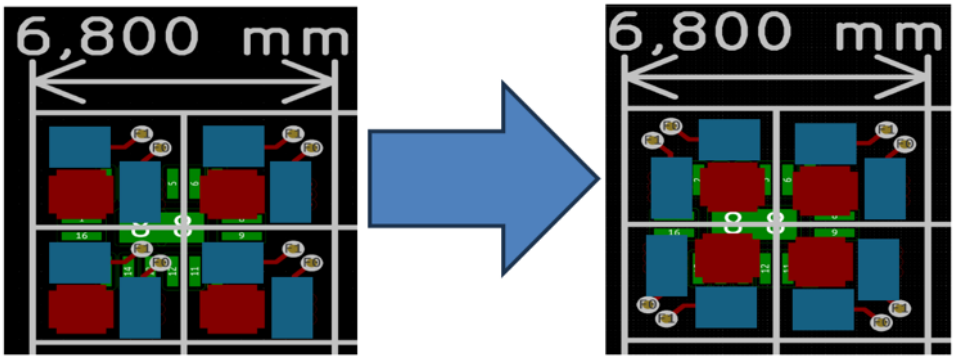

FIGURE 27: LAYOUT DESIGN OF THE PIXEL DESIGN

METASURFACE CONTROL AND ANTENNA OPTIMIZATION

The procedure of antenna optimization is based on metasurface control. Through the process, several configurations are applied to the metasurface, this means that a certain pattern of On and Off state is applied to each switching elements (diodes or switches) of the MTS.

Each one of these metasurface configuration results in a specific antenna behaviour (gain, radiation pattern, scan loss). The optimization algorithm is then run considering different MTS configurations (for different values of angle of incidence) and the best MTS configuration corresponding to the best optimization result is then considered. The goal of the algorithm is to find the best configuraton of the metasurface which provides the best antenna gain at the given direction at given frequency. Each final configuration of the metasurface inside the cavity leads to establishment of the specific cavity mode. This mode is optimal for the best antenna response and takes into account all the features of the cavity, including pixels shapes, position, cavity dimensions, antenna feeder dimensions and position etc. That is given technology doesn't need to have a proper homogeneous and known distribution of the antenna elements. The antenna optimization (or calibration) procedure already takes into account all the features of the particular given metasurface and cavity.

4.3.1.5 Bistatic Measurement Setup and Results

Before fabricating the complete Metasurface, we employ a Mini-Metasurface for preliminary validation. This ensures that we assess key design parameters such as dissipation level, phase difference, and resonance frequency alignment with simulation results. The Mini-Metasurface comprises a 6x6 unit cell configuration (see Figure 29). To characterize this Mini-Metasurface, we use a Bistatic measurement setup that has essential components, shown in Figure 28. This setup includes the Mini-Metasurface itself, two horn antennas for transmitting and receiving electromagnetic waves, various holders for holding different components, a dielectric lens for focusing, a Vector Network Analyzer (VNA) for precise measurements, and a power supply to control the ON/OFF states of CMOS-based switches. In case of the mini-metasurface, the states of all pixels polarized in same direction is changed simultaneously, providing uniform phase pattern for given vertical or horizontal polarization of the mini-metasurface. Totally 4 measured states are possible (vertically polarized pixels ON/OFF and horizontally-polarized pixels ON/OFF stated).

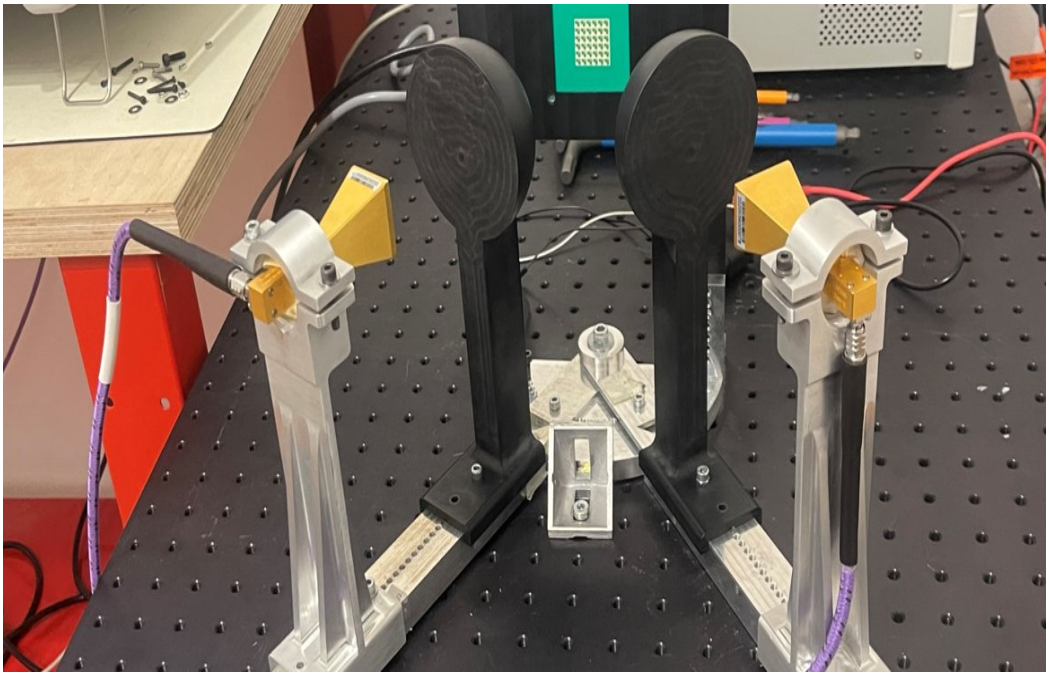

FIGURE 28: BISTATIC MEASUREMENT SETUP

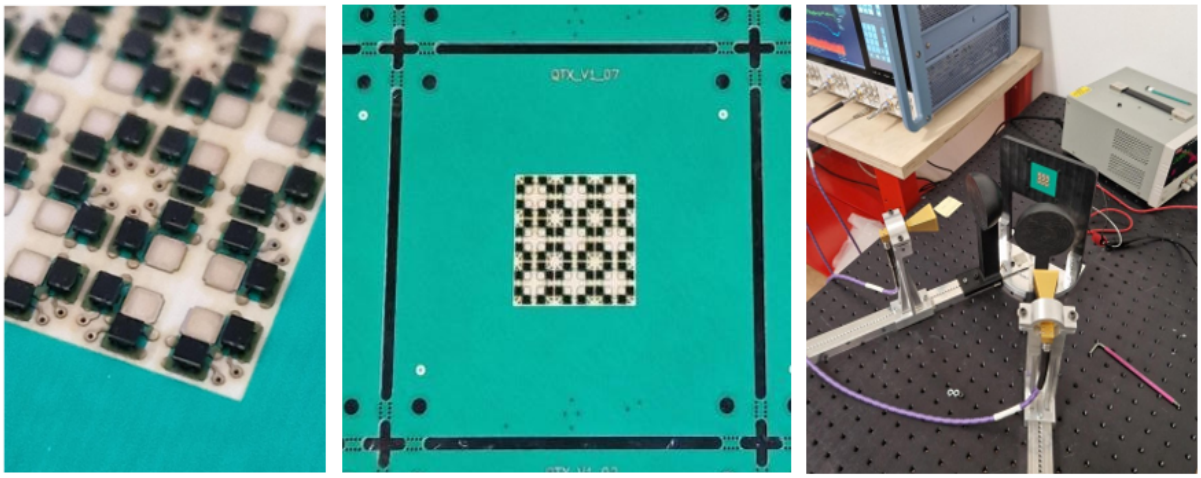

FIGURE 29: 6X6 MINI-METASURFACE

4.3.1.6 Results – Dissipation and Phase Difference (TE/TM polarizations):

In Fig. 31, we present measurement results for the previously presented pixel at VTx band. Since transmitting and receiving antennas are placed at a final distance from each other, there is some angle imposed to incident/ reflected wave. Given measurements were conducted with an incidence wave at 20°relatively to the MTS surface.

In order to minimize the noise during the measurements, time gating has been performed.

Since every pixel has two diodes and each diode interacts with one of the polarizations (TE/TM), The switch corresponding to the desired polarizations is then turned On and Off in order to have both MTS behaviors (presented by TE_ON/TE_OFF and TM_ON/TM_OFF in figures below). Here 'TE' means that the electrical component of the incident field is polarized parallel to the MTS surface, and TM means that the magnetic component of the incident field

is polarized parallel to the MTS surface. In both cases angle of incidence/reflection is fixed to 20 degrees.

We see from figure 31(a) that dissipation level in the operational frequency band lies in the range -7.5 to -5 dB. Ideal value of dissipation should be 0 dB, indicating that all the energy has been reflected without loss.

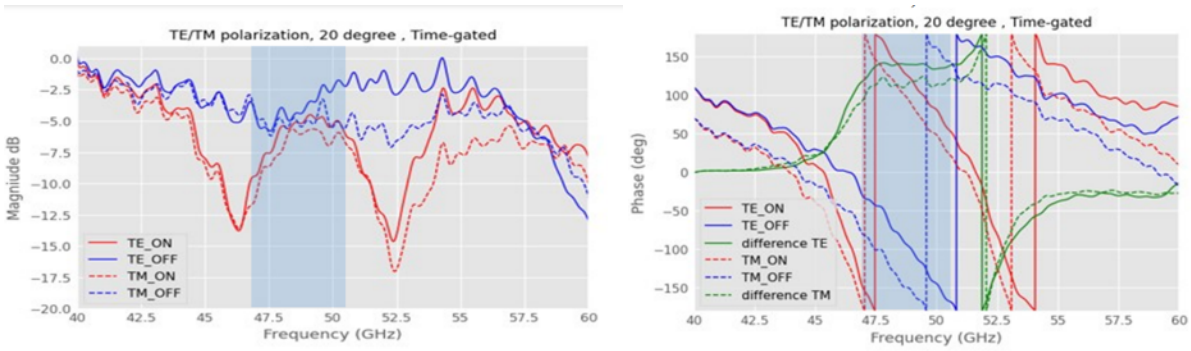

(a) dissipation levels

(b) phase response

FIGURE 30: MEASURED RESULTS OF THE DESIGNED SAMPLE AT 20◦ ANGLE OF WAVE INCIDENCE Θ0 FOR THE TE & TM POLARIZATION OF THE INCIDENT WAVE: (A) DISSIPATION LEVELS AND (B) PHASE RESPONSE

4.3.1.7 Conclusion

Overall, the proposed design along with the fabricated and measured samples, demonstrates an acceptable dissipation level and good phase difference between two states for two orthogonal polarizations of the incident wave. The selected Mini-Metasurface will be used for the fabrication of the full size Metasurface to be used in the leaky wave antenna technology for the proof-of-concept demonstration of the antenna operating at Q/V bands.

4.3.2 Antenna Feeder System: Simulation

The designed antenna feeder system has two subsystems:

1. H-plane splitter.
2. Radiating unit-cell (Tx and Rx).

4.3.2.1 H-Plane Splitter

The H-plane splitter is used to initially split the energy between to branches of the feeding system (Figure 31). The two branches of the feeding system are split into two and then four additional branches. Each one of these branches (16 in total) is ended by a radiating unit cell that illuminates uniformly (ideally) the metasurface.

The splitter consists of three λ/4 matching sections. The cutoff frequency of the waveguide (WG) is 31.3336 GHz. The band of interest for this project is from 37.5 GHz to 50.2 GHz. The subsystem is simulated, and its results are reported in Figure 32. A reflection coefficient that is lower than -35 dB over the whole band of interest is noticed. This ensures a very stable operation and results in a semi-transparent subsystem.

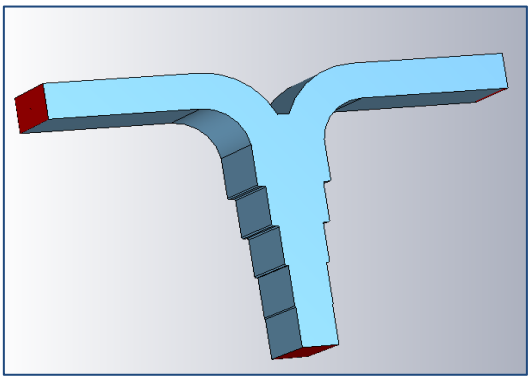

FIGURE 31: H-PLANE SPLITTER WITH THREE Λ/4 MATCHING SECTIONS.

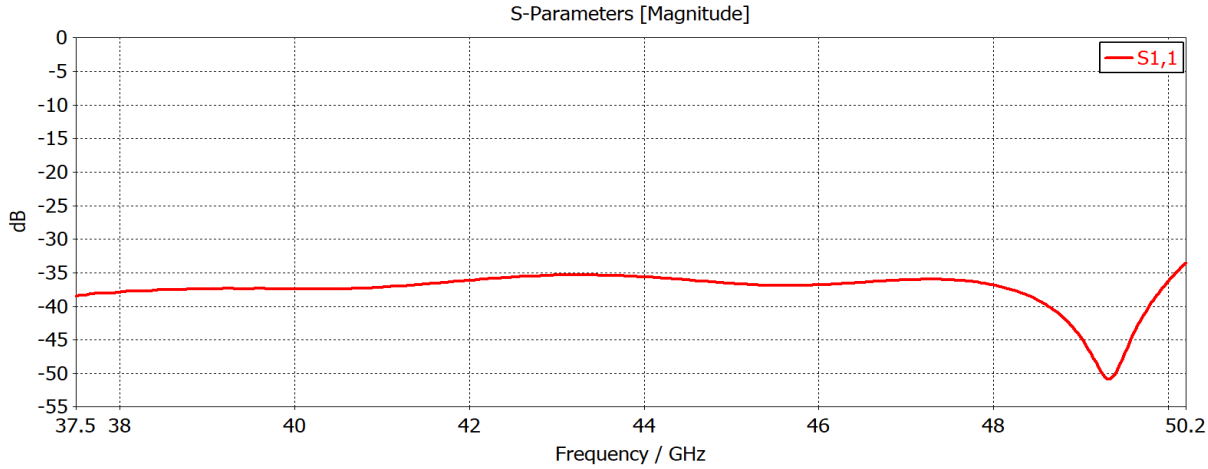

FIGURE 32: SIMULATED REFLECTION COEFFICIENT OF H-PLANE SPLITTER. A REFLECTION COEFFICIENT THAT IS LOWER THAN -35 DB OVER THE WHOLE BAND OF INTEREST IS NOTICED.

4.3.2.2 Radiating Unit-Cell

This section presents the radiating unit cell (subsystem) design and simulation results. Figure 33. shows images of the subsystem. Two radiating unit cells were designed, one for the RX antenna and the other for the TX antenna. The RX subsystem is matched using four λ/4 sections, The TX subsystem is matched using three λ/4 sections, A 6 mm aperture was considered for both systems. The radiating unit cell can also be referred to as a discrete source (DS).

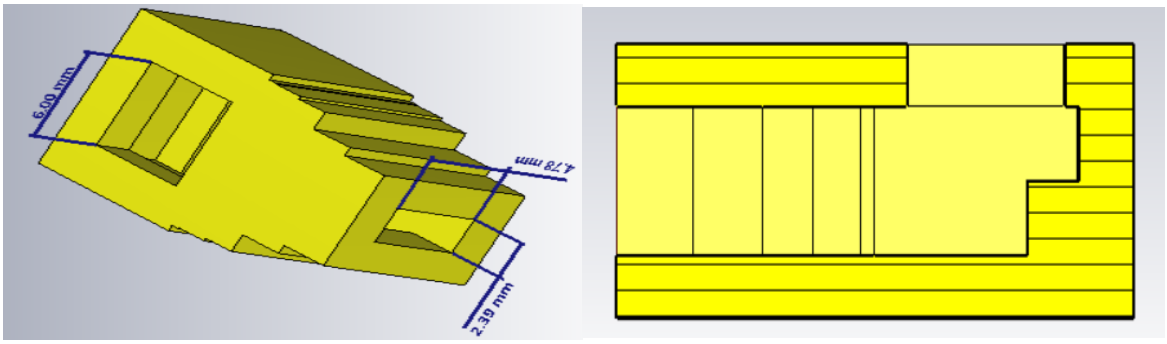

FIGURE 33: RX DS SHOWING WG AND APERTURE DIMENSIONS CROSS-SECTION (FOUR Λ/4 MATCHING SECTIONS ARE CONSIDERED

1. RX Q BAND (37.5-42.5 GHZ)

The RX band of interest is from 37.5 GHz to 42.5 GHz. The reflection coefficient of the RX element is lower than -27.5 dB, over the band of interest as shown in Figure 34.

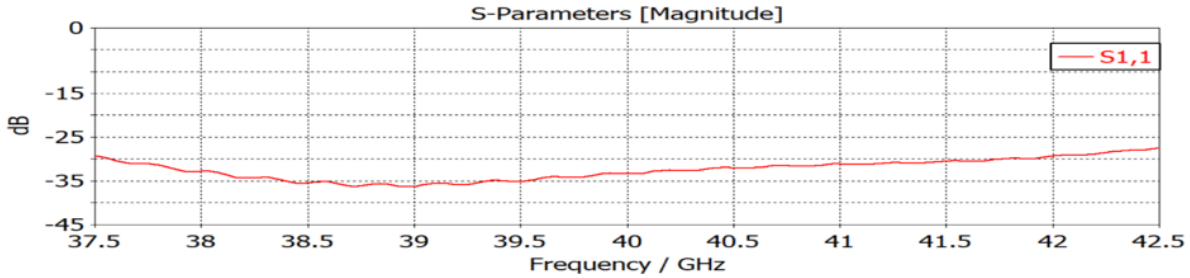

FIGURE 34: SIMULATED REFLECTION COEFFICIENT OF RX DS. A REFLECTION COEFFICIENT OF LOWER THAN -27.5 DB, OVER THE BAND OF INTEREST IS NOTICED.

2. TX V BAND (47.2-50.2 GHZ)

The TX band of interest is 47.2 GHz to 50.2 GHz. For the TX, the reflection coefficient is lower than -28.5 dB over the band of interest as shown in Figure 35.

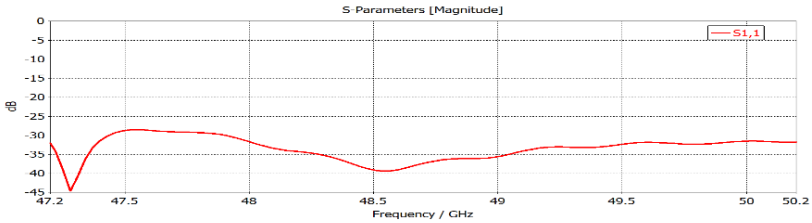

FIGURE 35: SIMULATED REFLECTION COEFFICIENT OF TX DS. A REFLECTION COEFFICIENT OF LOWER THAN -28.5 DB, OVER THE BAND OF INTEREST IS NOTICED.

4.3.2.3 KPIs

Leakage translates how much field or power is leaking from the feeder's sources directly to the direction of the antenna aperture without any interaction with the metasurface. Leakage KPI is computed using the following equation:

$$Leakage\ KPI\ (\%) = \frac{|E_{Aperture}|^2}{|E_{Aperture}|^2 + |E_{MTS}|^2} \times 100\% \qquad (1)$$

Where $|E_{Aperture}|$ is the magnitude of the E-field at the aperture level and $|E_{MTS}|$ is the magnitude of the E-field at the metasurface (MTS) level. To compute the leakage KPI's, we considered 2 cases where the distances from the aperture or MTS to the DS is either 3 mm or 3 cm (see Figure 37c).

4.3.2.4 RX KPIs

The KPIs are calculated for the following frequencies: 37.5 GHz (minimum), 40.5 GHz and 42.5 GHz (maximum). Results are reported in Table 26 where d_stp is the distance from the aperture or MTS to the DS.

TABLE 26: RX LEAKAGE KPIS FOR DIFFERENT FREQUENCIES AND D_STP

Frequency [GHz]	37.5	38.5	39.5	40.5	41.5	42.5
Leakage KPI [%] (1) [3 mm spacing]	10.1	9.85	9.52	9.24	8.9	8.59
Leakage KPI [%] (2) [3 mm spacng]	1.25	1.18	1.1	1.03	0.94	0.87
Leakage KPI [%] (1) [3 cm spacng]	12.3	11.8	11.4	10.94	10.38	9.96
Leakage KPI [%] (2) [3 cm spacng]	1.91	1.76	1.63	1.49	1.33	1.21

The smaller the leakage KPIs, the better the antenna behaves. Having very small leakage KPI means that most of the radiated power is focused on the MTS and so, controlled and shaped by the MTS. Controlling the maximum radiated wave by the feeder enhances the overall behaviour of the antenna.

4.3.2.5 TX KPIs

The KPIs are calculated for the following frequencies: 47.2 GHz (minimum), 49.2 GHz and 50.2 GHz (maximum). Results are reported in Table 27 where d_stp is the distance from the aperture or MTS to the DS.

TABLE 27: TX LEAKAGE KPIS FOR DIFFERENT FREQUENCIES AND D_STP

Frequency [GHz]	47.2	49.2	50.2
Leakage KPI [%] (1) [d_stp=3 mm]	7.53	6.37	6.10
Leakage KPI [%] (2) [d_stp=3 mm]	0.66	0.46	0.42
Leakage KPI [%] (1) [d_stp=3 cm]	7.46	7.13	7.37
Leakage KPI [%] (2) [d_stp=3 cm]	0.65	0.59	0.63

4.3.2.6 Full Antenna Feeder System

The two antenna feeder systems designed and analysed are:

1. Rx antenna feeding system (37.5-42.5 GHz)
2. Tx antenna feeding system (47.2-50.2 GHz)

4.3.2.7 Tx antenna feeding system (47.2-50.2 GHz)

Figure 36 shows the Tx Antenna Feeder System, The cavity measures (210 mm × 210 mm × 43.78 mm). The Return loss of the feeding system is shown in Figure 37. A reflection coefficient that is lower than -20 dB over the whole band of interest is noticed.

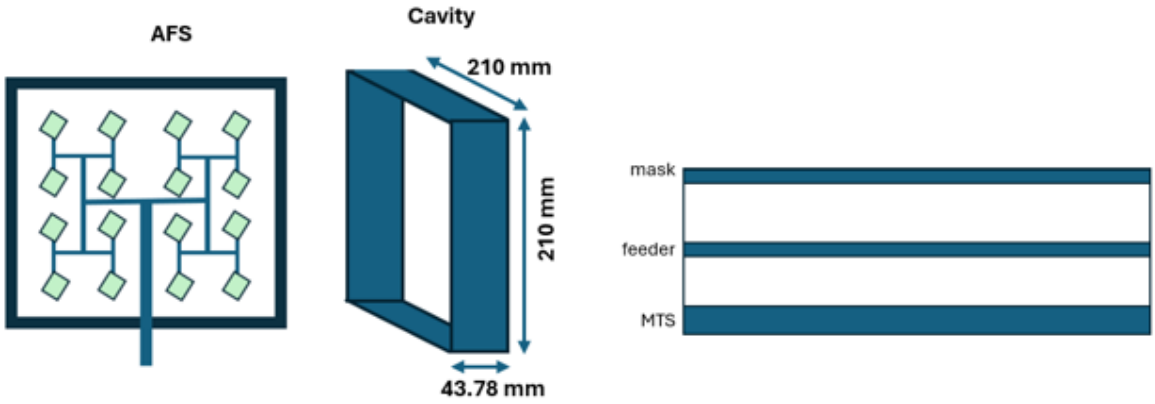

FIGURE 36: VTX FEEDING SYSTEM: (A) CAVITY WITH 16 DS (B) CAVITY DIMENSIONS, (C) SCHEMATIC PLACEMENT OF ANTENNA ELEMENTS.

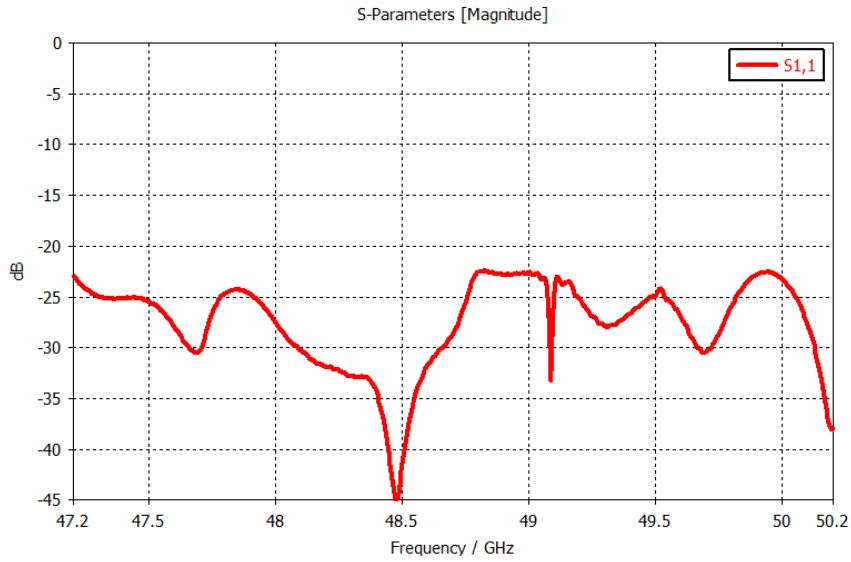

FIGURE 37: SIMULATED REFLECTION COEFFICIENT OF THE TX FEEDING SYSTEM. A REFLECTION COEFFICIENT THAT IS LOWER THAN -20 DB OVER THE WHOLE BAND OF INTEREST IS NOTICED.

V-TX FEEDING SYSTEM KPIS

Two KPIs are evaluated for the AFS are the Uniformity of the field (UOF) and Leakage. UOF is defined as the ratio of the standard deviation of E-tan and its mean value measured at the MTS plane as presented in Figure 39 (a,b,c and d) and Table 22 for different frequencies. Leakage is the ratio of the power measured at the Aperture plane and the total measured power (at both planes) presented in Table 22.

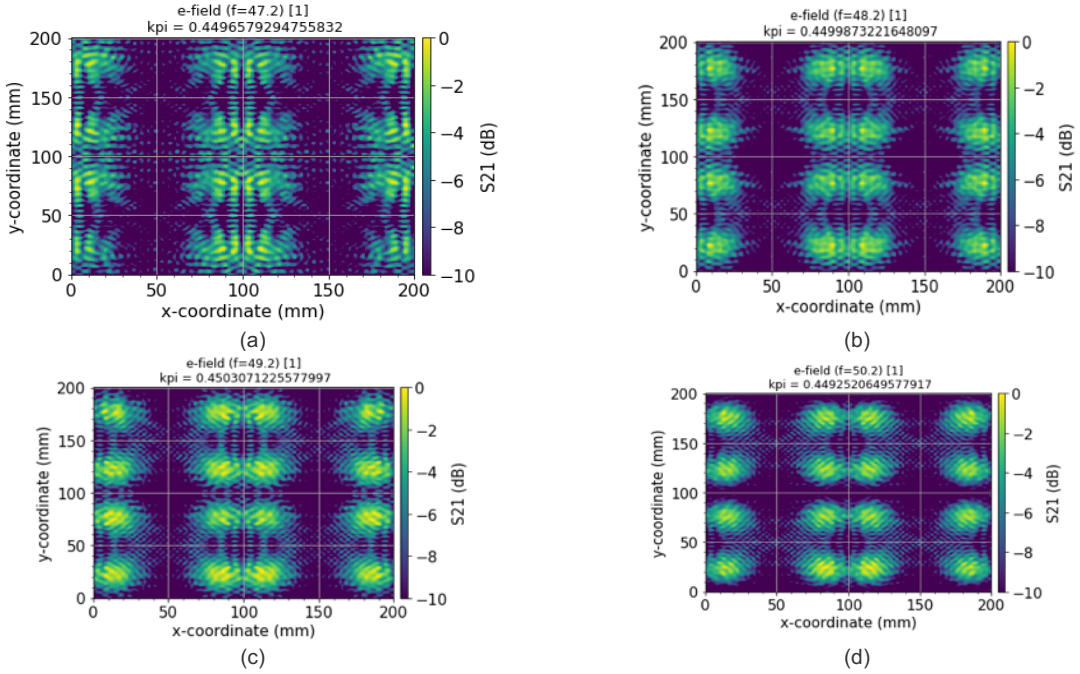

FIGURE 38: VTX UNIFORMITY OF THE FIELDS AT (A) 47.2 GHZ (B) 48.2 GHZ (C) 49.2 GHZ AND (D) 50.2 GHZ.

KPIs values are presented in linear (Table 28). For both KPIs, the lower the value, the better, since it is the ratio of the field's standard deviation to its mean value. The results presented here are for the best fabricated sample, chosen using these KPIs.

TABLE 28: VTX FEEDING SYSTEM LEAKAGE KPIS FOR DIFFERENT FREQUENCIES.

Frequency [GHz]	47.2	48.2	49.2	50.2
UOF	0.45	0.45	0.45	0.45
Leakage KPI [%] (lower – better)	4.93	3.88	3.82	3.36

4.3.2.8 Rx antenna feeding system (37.5-42.5 GHz)

Figure 39 shows the Rx AFS. The cavity measures (210 mm × 210 mm × 43.78 mm). The Return loss of the feeding system is shown in Figure 40. A reflection coefficient that is lower than -20 dB over the whole band of interest is noticed.

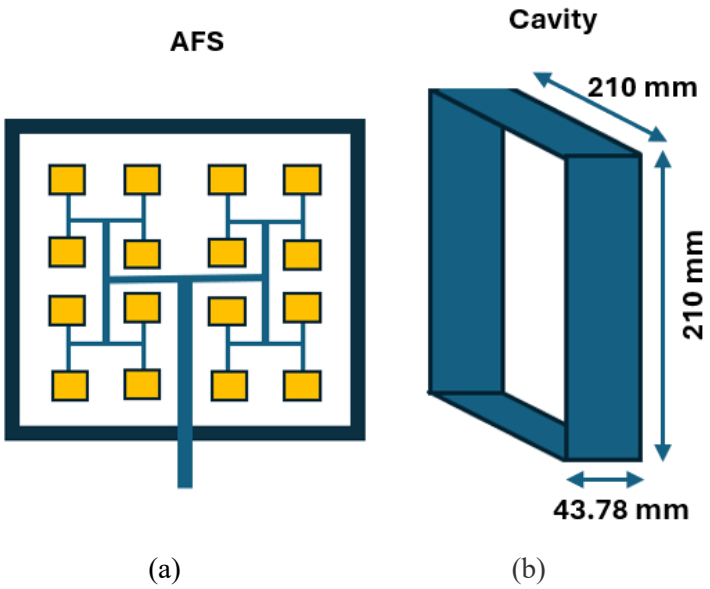

FIGURE 39: RX FEEDING SYSTEM: (A) AFS WITH 16 DS (B) CAVITY DIMENSIONS

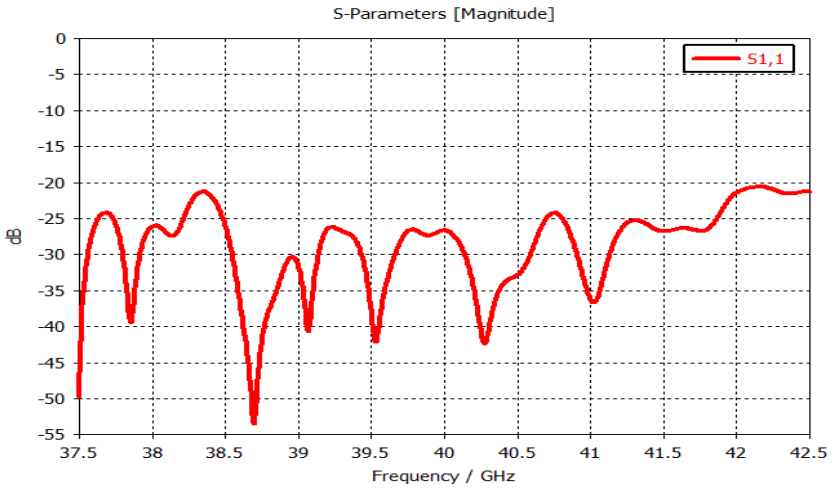

FIGURE 40: SIMULATED REFLECTION COEFFICIENT OF THE RX AFS. A REFLECTION COEFFICIENT THAT IS LOWER THAN -20 DB OVER THE WHOLE BAND OF INTEREST IS NOTICED.

Q-RX FEEDING SYSTEM KPIS

Two KPIs are evaluated for the AFS: the UOF and Leakage.

Figure 42 (from a to f) includes results for the E field distribution for different frequencies, uniformity KPI is presented in Table 29. The same table includes leakage KPIs also.

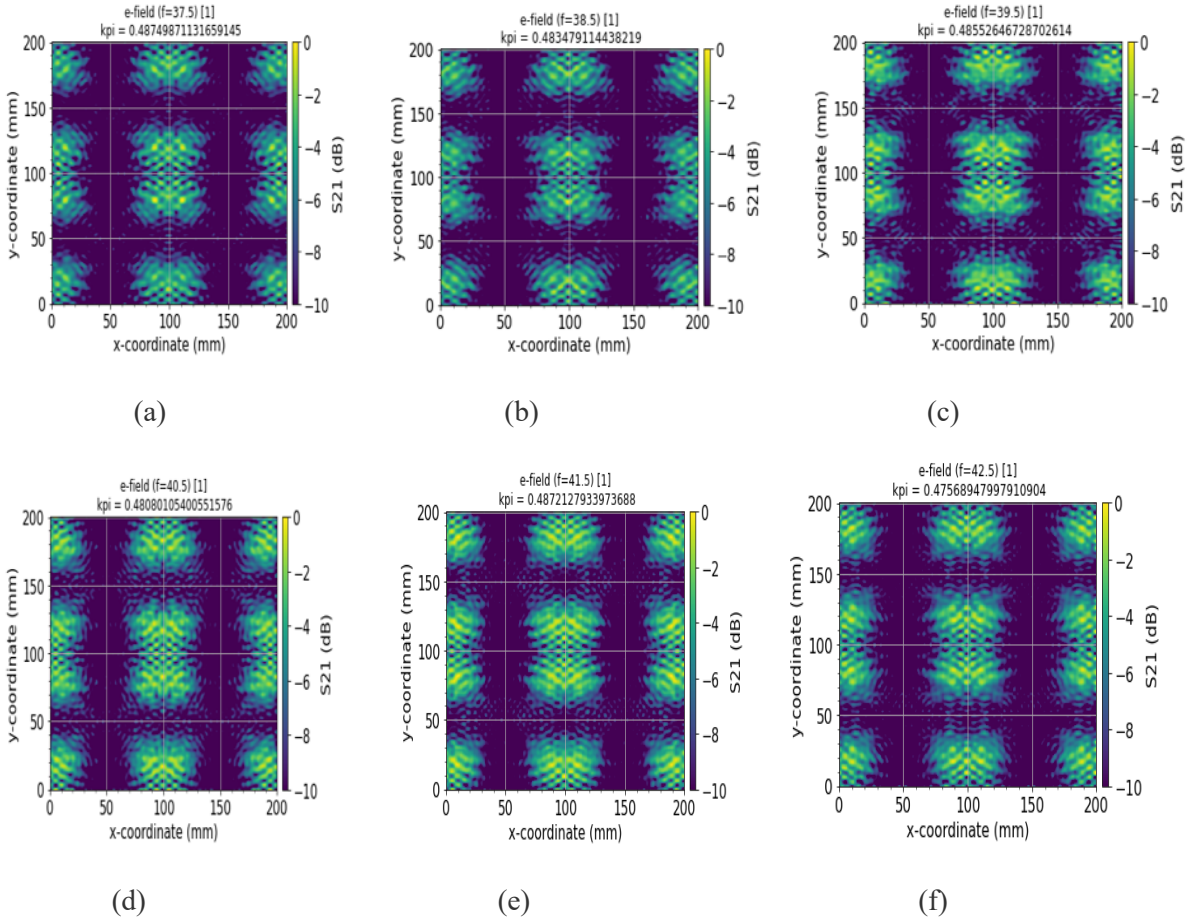

FIGURE 41: QRX UOF AT (A) 37.5 GHZ (B) 38.5 GHZ (C) 39.5 GHZ (D) 40.5 GHZ (E) 41.5 GHZ AND (F) 42.5 GHZ

TABLE 29: RX FEEDING SYSTEM LEAKAGE KPIS FOR DIFFERENT FREQUENCIES.

Frequency [GHz]	37.5	38.5	39.5	40.5	41.5	42.5
UOF	0.49	0.48	0.49	0.48	0.49	0.48
Leakage KPI [%]	7.75	8.13	9.08	6.63	6.15	5.20

For the Rx AFS best UOF of 0.48 was observed at (38.5 GHz, 40.5 GHz, and 42.5 GHz).

4.3.3 Antenna Feeder System: Characterization

4.3.3.1 S11 (Return Loss)

The Return Loss and the mismatching factor are shown in Figure 42 (a) and in Figure 42 (b), respectively.

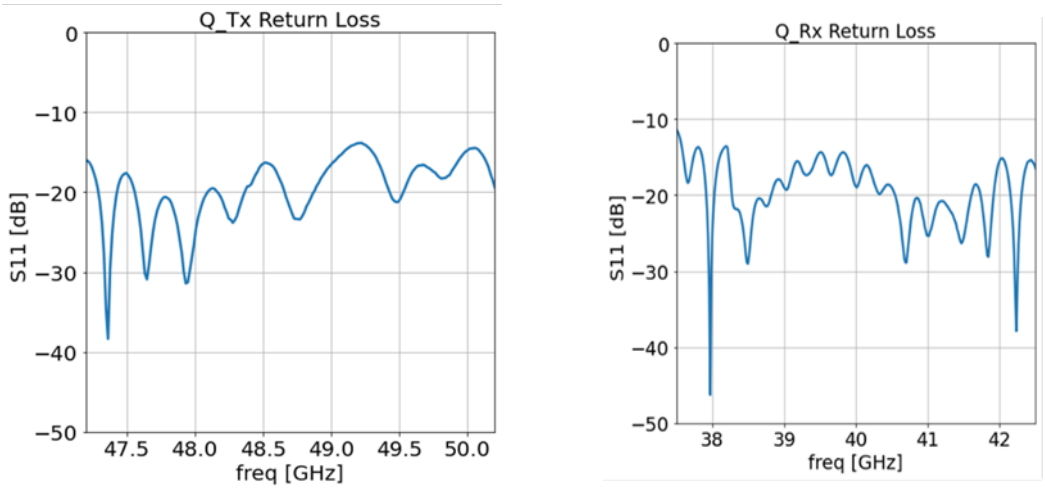

(a) (b)

FIGURE 42: MEASURED RETURN LOSS (A) TX (B) RX.

The measured return loss shows a good result which is below the -15 dB for almost the whole frequency bands of interest for the Tx and Rx AFSs.

4.3.3.2 Near-Field Planar Scan Results

The planar near-field (NF) scans are performed at the desired planes.

The Tx near-field scan plots are presented in the tables provided below, along with the far-field plots (near-field to far-field transformation) at 47.2 GHz (3.1.2.1) and 49.2 GHz (3.1.2.2) covering the whole desired V band.

The Rx near-field scan plots are presented in the tables provided below, along with the far-field plots (near-field to far-field transformation) at 37.5 GHz (3.1.2.1) and 40.5 GHz (3.1.2.1) covering the whole desired V band.

4.3.3.3 FREQUENCY 47.2 GHZ

The values of the field presented below are normalized to the maximum value and plot with a range 0 to -10dB or 0 to -20 dB.

1. NORMALIZATION WITH -10 DB

The NF measured results which are normalized with -10 dB are shown in Figure 43.

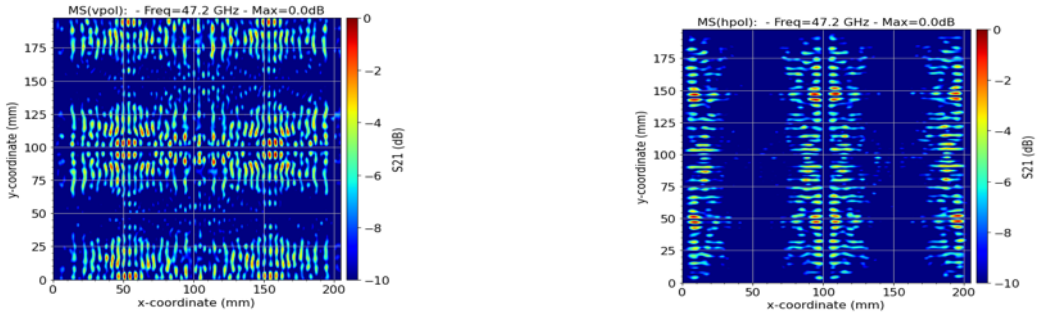

(a) (b)

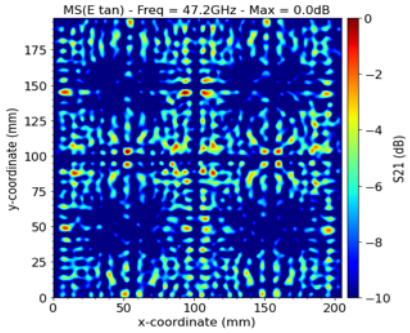

(c)

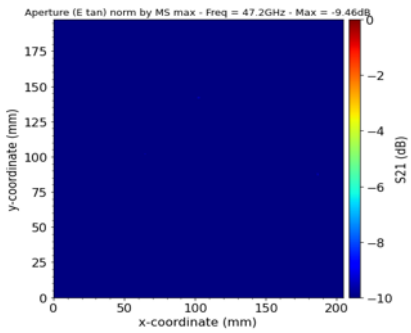

(d)

FIGURE 43: NF SCAN RESULTS AT 47.2 GHZ NORMALIZED WITH -10 DB: (A) V-POL, (B) H-POL AND (C) TOTAL TANGENTIAL E-FIELDS AT THE MTS PLANE. (D) TOTAL TANGENTIAL E-FIELDS AT THE MASK PLANE.

2. NORMALIZATION WITH -20 DB

The NF measured results are also normalized with -20 dB (Figure 44). This normalization helps to illustrate the distribution of the lower values of the field.

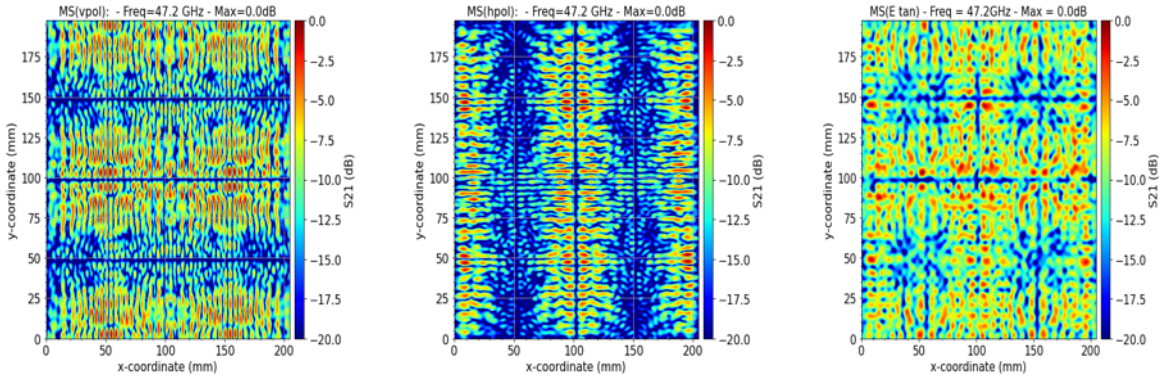

(a) (b) (c)

FIGURE 44: NF SCAN RESULTS AT 47.2 GHZ NORMALIZED WITH -20 DB: (A) V-POL, (B) H-POL AND C) TOTAL TANGENTIAL E-FIELDS AT THE MTS PLANE.

4.3.3.4 FREQUENCY 49.2 GHZ

1. NORMALIZATION WITH -10 DB

The NF measured results normalized with -10 dB are shown in Figure 46 below, (a), (b) and (c) figures represent the normalized field for H polarization, V polarization and total E field at the MTS plane. (d) figure represents the total E field at the mask plane.

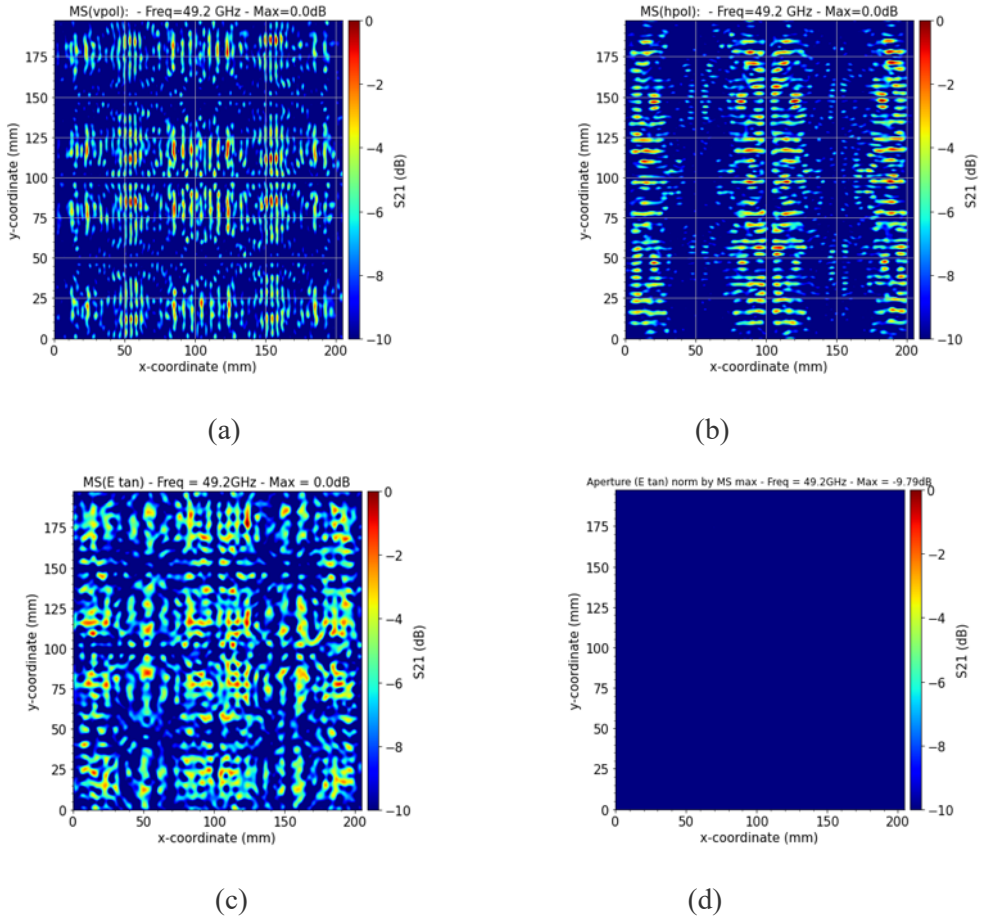

FIGURE 45: NF SCAN RESULTS AT 49.2 GHZ NORMALIZED WITH -10 DB: (A) V-POL, (B) H-POL AND (C) TOTAL TANGENTIAL E-FIELDS AT THE MTS PLANE. (D) TOTAL TANGENTIAL E-FIELDS AT THE MASK PLANE.

2. NORMALIZATION WITH -20 DB

The NF measured results which are normalized with -20 dB are shown in Figure 46.

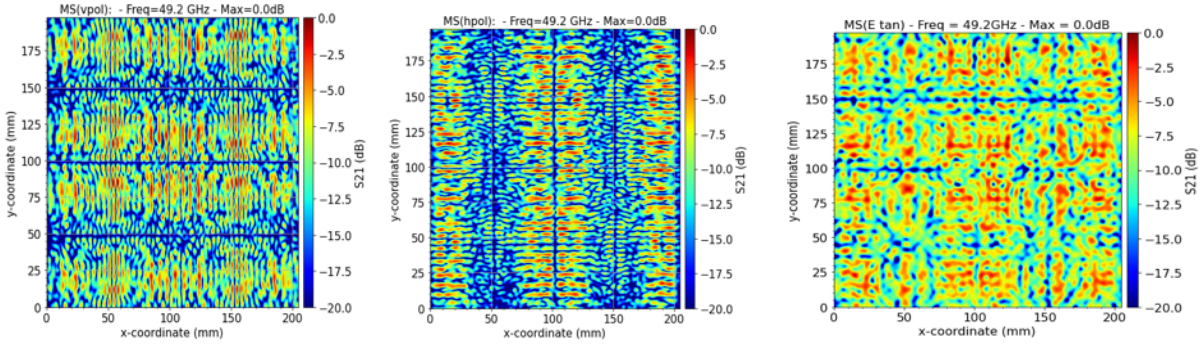

FIGURE 46: NF SCAN RESULTS AT 49.2 GHZ NORMALIZED WITH -20 DB. (A) V-POL, (B) H-POL AND (C) TOTAL TANGENTIAL E-FIELDS AT THE MTS PLANE.

4.3.3.5 Frequency 37.5 GHz

NORMALIZATION WITH -10 DB

The NF measured results which are normalized with -10 dB are shown in Figure 47 below.

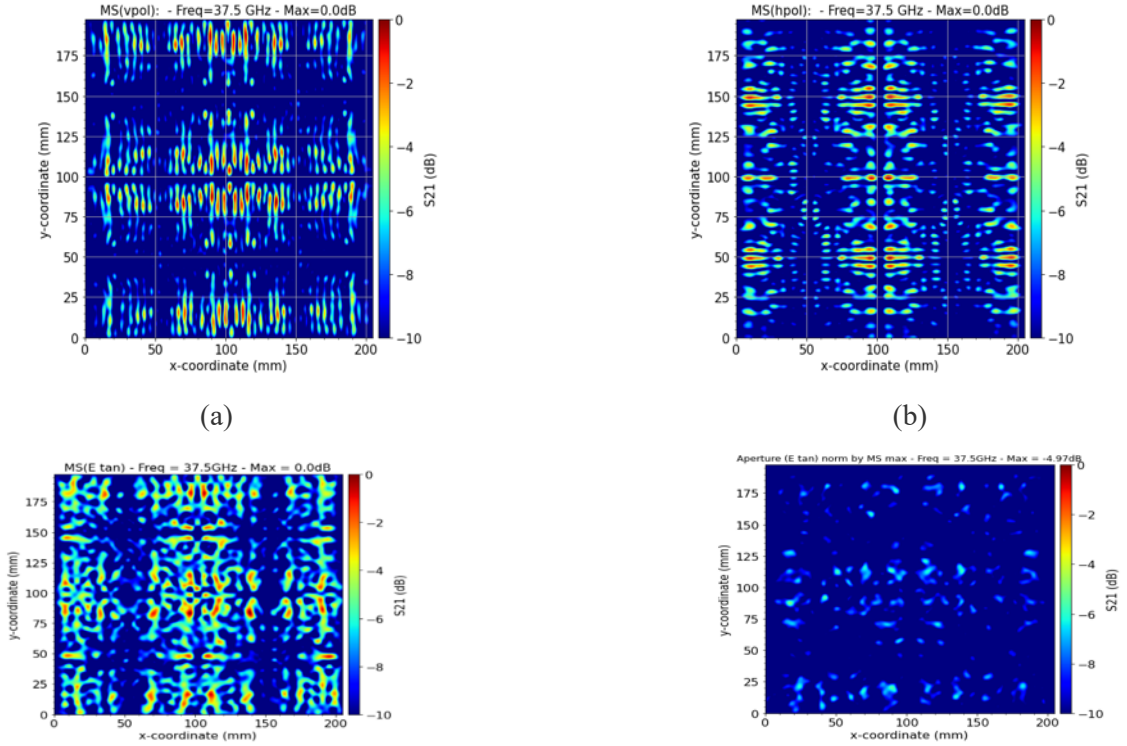

FIGURE 47: NF SCAN RESULTS AT 37.5 GHZ NORMALIZED WITH -10 DB: (A) V-POL, (B) H-POL AND (C) TOTAL TANGENTIAL E-FIELDS AT THE MTS PLANE. (D) TOTAL TANGENTIAL E-FIELDS AT THE MASK PLANE.

NORMALIZATION WITH -20 DB

The NF measured results which are normalized with -20 dB are shown in Figure 48 below.

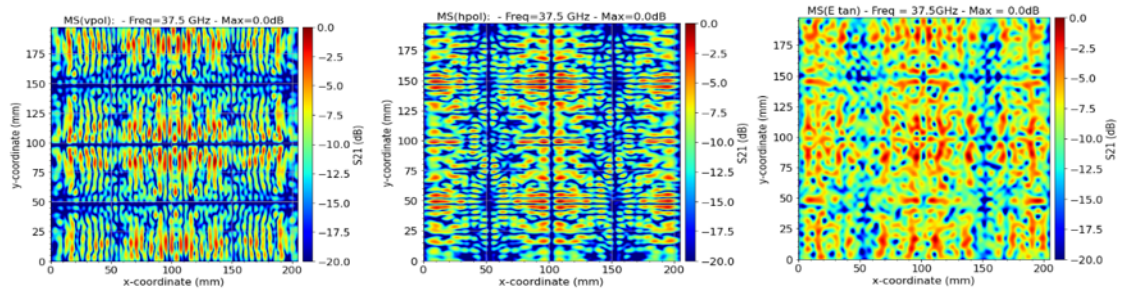

FIGURE 48: NF SCAN RESULTS AT 37.5 GHZ NORMALIZED WITH -20 DB: (A) V-POL, (B) H-POL AND (C) TOTAL TANGENTIAL E-FIELDS AT THE MTS PLANE.

The normalized field at the aperture level is not shown here since it has no interest.

4.3.3.6 Frequency 40.5 GHz

NORMALIZATION WITH -10 DB

The NF measured results which are normalized with -10 dB are shown in Figure 49 below.

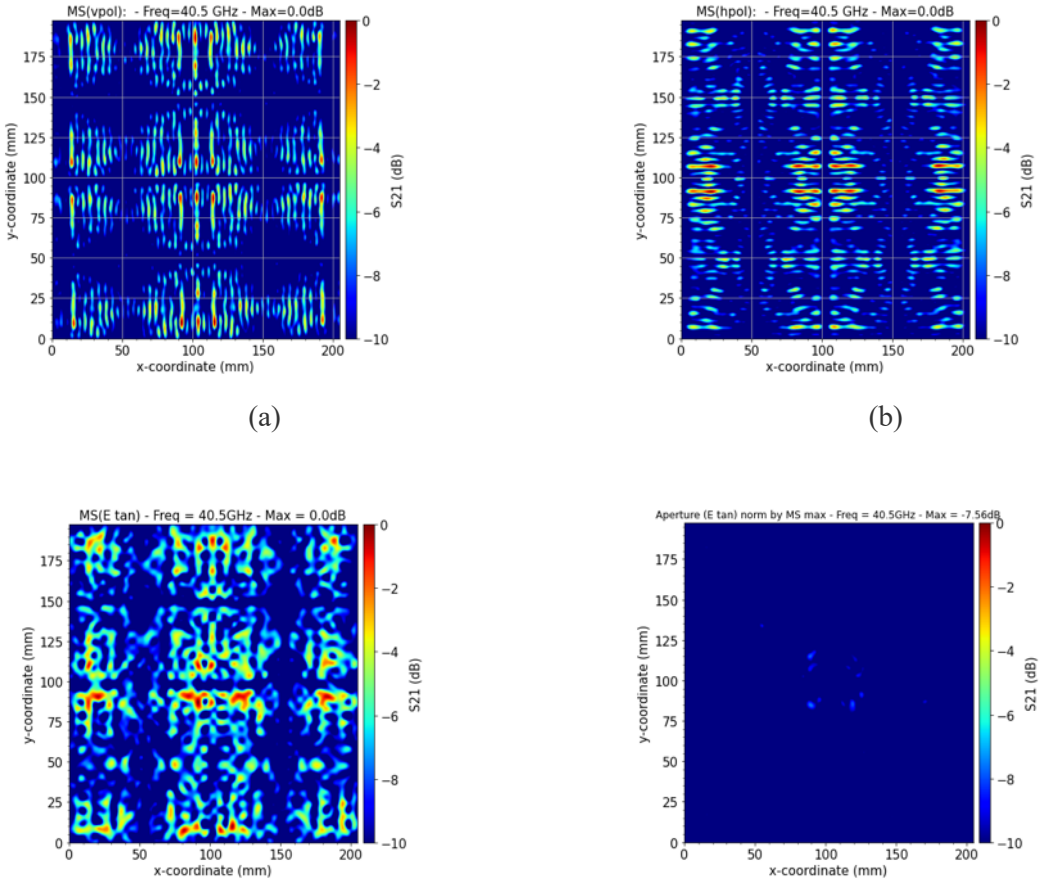

FIGURE 49: NF SCAN RESULTS AT 40.5 GHZ NORMALIZED WITH -10 DB: (A) V-POL, (B) H-POL AND (C) TOTAL TANGENTIAL E-FIELDS AT THE MTS PLANE. (D) TOTAL TANGENTIAL E-FIELDS AT THE MASK PLANE.

NORMALIZATION WITH -20 DB

The NF measured results which are normalized with -20 dB are shown in Figure 50 below.

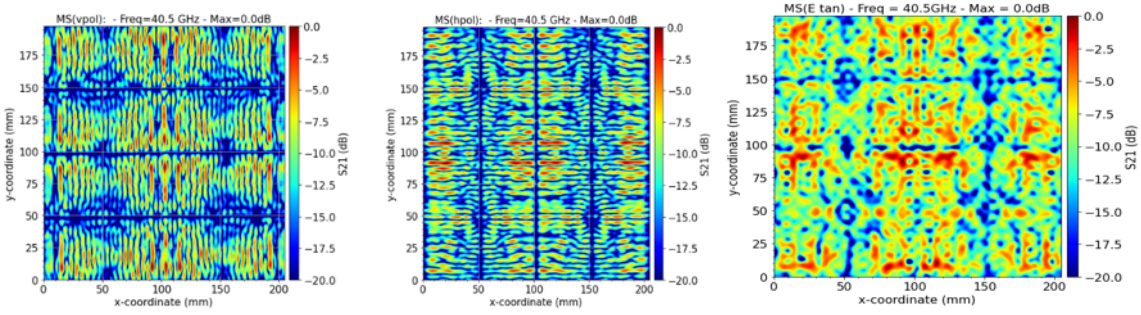

FIGURE 50 NF SCAN RESULTS AT 40.5 GHZ NORMALIZED WITH -20 DB: (A) V-POL, (B) H-POL AND (C) TOTAL TANGENTIAL E-FIELDS AT THE MTS PLANE.

The normalized field at the aperture level is not shown here since it has no interest.

4.3.3.7 KPIs and Direct leakage

The UOF is defined by the ratio of the standard deviation of E-tan and its mean value measured at the MTS plane. Results are presented in Table 30 for VTx AFS and in Table 31 for QRx AFS.

TABLE 30: SUMMARY OF VTX AFS KPI: UOF AND LEAKAGE AT PREDEFINED FREQUENCY POINTS

	47.2 GHz	48.2 GHz	49.2 GHz	50.2 GHz
UOF	0.41	0.39	0.39	0.39
Leakage (%)	8.0	8.13	9.1	8.73

TABLE 31: SUMMARY OF QRX AFS KPI: UOF AND LEAKAGE AT PREDEFINED FREQUENCY POINTS.

	37.5 GHz	38.5 GHz	39.5 GHz	40.5 GHz	41.5 GHz	42.5 GHz
UOF	0.41	0.42	0.41	0.41	0.40	0.40
Leakage (%)	9.16	8.9	9.18	6.4	7.36	8.57

4.3.3.8 Conclusion

The measured return loss is below -15 dB for almost the entire QV band.

For VTx KPIs, a very low uniformity KPI (0.39) was obtained at most of the frequencies. This value is minimum across all measured samples, which indicates the best achieved uniformity of the radiation of the metasurface. A minimum direct leakage of 0.8% is obtained at 47.2 GHz and a maximum level of 9.1% is obtained at 49.2 GHz.

The best QRx KPI (0.40) was found at 41.5 GHz and 42.5 GHz with a direct leakage of around 7.36 % and 8.57% respectively. Meanwhile, the lowest direct leakage (6.4 %) can be found at 40.5 GHz with a KPI of about 0.41.

4.3.4 Antenna Mask

The antenna mask is placed on the top of the antenna cavity (see Fig. 37c). This part of the antenna is semi-transparent. This means that it allows us to transmit a certain level of power (radiate through the antenna aperture) and reflect the remaining part towards the Metasurface to be shaped and stirred to the desired direction. Multiple reflections accrue then between the Metasurface and the mask inside the antenna cavity and a part of the power is always radiated outside of it. Multiply reflections between the mask and metasurface efficiently increase the efficiency of metasurface interaction with the field inside the cavity and consequently the weight of each pixel of metasurface.

4.3.4.1 QRx and VTx masks design

The technical details of the two masks are:

1. Frequency of interest: Q-Rx => [37.5 GHz – 42.5 GHz]
   Q-Tx => [47.2 GHz – 50.2 GHz]

2. Geometry: Flat, uniform and one layer PCB based.
3. Dissipation: 0.01
4. Transmission: 65%
5. CrossPol < -20 dB
6. Material: Rogers 4003C

Some KPIs need to be reached in order to validate the designed masks. The fabrication of the mask is based on a fixed goal (% of transmission) and KPIs reflecting the TE and TM modes symmetry as function of incidence angle Theta.

4.3.5 Antenna Mask Characterization

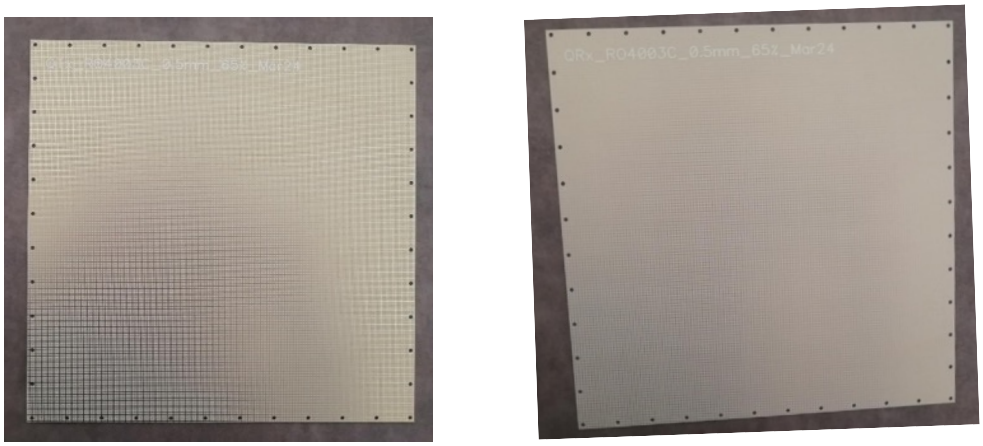

FIGURE 51: VTX (LEFT) AND QRX (RIGHT) MASKS

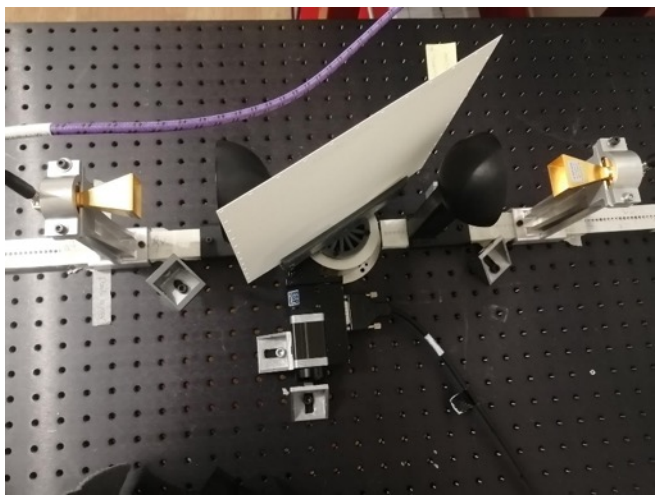

FIGURE 52: MASKS CHARACTERIZATION SETUP

Fabricated masks are presented in Figure 51. Both masks transmission coefficients were measured for different angles [0°-50°]. Results are presented in Table 32 and compared to simulation.

TABLE 32: QRX AND VTX CHARACTERIZATION RESULTS COMPARED TO SIMULATION

	Mask QRx [Bandwidth : 12%]	**Mask VTx [Bandwidth: 6%]**
Measurement	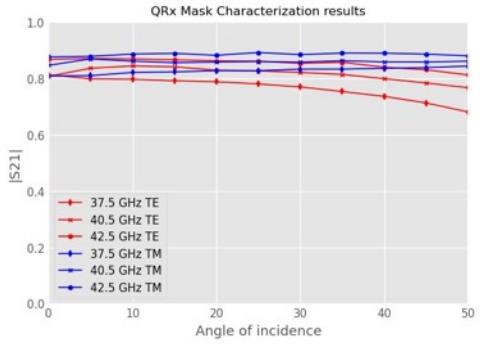	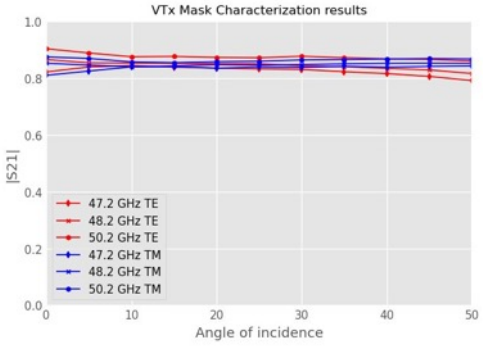
Simulation	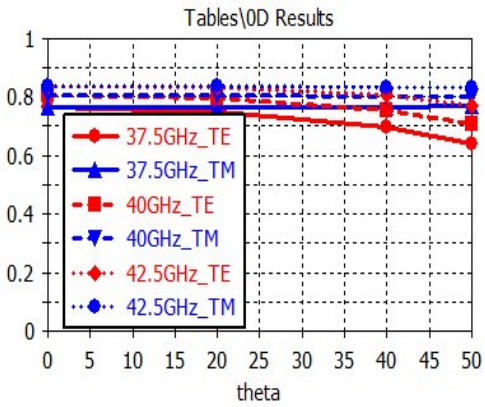	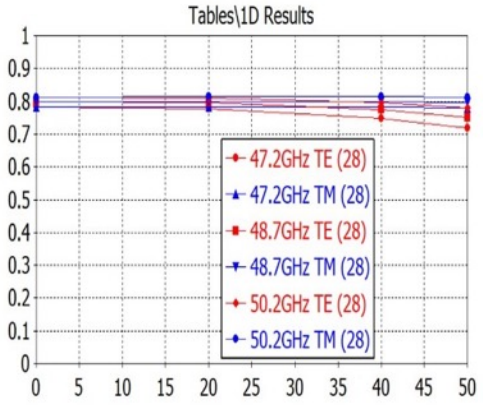

The desired transmission level of power was 0.65% (0.8% S21 level).

Both masks present good coherence between measurement and simulation result in measurement are around 5% higher than simulation for both masks.

4.4 CONCLUSION

A novel Q/V-band 1-bit reconfigurable metasurface for 6G-NTN applications has been designed, simulated and measured. Since initial metasurface design exhibited high reflection dissipation and low phase difference between ON and OFF states of pixels, the new metasurface design has been initiated. A new design is based on a different switching element to mitigate the hight dissipation levels.

The designed Q- and V-masks present good coherence between measurement and simulation result with a higher level of transmission in measurement compared to simulation, estimated around 5% for both masks.

Antenna Feeder System for both Q and V bands has been designed, simulated, and measured. Overall, the parameters of the antenna feeder are sufficient for the antenna to meet the defined project specifications.

5 ANTENNA CHARACTERIZATION

Mini MTS characterization results presented previously in section 4.3.1.7 showed results that are far from KPIs, these differences were mainly related to the performance of the switch. Therefore, a second iteration (V2) for the MTS design was suggested based on a different switching component (Macom diode).

In the second part of this report, we will focus on the second iteration of MTS design (V2 QRx & V2 VTx). Simulation and characterization results will be presented and compared. Since some delays occurred in the manufacturing process of V2 VTx MTS, we will focus on characterization results of V2 QRx MTS only. Regarding the full QV antenna characterization, only QRx related results will be presented for the same reasons presented previously. Characterization results for VTx module are going to be presented later in section 5.3.

5.1 V2 METASURFACE (DIODE BASED)

5.1.1 V2 QRx mini-MTS

V2 QRx mini-MTS design is based on a Macom PIN diode as a switching element to replace the CMOS switch used in the first version.

The same KPIs should be met for this design:

- Phase difference between two consecutive states: 180+/- 40 degree
- Average dissipation: less than -2 dB
- Frequency bands: 37.5 – 42.5 GHz
- Size: < λ/2 over all frequency band
- Bandwidth: 5 GHZ

5.1.2 V2 QRx Pixel design

The pixels consist of 3 main important elements as shown in Figure 53 which could generate the response mentioned in the objectives

- Patch – Main radiating element
- Parasitic element – helps generate the phase shift between the two states
- Diode – To switch between the two states.

The phase shift between the two-pixel states is obtained by introducing a longer electrical length element, a parasitic element, in the ON state.

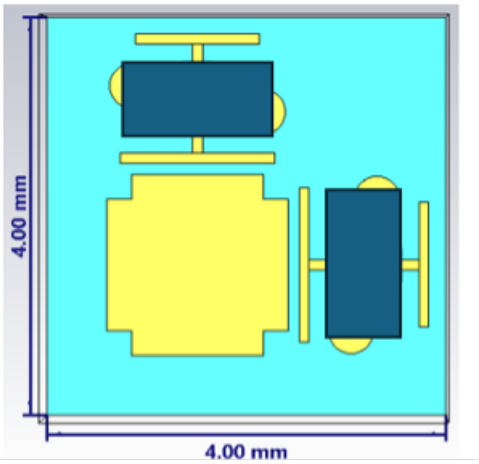

FIGURE 53: V2 QRX PIXEL DESIGN (DIODE BASED)

The main reflector patch also has truncated corners to reduce cross coupling. For each diode there is one GND vias and 1 enable via. Bigger vias were used to reduce the cost per pixel.

Due to hardware constraints, the periodicity of the pixel became 4 mm.

Parameter details:

- Substrate height = 0.5 mm
- Via diameter = 0.15 mm
- Via pad diameter = 0.45 mm

During the design of a dual polarized pixel, the diode and the parasitic resonator are mirrored with respect to the center of the patch to keep the symmetry for each polarization. A periodic structure of 3 pixels x 3 pixels is presented in Figure 54 illustrating the periodic pattern of the MTS.

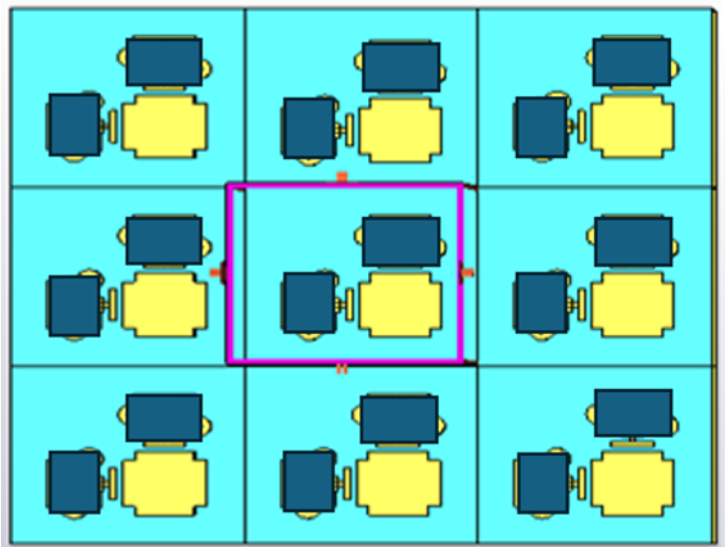

FIGURE 54: SIMULATED PERIODIC STRUCTURE BASED ON V2 QRX PIXEL

5.1.3 Simulation results of V2 QRx pixel

In pixel simulation, we are interested in the amplitude and the phase of the reflected electromagnetic wave by our pixel. We mainly focus on Co-polarization and Cross polarization (X-polarization).

Co-polarization, represented by TE and TM is related to the reflected/dissipated wave energy in the same incident polarization (either TE or TM) while cross polarization is related to the reflected/dissipated wave energy in a different polarization from the incident one.

The Co-polarization (TE/TM) , X-polarization and phase difference simulation results are illustrated in Table 33.

- The phase difference between the two states: **180+/- 30 degree**
- An average dissipation of **1.2 dB**
- Bandwidth: **more than 5 GHZ**
- X-pol Dissipation Level: **below -14 dB**

TABLE 33: CO-POLARIZATION, X-POLARIZATION, AND PHASE DIFFERENCE RESULTS

	|S11| (dB)	Phase (°)
TE	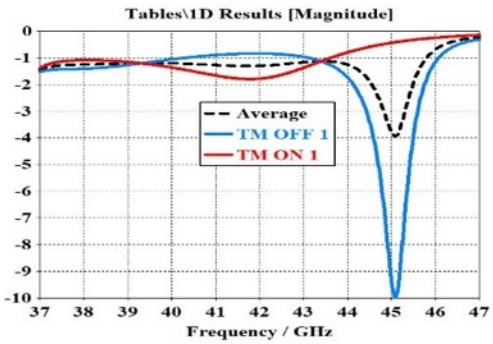	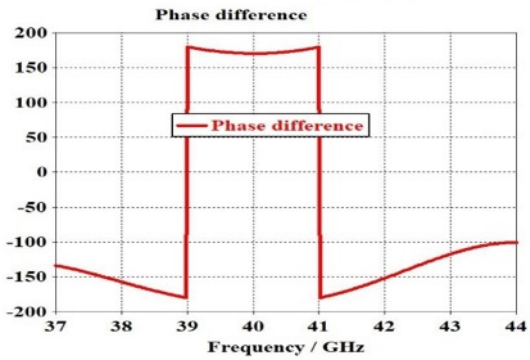
TM	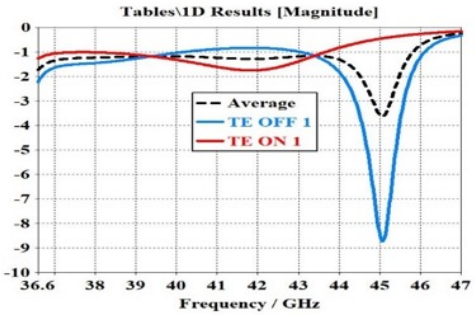	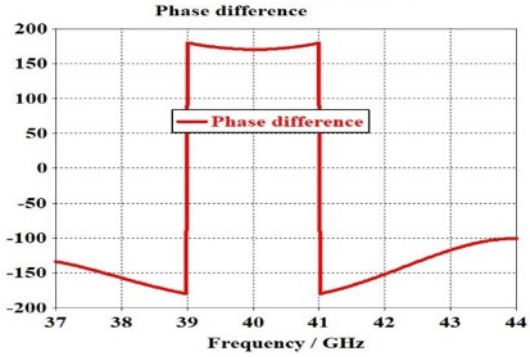

Cross pol	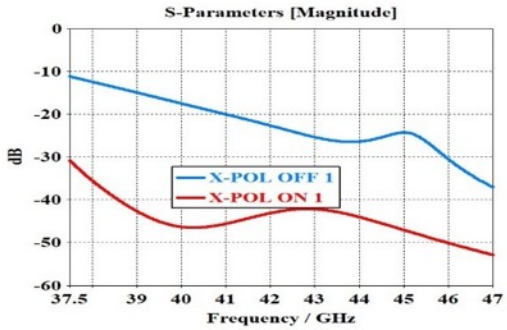

Results show that V2 QRx pixel design meets the KPI, the design is then validated. The V2 mini-QRx MTSs are sent for fabrication and characterization results are shown in the next section.

5.1.4 Measurement results for V2 QRx mini-MTS

This measurement was done in the first place to validate the RF design, the V2 QRx mini-MTS is composed of 6x6 diode-based pixels.

The measurement setup (as presented below) consists of doing a bistatic measurement of the mini-MTS using two identical horn antennas and two lenses in order to focus the wave on the mini-MTS sample. Power supply is used to control the diodes (On/Off states). S21 parameter is measured using a VNA for both TE, TM polarizations and x-polarization.

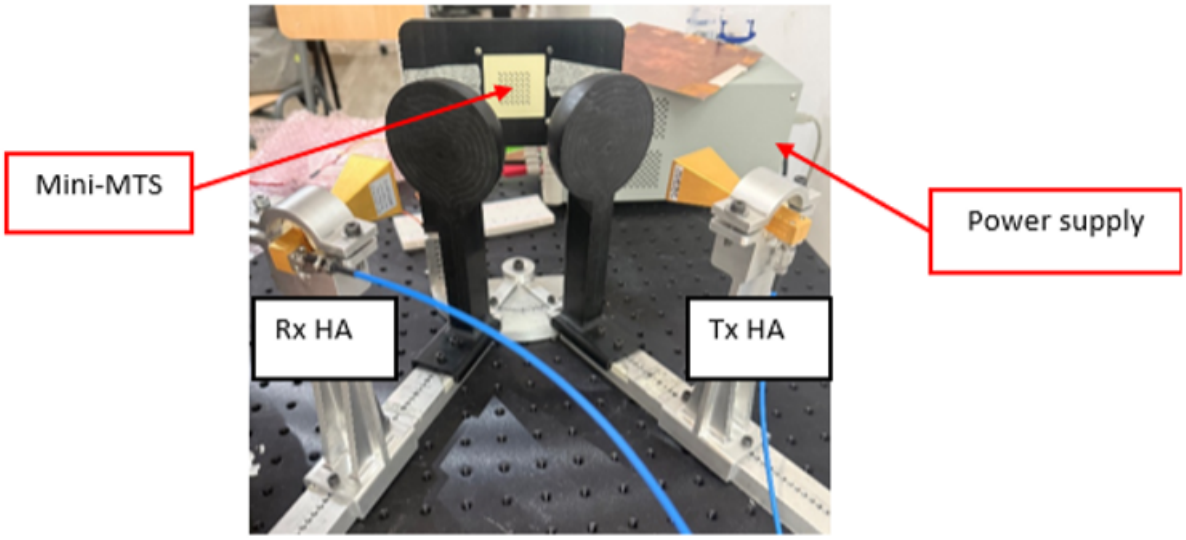

FIGURE 55: BISTATIC MINI-MTS CHARACTERIZATION SETUP: VNA, 2 HORN ANTENNAS, POWER SUPPLY, LENSES AND CABLES.

Table 34 provides a comparison between two measurements of QRx Mini-MTS sample .

TABLE 34: CO-POLARIZATION, X-POLARIZATION, AND PHASE DIFFERENCE FOR TWO DIFFERENT MINI MTS MEASUREMENTS

	V2 measurements	V1 measurements
Amplitude	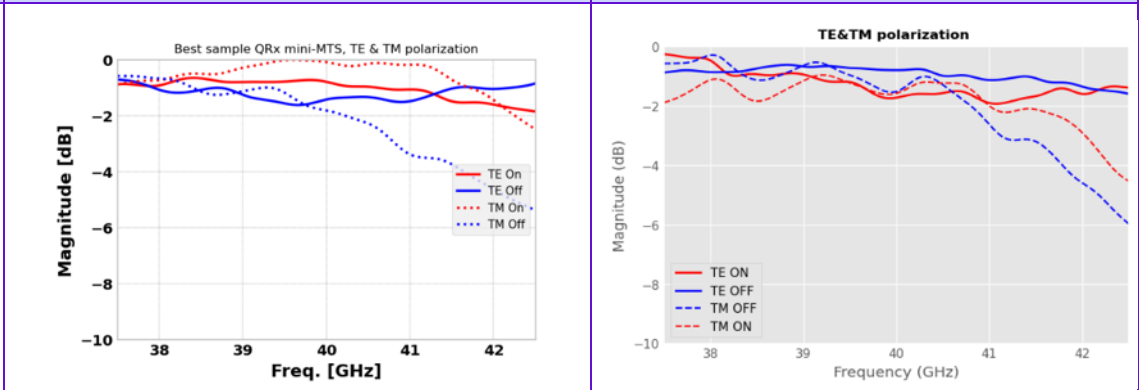	
Phase	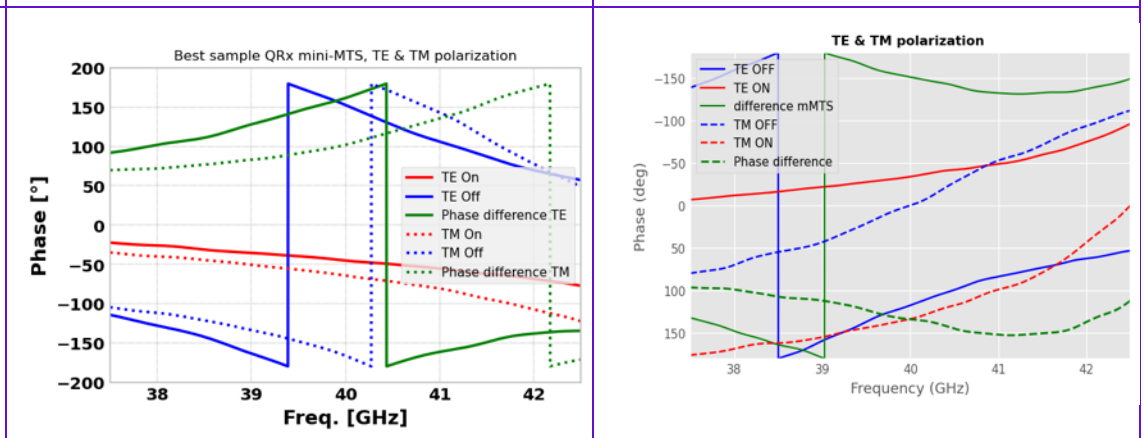	
Cross pol	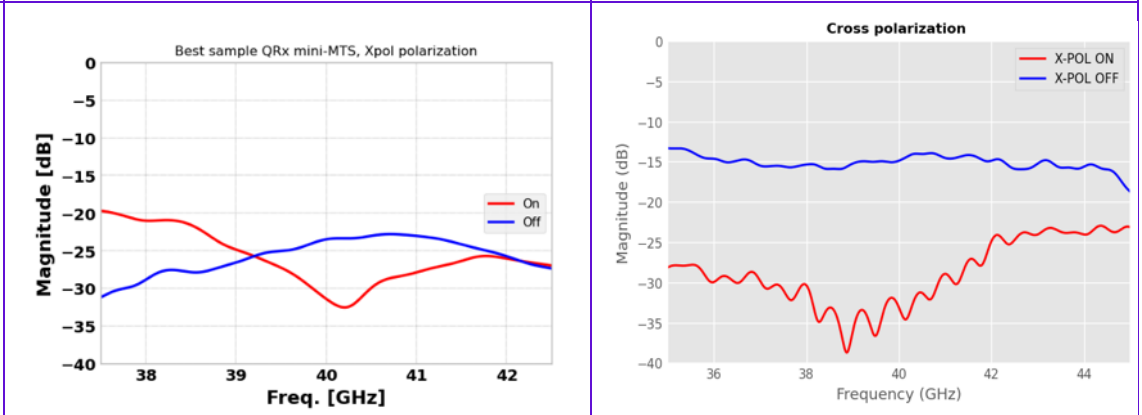	

As presented in Table 34:

- Average dissipation level is **around -1 dB** for TE polarization, and for TM polarization dissipation level is **around – 1 dB** for frequencies lower than 40.5 GHz. Above 40.5 GHz, the |S11| drops to **- 4 dB** (average value).
- The phase difference between the two states is higher than **95°** for all the frequency band in TE polarization **(>140°** for more than half of the band). For TM, the phase difference is higher than **100°** for half of the frequency band but drops to **70°** at the lower frequencies.
- X-pol dissipation level is good (**below -14 dB)**

5.1.5 Measurement results for V2 QRx MTS

The size of the MTSs is 10cmx10cm and every MTS has a total of 576 pixels (24 pixels x 24 pixels). The QRx antenna size is around 21cm x 21cm, and it is composed of 4 MTSs.

A total of 5 MTSs were fabricated (4 MTSs for the antenna and one spare).

In the next section, we will present the measurement setup and results for bistatic characterization of V2 QRx MTSs.

5.1.5.1 V2 QRx MTS measurements Setup

Bistatic characterization procedure and setup is similar to the previously explained measurement for QRx mini-MTSs and it focuses on TE, TM and Cross polarization measurement for all the 5 MTs.

As presented below, the same horn antennas and lenses are used. But, for this measurement we need a control board to set the pixel configurations. In this test we only consider all on and all off states of the diodes. The same control board is used for each of the four MTSs used in the antenna.

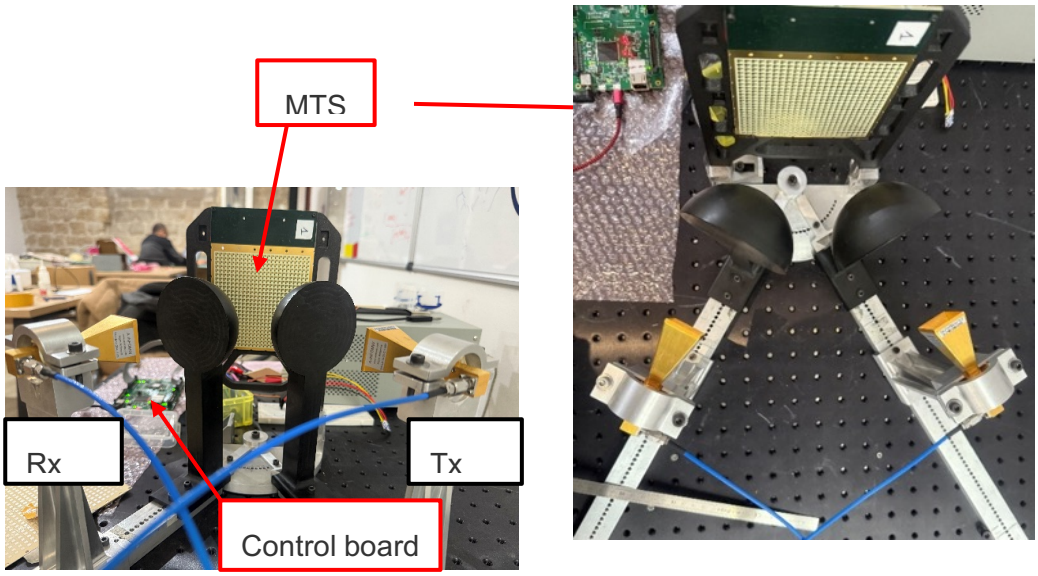

FIGURE 56: CHARACTERIZATION SETUP: VNA, CONTROL BOARD, 2 HORN ANTENNAS, LENSES AND CABLES.

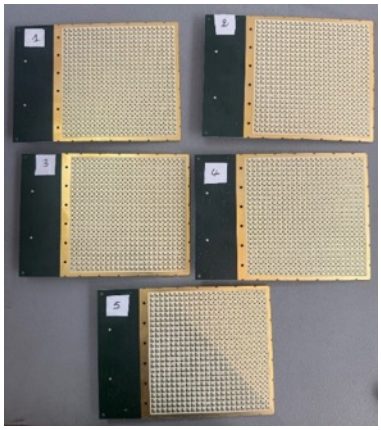

FIGURE 57: THE CHARACTERIZED 5 SAMPLES OF V2 QRX

The used setup elements are presented in Table 35.

TABLE 35: SETUP NEEDS FOR MTS BISTATIC CHARACTERIZATION

Item	Description
VNA	Rohde & Schwarz ZNA67
RHA (reference horn antennas)	Reference horn antennas (Rx and Tx)
Control board	To control the Pixel states (Ref: CBFV2.1)
Power supply	12 V: to power the MTS & CB
Cables / transitions	2 coax cables: 0.9 m + ribbon cable
Lenses / holders / support	Mechanical part of the setup

Measurement results for the five fabricated MTSs are presented in tables below (for TE, TM and x-pol)

5.1.5.2 TE polarization

TABLE 36: CO-POLARIZATION (TE) MEASUREMENTS RESULTS FOR THE 5 MTSS

MTS	Amplitude	Phase
MTS1	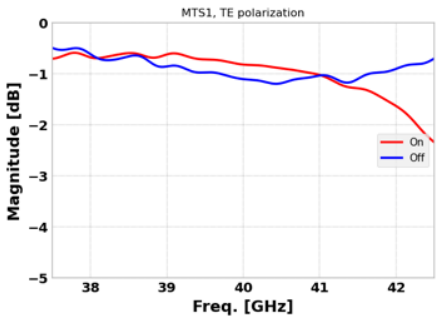	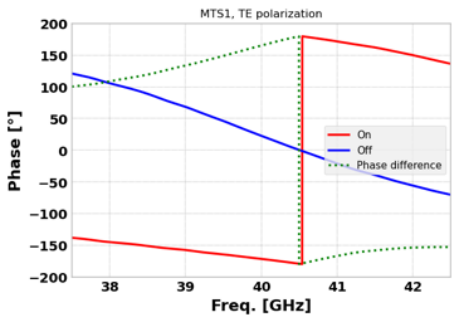

MTS2	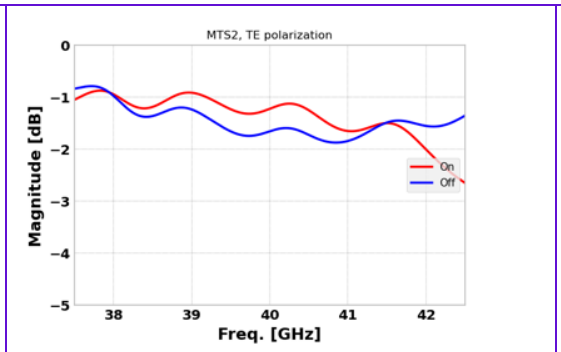	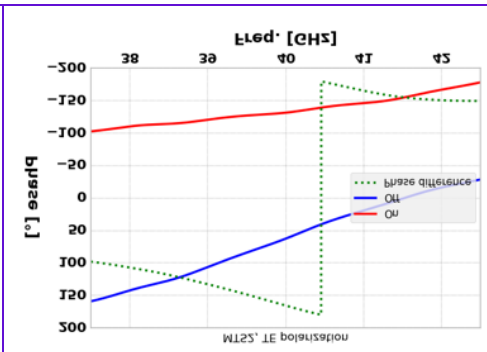
MTS3	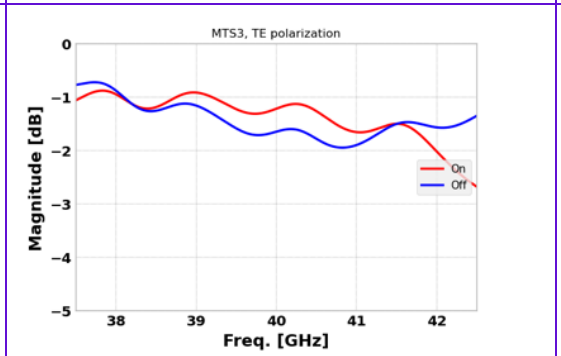	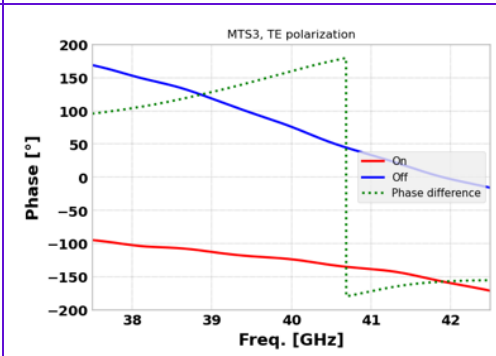
MTS4	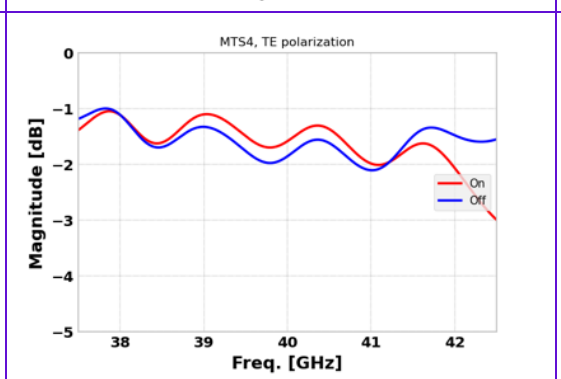	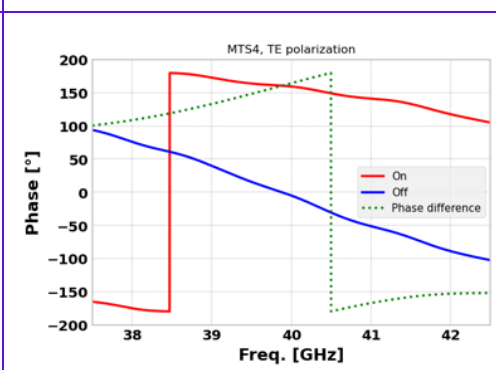
MTS5	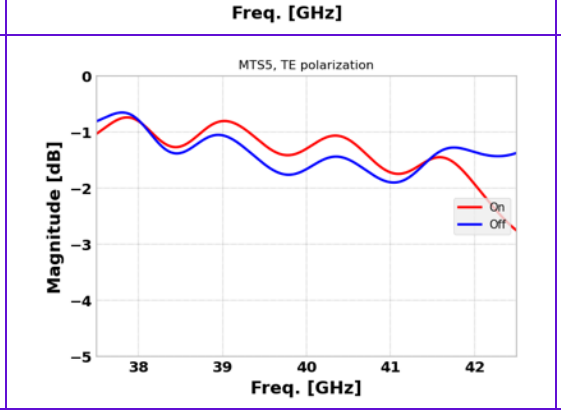	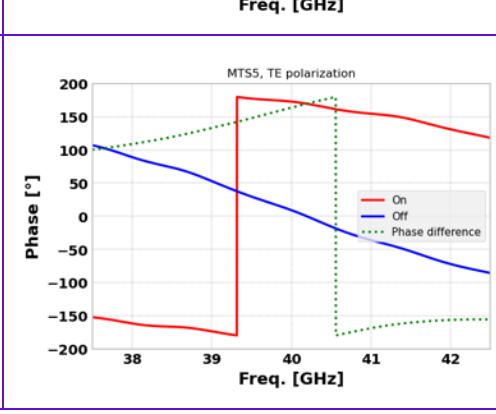

5.1.5.3 TM polarization

TABLE 37: CO-POLARIZATION (TM) MEASUREMENTS RESULTS FOR THE 5 MTSS

MTS	Amplitude	Phase
MTS1	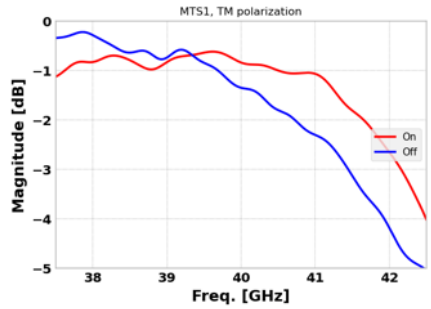	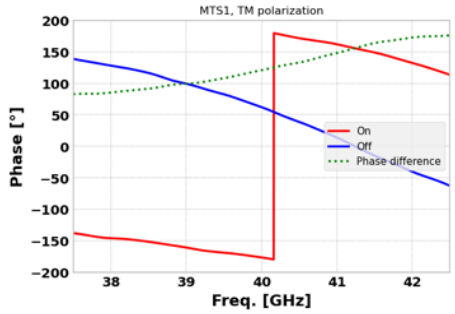
MTS2	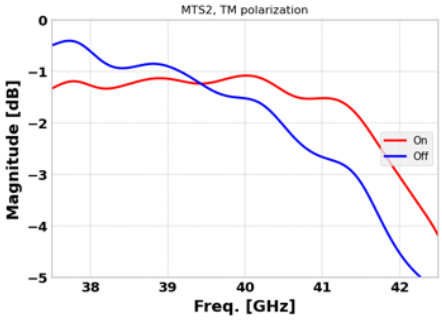	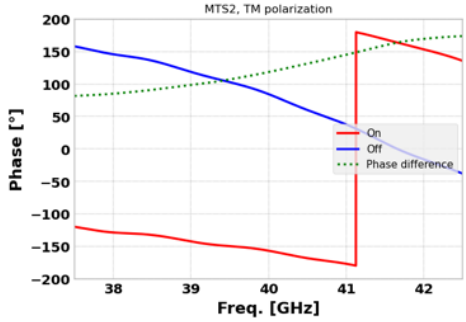
MTS3	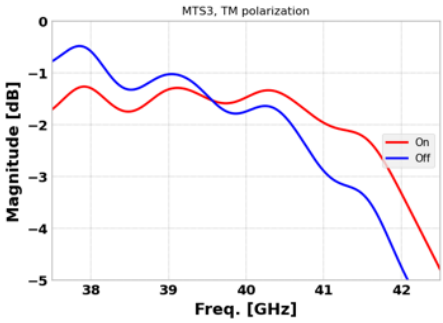	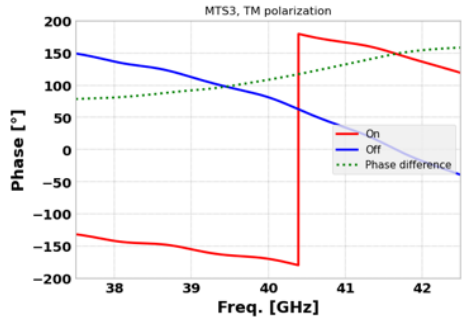
MTS4	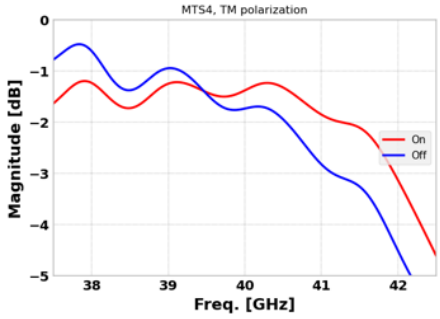	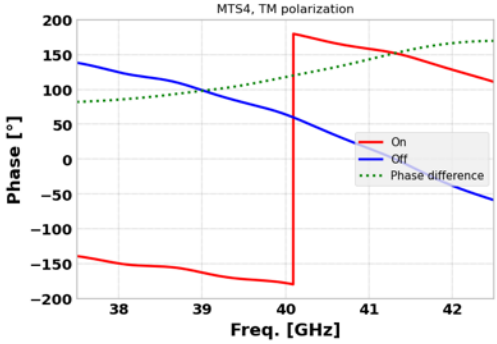

MTS5	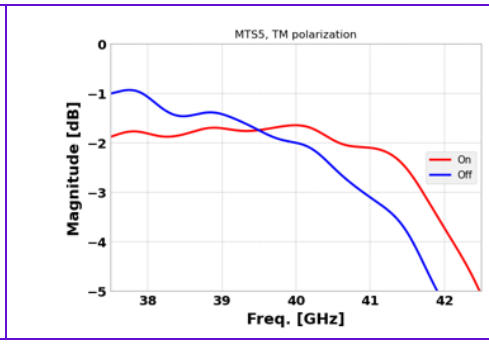	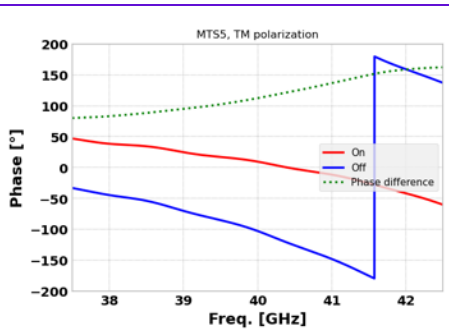

5.1.5.4 Cross polarization:

TABLE 38: CROSS-POLARIZATION MEASUREMENTS RESULTS FOR THE 5 MTSS

MTS	Amplitude	MTS	Amplitude
MTS 1	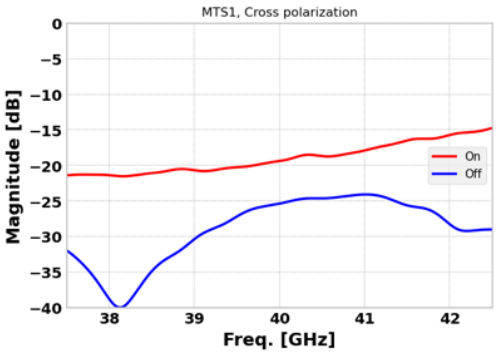	MTS 2	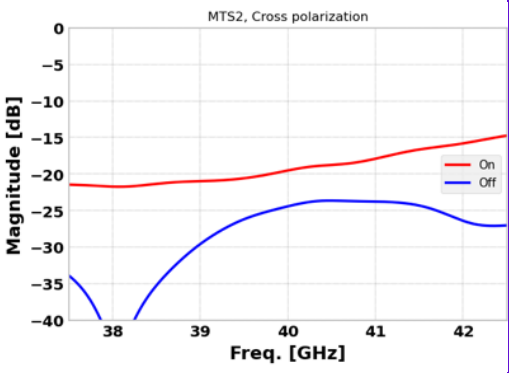
MTS 3	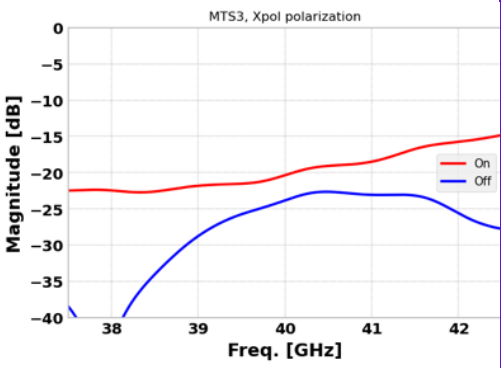	MTS 4	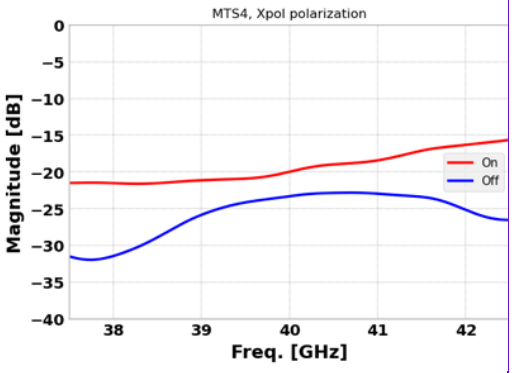
MTS 5	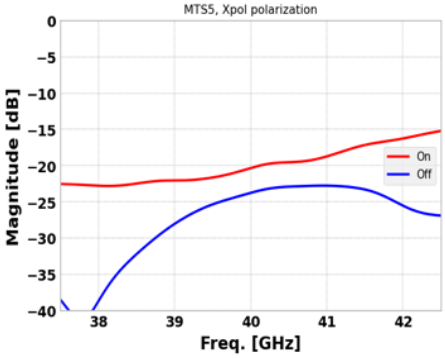		

Bistatic measurement results (Table 36, Table 37, Table 38) for QRx MTS showed very good agreement with the best mini MTS sample measurements. This validates the performance and the fabrication of the MTS considering the selected design (Sample 1 of QRx mini-MTS).

All 5 MTS were tested. As part of our test procedure, we first start by testing the switching elements, i.e., the diodes. Here, all the MTS diodes were fully detected. (that means consistency of electronic components operation). Bistatic measurement results for the 5 MTS samples are very similar.

If we consider MTS1 sample:

- Dissipation: TE=> -1 dB average, TM=> above -2 dB over 64% of the band minimum of (-4.5dB), Cross pol: bellow –15 dB
- Phase difference: TE => above 100° for all the frequency band and above 140° for 62% of the band, TM => above 84° for all the frequency band and above 100° for 50% of the band and above 140° for 30% of the band.

For the QRx antenna assembly 4 V2 QRx MTSs are needed. The next part of the report will be dedicated to the QRx antenna characterization results.

5.2 QRX ANTENNA CHARACTERIZATION

5.2.1 Presentation of the AUT

The antenna under test is: QRx antenna

- Metasurface: V2 QRx
  - **Design:** one layer diode-based MTS (total of 4608 diodes)
  - **Size:** MTS 20cmx20cm composed of four 10cmx10cm MTSs
- **Cavity**: aluminum of 4.37cm height.
- **Antenna Feeder**: aluminum, 16 sources and WR19 input port
- **Mask:** one layer PCB mask with slot pattern (facing the inside of the cavity), uniform with 65% transmittance

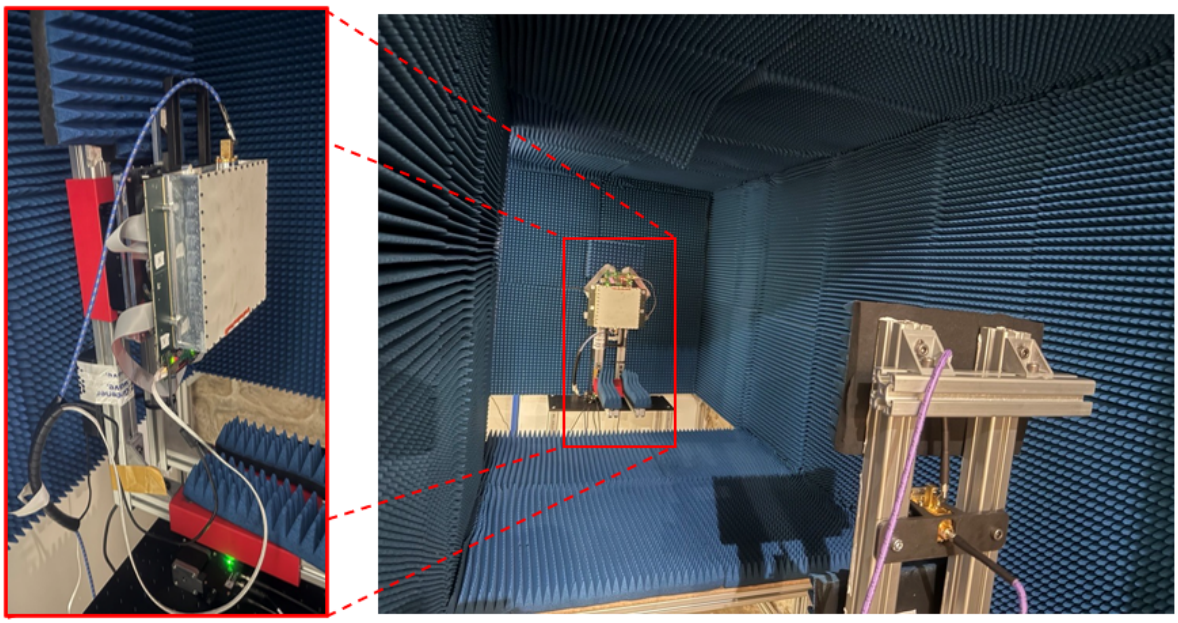

FIGURE 58 AUT ON THE CHARACTERIZATION SETUP.

5.2.2 Experimental setup

QRx antenna characterization was conducted in Nemo spherical near field setup located in Greenerwave's premises in Paris (Figure 58). For this measurement setup, we needed the following components:

- VNA: Rohde & Schwarz ZNA67
- Reference horn antenna: **DH-400SGAHLMB15**
- Probe antenna (measurement antenna): Choke Flange horn antenna (in-house designed antenna)
- Amplification chain as in Table 37
- OMT: Orthomode transducer (Datasheet OTM)
- Power supply: To power the amplifier
- Motor/ cables/ mechanical holders/ transitions

TABLE 39: AMPLIFICATION CHAIN FEATURES

LNA (2 items): **30 dB gain**	SBL-3335033040-2F2F-S1
PA (1 item): **35 dB gain**	SBP-3537033520-VFVF-S1
Heatsinks for PA + LNAs	Used to dissipate the heat of PA & LNAs

5.2.3 Measurement process

QRx antenna characterization process is organized as follows:

1. Reference horn antenna measurement

2. S11 measurements
3. QRx antenna measurement
    - Boresight measurement
    - Scan loss
    - Radiation pattern

5.2.4 Measurement results

5.2.4.1 Reference horn antenna (RHA) measurement

First, we evaluate the RHA correction factor that we are going to use later for the antenna measurement (figure below on the right). This parameter is simply the ratio of S21 measured between RHA and probe antenna for V pol to the same S21 measured for H polarization. This correction allows us to avoid gain error due to misalignment of the DUT antenna with respect to the setup elements.

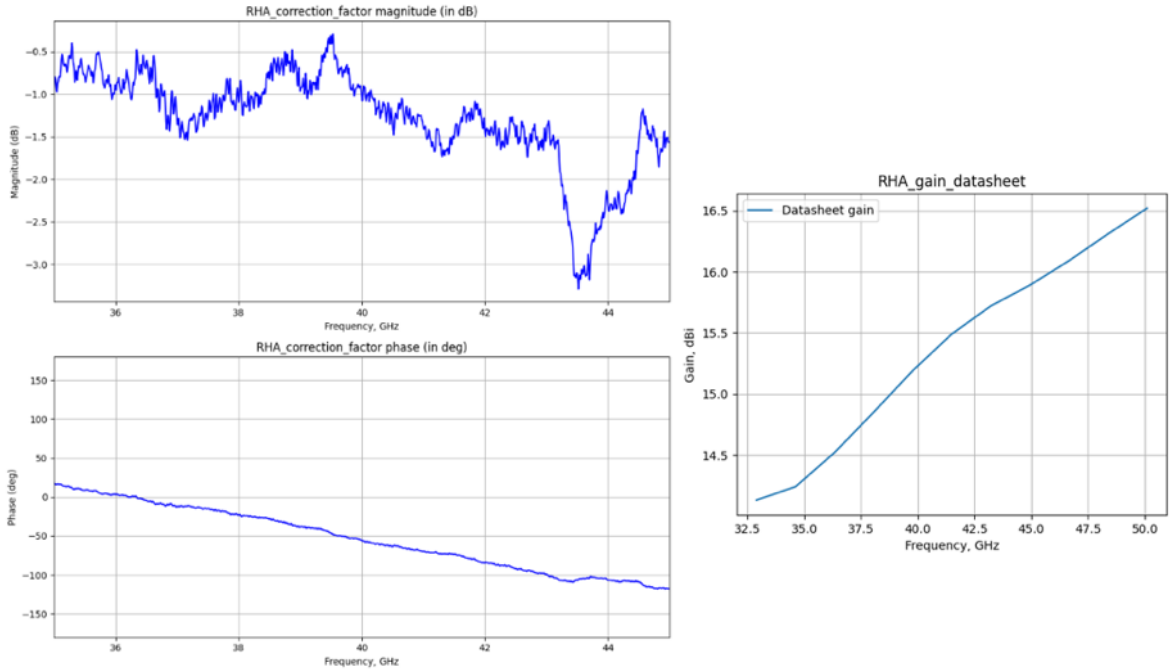

(a) *(b)*

FIGURE 59: GAIN OF THE REFERENCE HORN ANTENNA AND ITS CORRECTION FACTOR.

Figure 59 - (b) represents the gain of RHA as given in the data sheet.

The measured radiation pattern of the antenna is presented in Figure 60. The radiation pattern is plotted as a function of azimuth angle of scan Theta and rotation angle Phi.

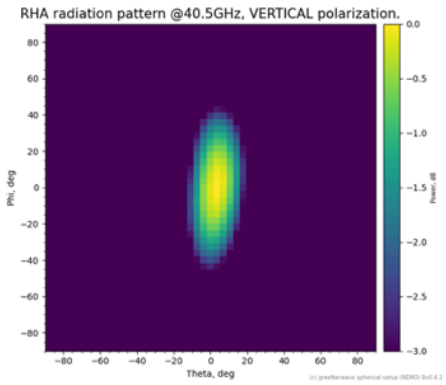

FIGURE 60: RADIATION PATTERN OF RHA

5.2.4.2 Return loss

For this measurement, the AUT's S11 was calculated indirectly using uncalibrated S11 measurements for the AUT and Reference Horn Antenna (RHA), then using the RHA's S11 from datasheet, we can calculate the calibrated S11 of our AUT.

The RHA S11 extracted from the datasheet is calculated using the provided SWR values:

$$|S11| = (SWR - 1)/(SWR + 1)$$

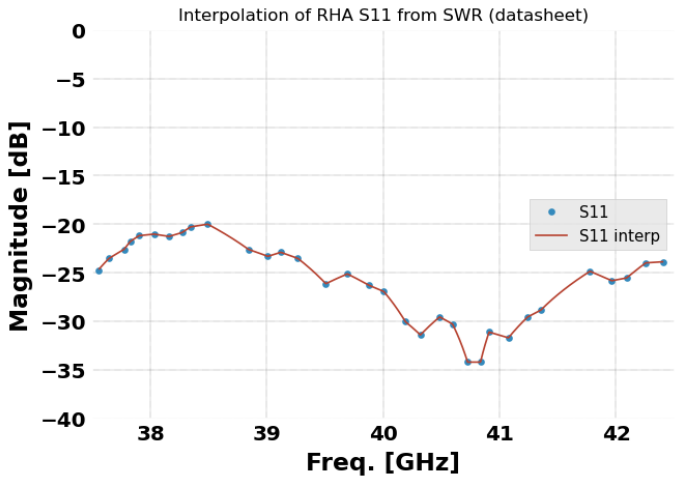

FIGURE 61: RHA S11 EXTRACTED FROM SWR PROVIDED IN DATASHEET

We perform S11 measurement for both AUT and RHA antennas considering the exact same setup. In the case of the AUT, all off configuration is considered for the MTS.

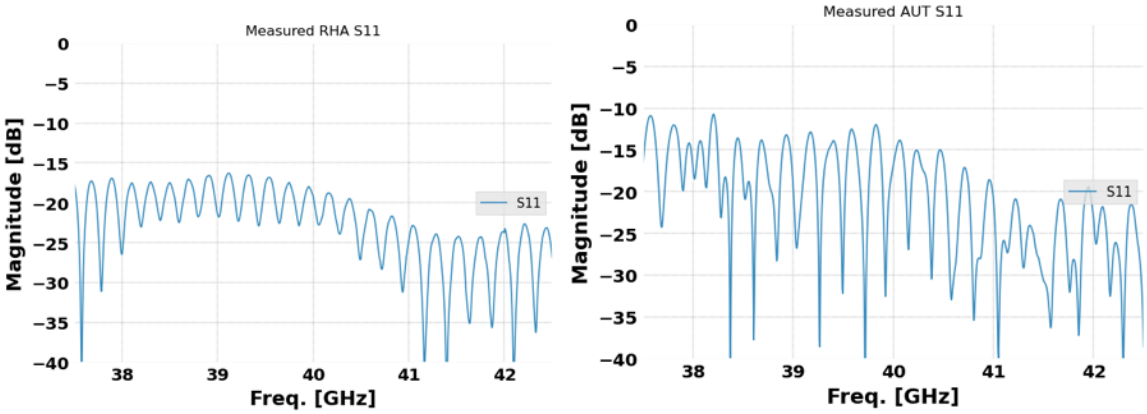

FIGURE 62: MEASURED S11 OF AUT AND RHA WITH UNCALIBRATED MEASUREMENT SETUP

Using the parameters presented before, we can calculate the AUT's S11:

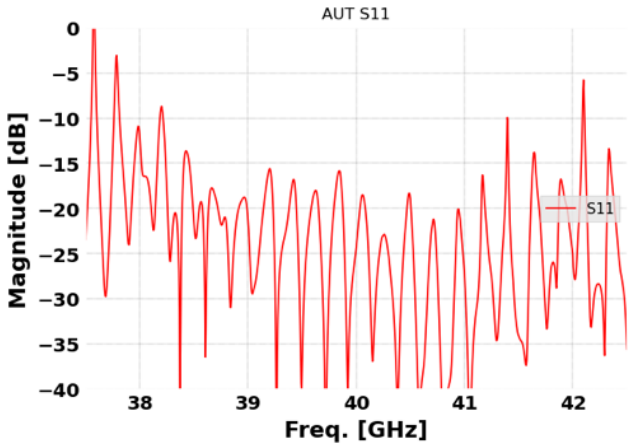

FIGURE 63: RETRIEVED S11 OF QRX ANTENNA

We see that we have some high fluctuations in the resulting AUT S11, this is related to the calculations. We only have few values exceeding the -10 dB at the lower frequency band and the upper frequency band. For the rest of the frequencies, we identified a good antenna matching.

5.2.4.3 Broadside Gain vs. Frequency

Broadside measurement is done for 4 possible polarizations of the antenna radiation: linear (horizontally and vertically polarized) and circular (right and left circular polarization). Antenna calibration was performed with the following settings for RHA measurement:

TABLE 40: BROADSIDE MEASUREMENTS PARAMETERS

Parameters	Values
Frequency range	37.5 GHz – 42.5 GHz (25 points) (200 MHz step)
Inst. Bandwidth	100 MHz
Polarization	RHCP, LHCP, HLP, VLP

Optimization procedure	PbP – 5 loops with no kick (as first value)

Results for gain and realized gain are presented in the figures below (Table 41):

TABLE 41: BROADSIDE GAIN RESULTS

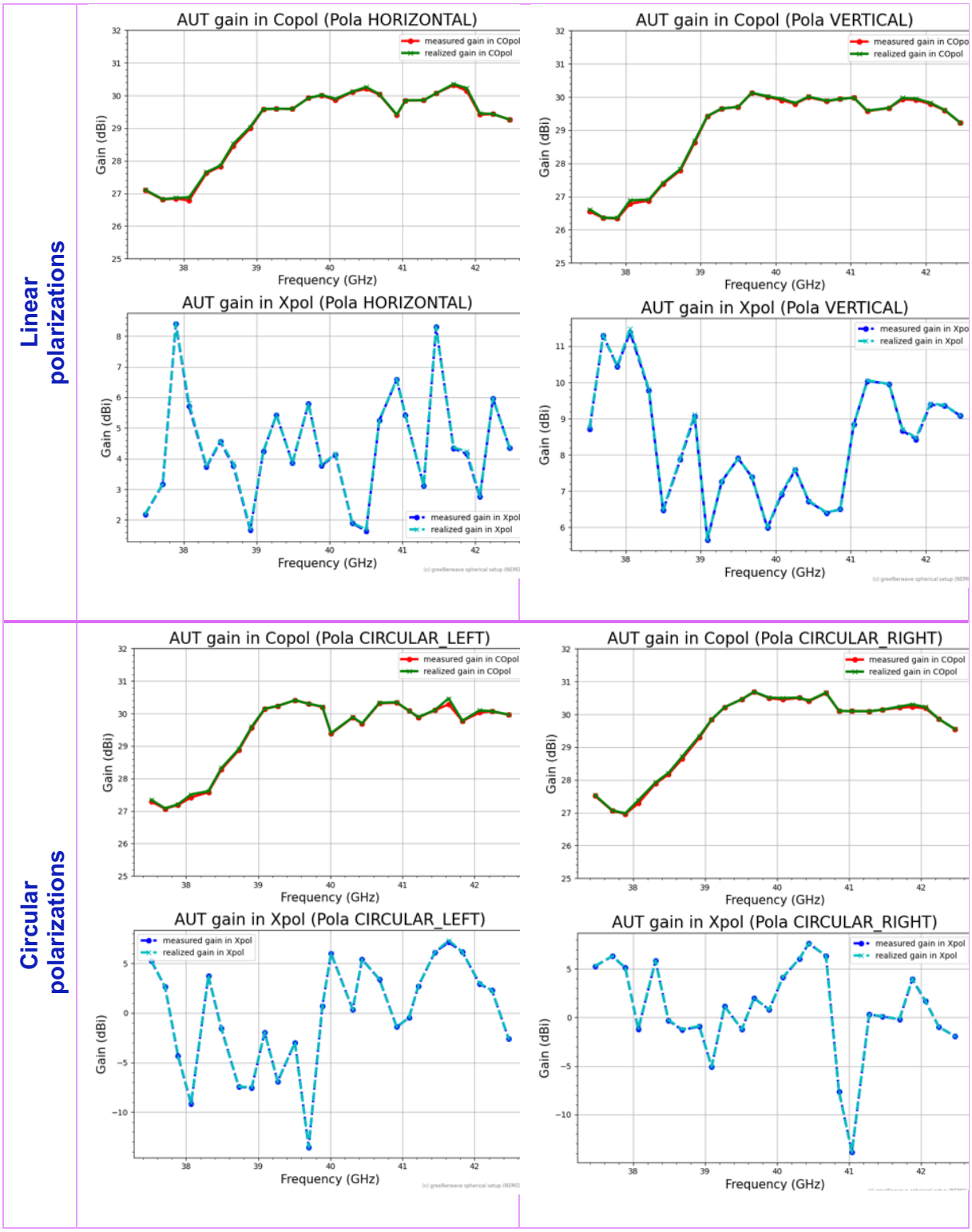

The gain of QRx antenna outperforms the gain values fixed in the specifications (25.5 dBi) for the four polarizations (H, V, RHCP, LHCP). Gain for linear polarizations (V and H) is higher

than 26.2 dBi for all the frequency band. For circular polarizations (LHCP, RHCP), the gain is higher than 27 dBi for all the frequency band.

For all the polarization, the gain presents a drop at the lower frequency band (37.5 GHz – 39.5 GHz) and slightly above 42 GHz, this could be related to MTS and feeder performances at these frequencies:

- In Table 38, for frequencies < 39 GHz, the MTS presents a low phase difference between On and Off states. However, the dissipation level is very good (|S11| > -1dB).
- For frequencies < 39.5 GHz and > 42 GHz, the feeder presents a higher leakage compared to the rest of the frequency band.

TABLE 42: MTS1 MEASUREMENT RESULTS

	Amplitude		Phase	
	TE	TM	TE	TM
MTS1	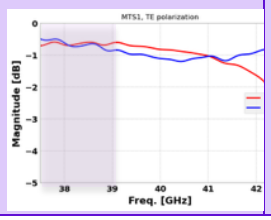	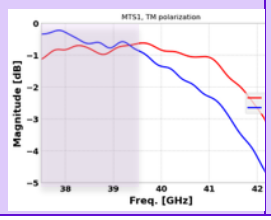	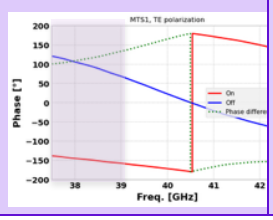	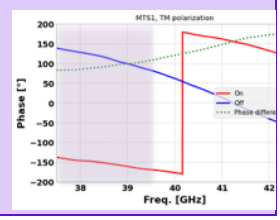

TABLE 43: AFS CHARACTERIZATION RESULTS

	37.5 GHz	38.5 GHz	39.5 GHz	40.5 GHz	41.5 GHz	42.5 GHz
UOF	0.41	0.42	0.41	0.41	0.40	0.40
Spillover (%)	**9.16**	**8.9**	**9.18**	6.4	7.36	**8.57**

Despite this drop in the gain, the QRx antenna is still above the expected gain specifications.

5.2.4.4 Scan loss

Scan loss represents the reduction in the gain of the steered beam as compared with the maximum gain at antenna broadside direction. For QRx antenna scan loss measurements, we considered the following measurement parameters (Table 44). The standard metasurface optimization procedure described above has been used to find and establish the proper configuration providing the antenna beamforming in the required direction at the required frequency.

TABLE 44: SCAN LOSS MEASUREMENTS PARAMETERS

Parameters	Values
Frequency range	37.5 GHz – 42.5 GHz (25 points) (200 MHz step)
Angular beamforming	-70°-70° /Step of Theta = 10°

Inst. Bandwidth	100 MHz
Polarization	HLP, VLP
Optimization procedure	PbP – 5 loops with no kick (as first value)

We consider three frequency points (**39.5 GHz**, **40.5 GHz** and **41.5 GHz**) and 5 different values of Phi angles including the broadside. Scan loss is then plotted for a Theta angle rage [-70° 70°] with a step of 10° and linear polarizations (V pol and H pol). Results are presented in Table 45 and Table 46:

Horizontal polarization

TABLE 45: SCAN LOSS RESULTS FOR H POLARIZATION

	39.5 GHz	**40.5 GHz**	**41.5 GHz**
Phi = 0°	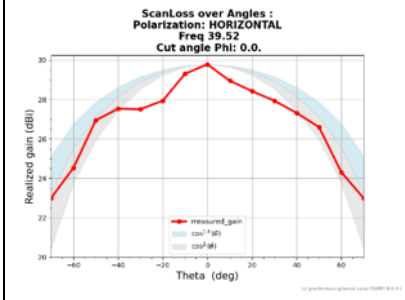	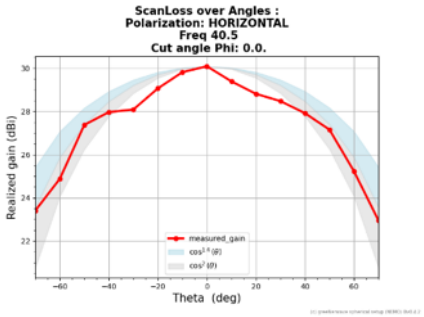	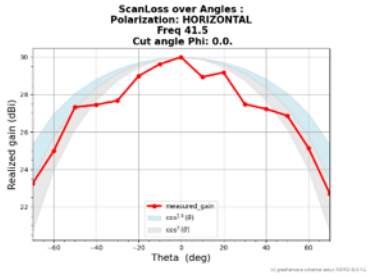
Phi = 45°	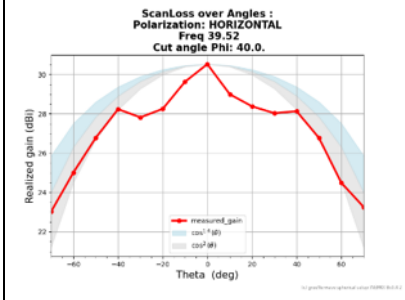	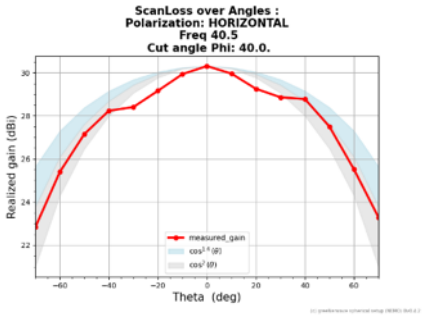	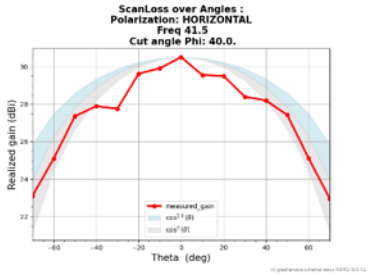

Phi = 90°	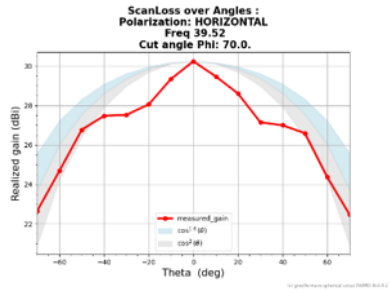	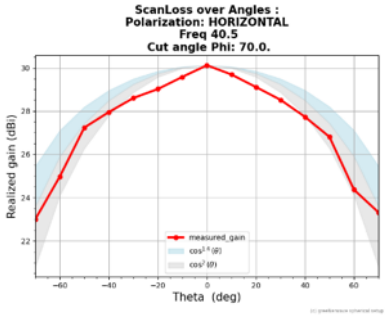	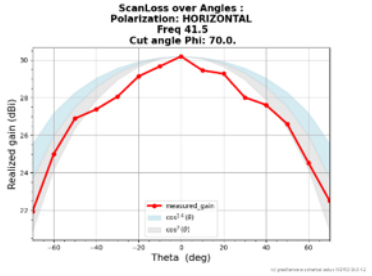

Vertical polarization

TABLE 46: SCAN LOSS RESULTS FOR V POLARIZATION

	39.5 GHz	40.5 GHz	41.5 GHz
Phi = 0°	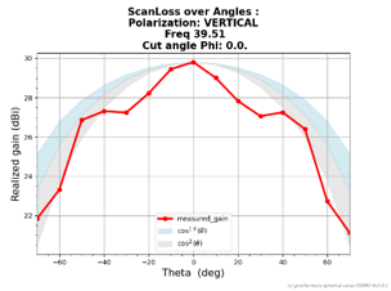	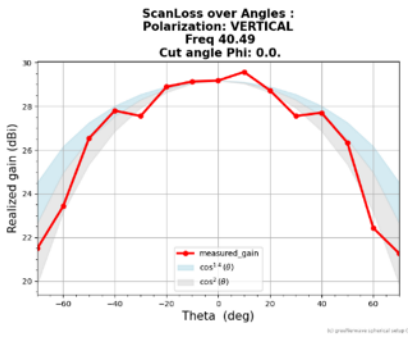	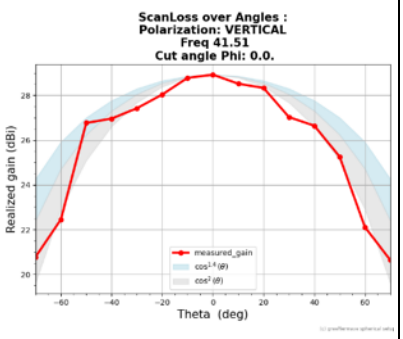
Phi = 45°	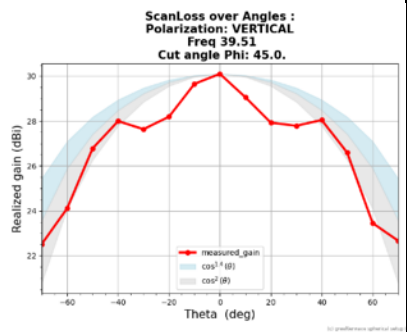	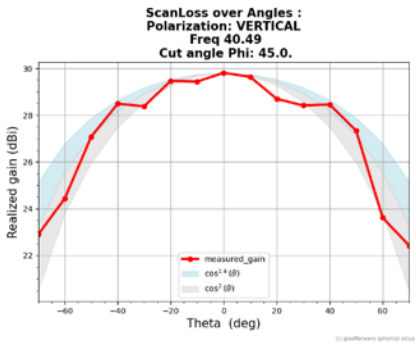	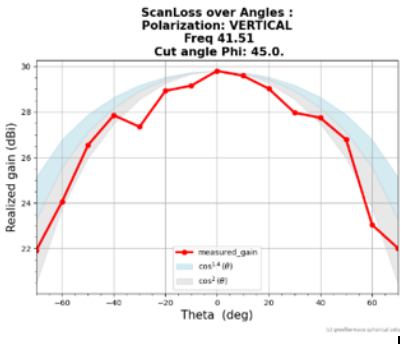

Phi = 90°	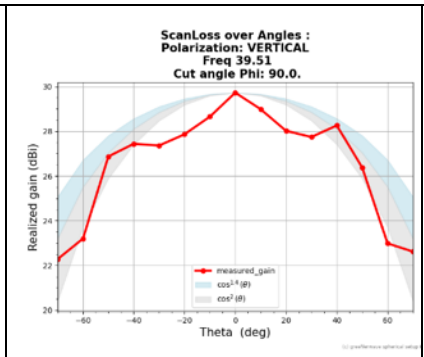	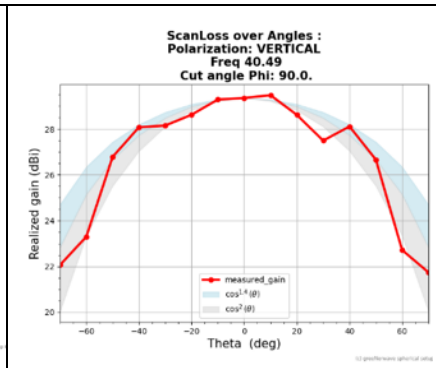	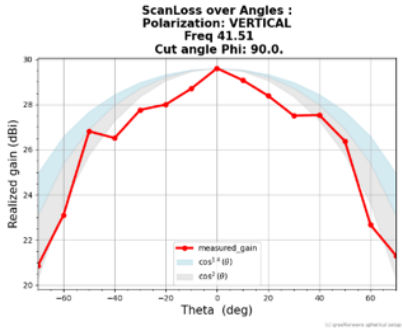

5.2.4.5 Directivity, aperture, rf and total efficiencies

The directivity was calculated through the combined maximum power radiated in both co-pol and cross-pol (for linear and circular polarizations).

Aperture efficiencies were calculated taking the aperture size as 200x200 mm2.

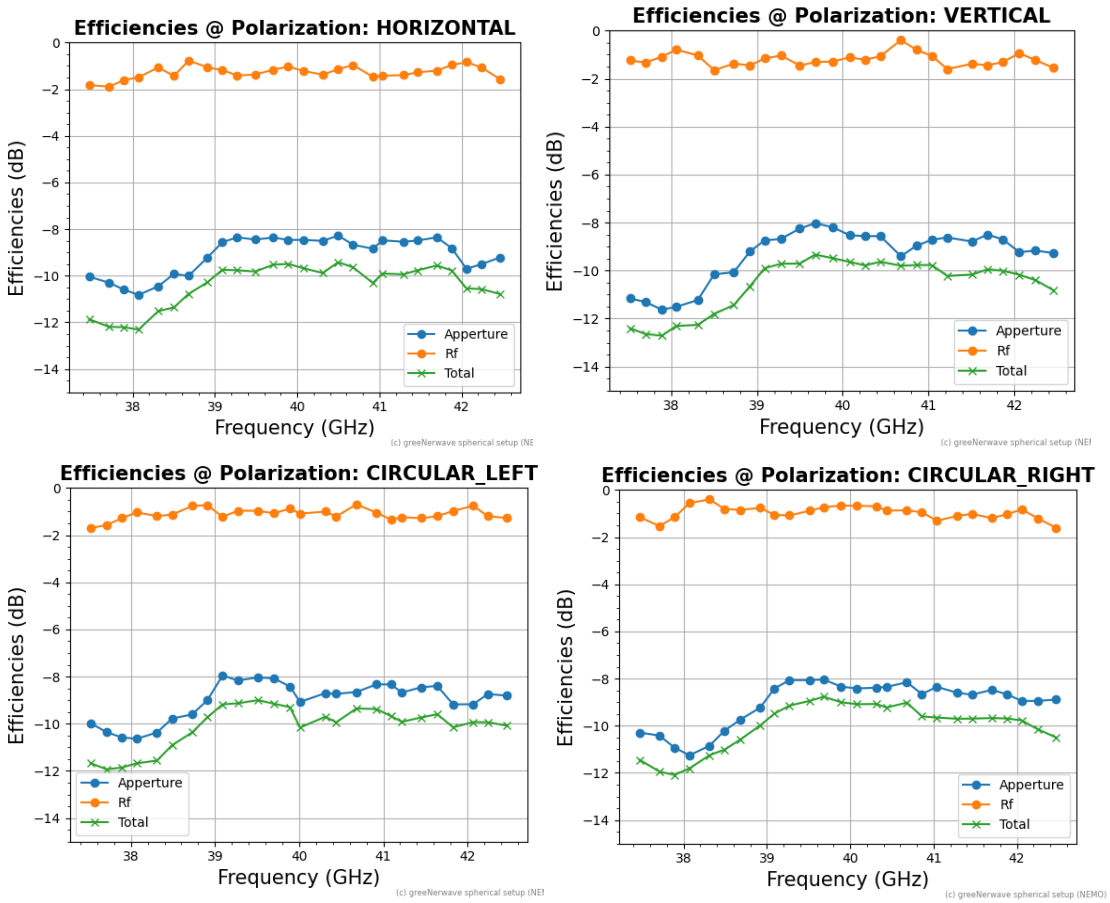

FIGURE 64: EFFICIENCIES VS FREQUENCY FOR DIFFERENT POLARIZATIONS

Total efficiency is around -10 dB for frequencies higher than 39 GHz, from 37.5 GHz to 39 GHz toral efficiency varies from -12.5 dB to -10 dB. These values outperform what is specified in the specs.

Radiation pattern

Results are presented for three frequency points from the QRx band (39.5 GHz, 40.5 GHz and 41.5 GHz) and for the four polarizations (V, H, RHCP, LHCP)

Radiation pattern measurements were performed considering the following settings

TABLE 47: RADIATION PATTERN MEASUREMENT PARAMETERS

Parameters	Values
Theta range	-70° : 70° / step of 10°
Phi range	0°, 45°, 90°
Frequency range VNA	37.5 GHz – 47.5 GHz (25 points) (200 MHz step)
Polarization	V, H, RHCP or LHCP

Radiation pattern at 39.5 GHz

TABLE 48: RADIATION PATTERN FOR PHI= 0°, 45° AND 90°

Vertical @ 39.5 GHz	**Horizontal @ 39.5 GHz**
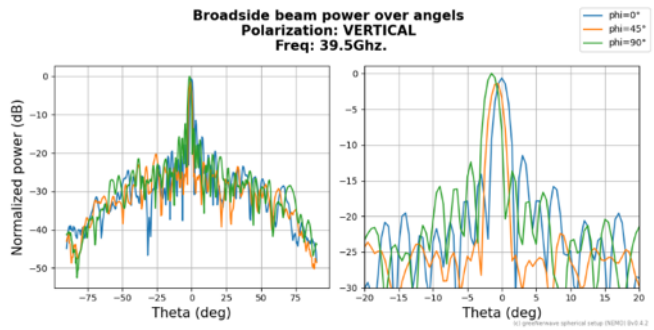	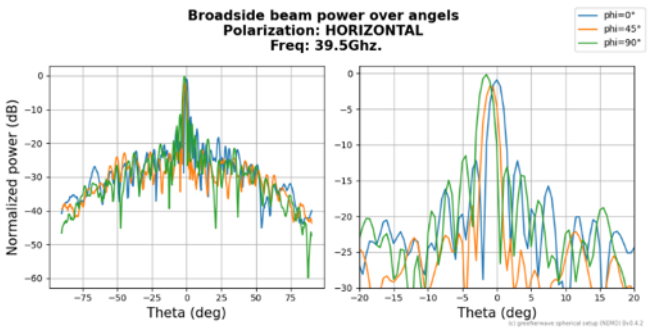
RHCP @ 39.5 GHz	**LHCP @ 39.5 GHz**

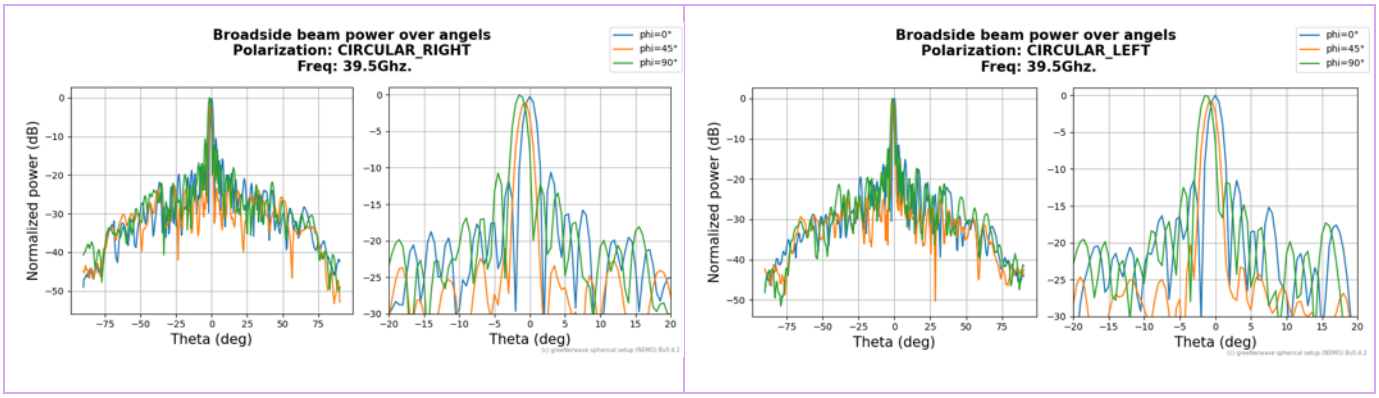

TABLE 49: RADIATION PATTERN FOR DIFFERENT POLARIZATIONS

Phi = 0° @ 39.5 GHz	Phi = 45° @ 39.5 GHz
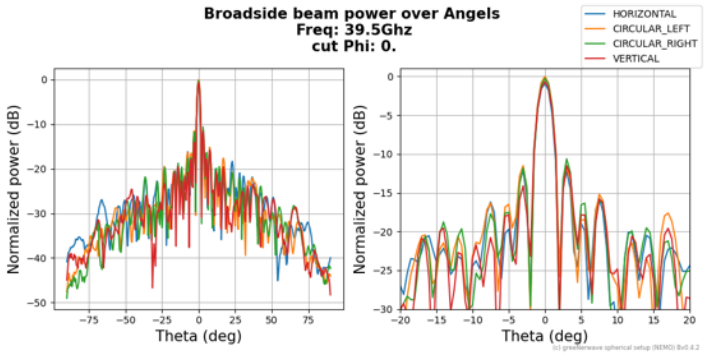	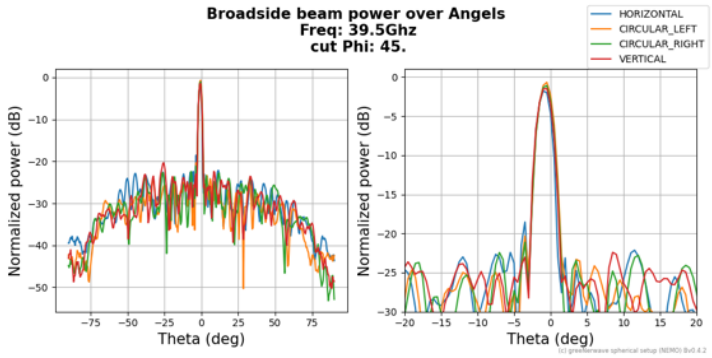
Phi = 90° @ 39.5 GHz	
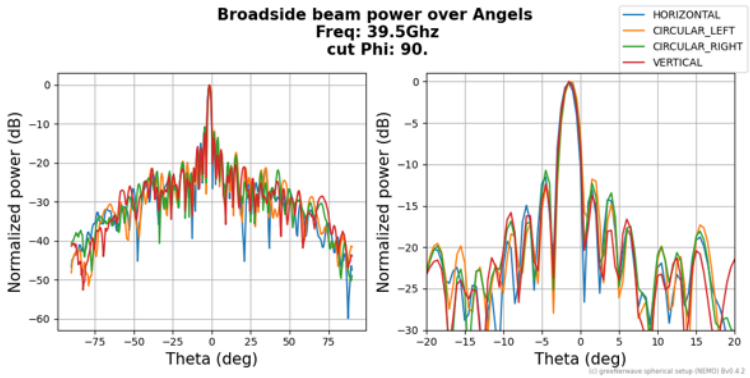	

Radiation pattern at 40.5 GHz

TABLE 50: RADIATION PATTERN FOR PHI= 0°, 45° AND 90°

Vertical @ 40.5 GHz	Horizontal @ 40.5 GHz

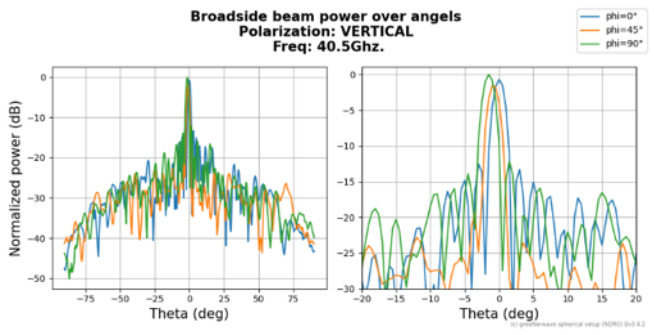	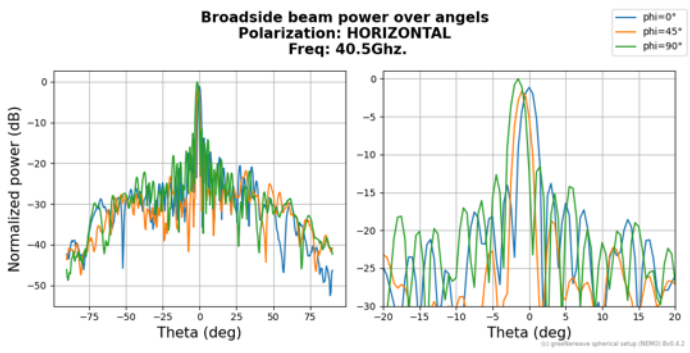
RHCP @ 40.5 GHz	**LHCP @ 40.5 GHz**
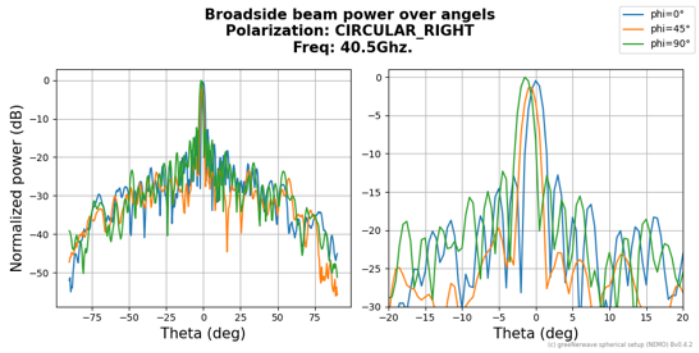	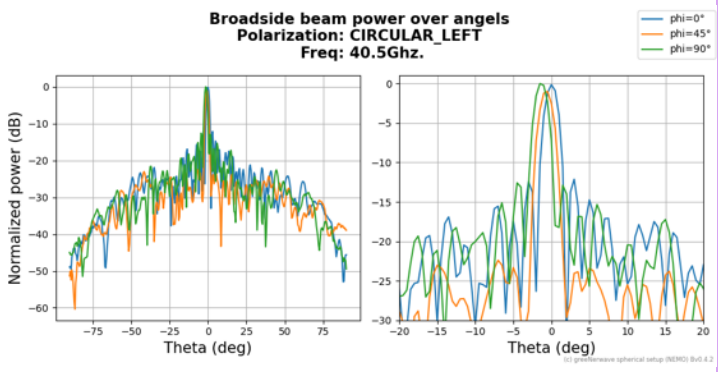

TABLE 51: RADIATION PATTERN FOR DIFFERENT POLARIZATIONS

Phi = 0° @ 40.5 GHz	**Phi = 45° @ 40.5 GHz**
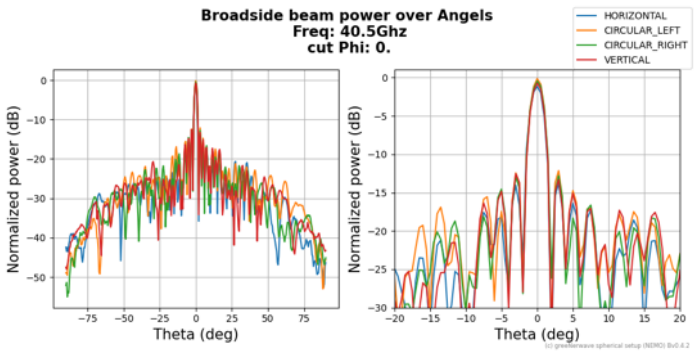	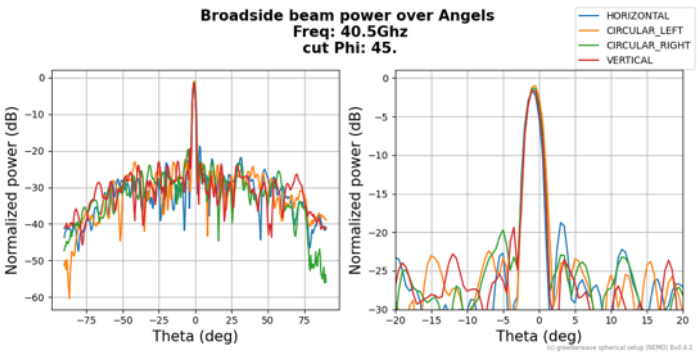
Phi = 90° @ 40.5 GHz	

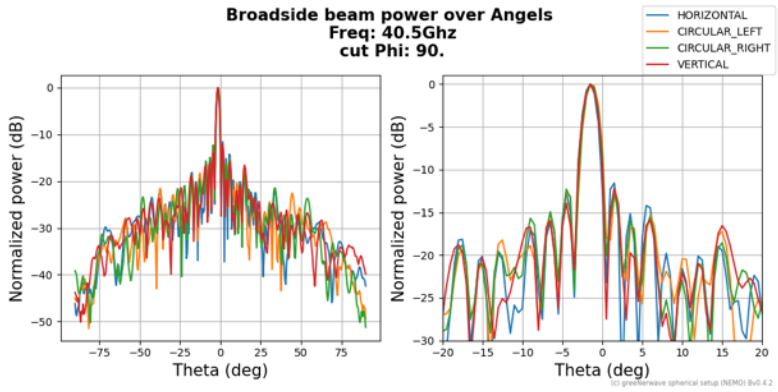

Radiation pattern at 41.5 GHz

TABLE 52: RADIATION PATTERN FOR PHI= 0°, 45° AND 90°

Vertical @ 41.5 GHz	Horizontal @ 41.5 GHz
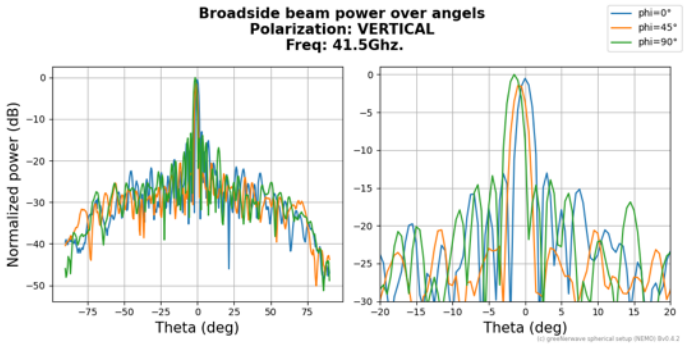	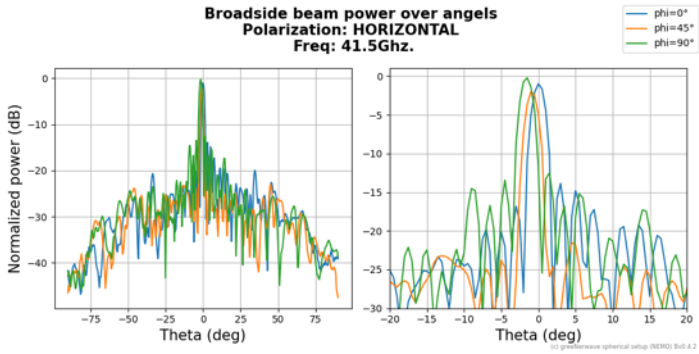
RHCP @ 41.5 GHz	**LHCP @ 41.5 GHz**
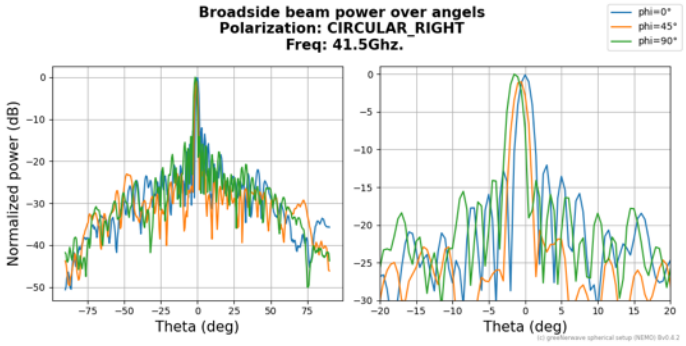	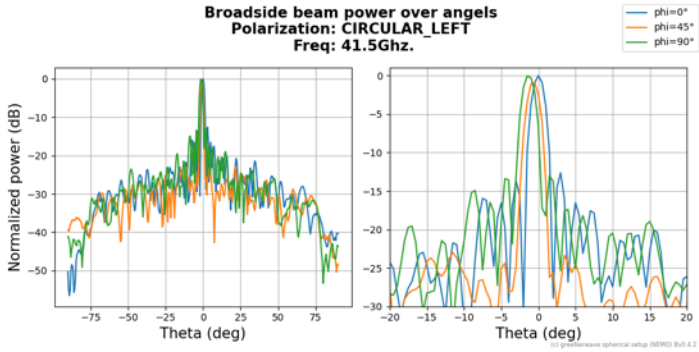

TABLE 52: RADIATION PATTERN FOR DIFFERENT POLARIZATIONS

Phi = 0° @ 41.5 GHz	Phi = 45° @ 41.5 GHz

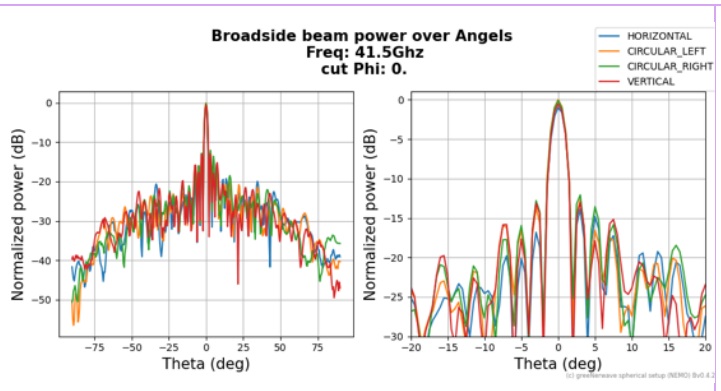

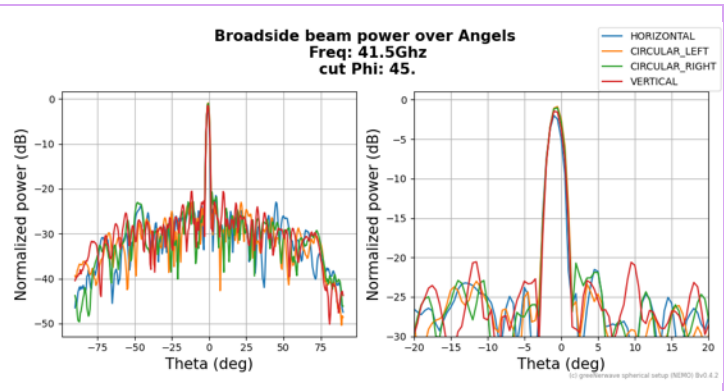

Phi = 90° @ 41.5 GHz

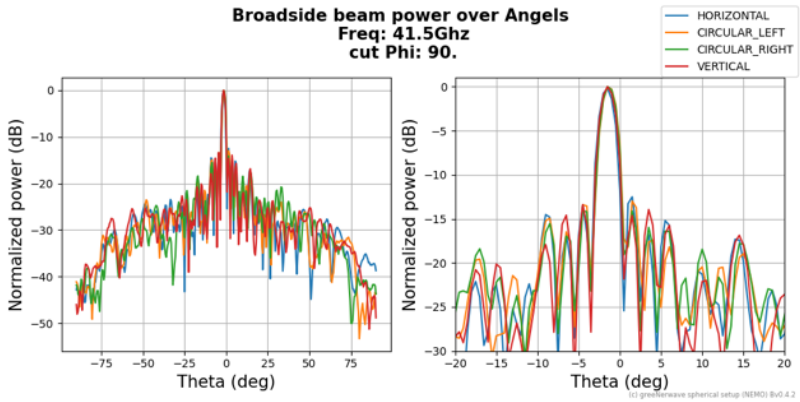

We identify a first side lobe level of -11 dB for 39.5 GHz and -12.5 dB to -15 dB for higher frequencies (40.5 GHz and 41.5 GHz). These values are higher than the SLL mentioned in the specifications.

The shift in the radiation pattern for different Phi angles might be related to a misalignment of the setup between AUT and the probe antenna.

5.3 VTX ANTENNA CHARACTERIZATION

In this part of the report, we will present characterization results related to VTx antenna, a first part will be dedicated to the V2 VTx diode based MTS chatracterization results.

Five (05) V2 VTx where fabricated (4 MTSs for the antenna and one spare). The size of the MTSs is 10cmx10cm and every MTS has a total of 576 pixels (24 pixels x 24 pixels). VTx antenna size is arround 21cm x 21cm, and, it is composed of 4 MTSs.

In the next section we will present the measurement setup and results for bistatic charcaterization of V2 VTx MTSs.

5.3.1 MTS measurements Setup

In the same bistatic measurement setup used for QRx MTSs, we performed VTx MTSs measurements: TE, TM and Cross polarization for all the 5 MTSs.

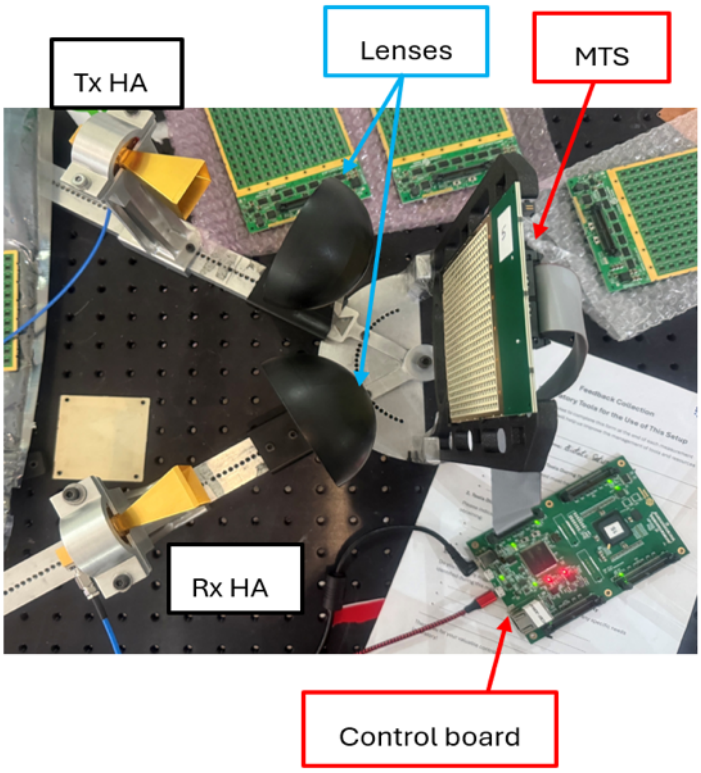

FIGURE 65: BISTATIC MTS CHARACTERIZATION SETUP: VNA, CONTROL BOARD, 2 HORN ANTENNAS, LENSES AND CABLES

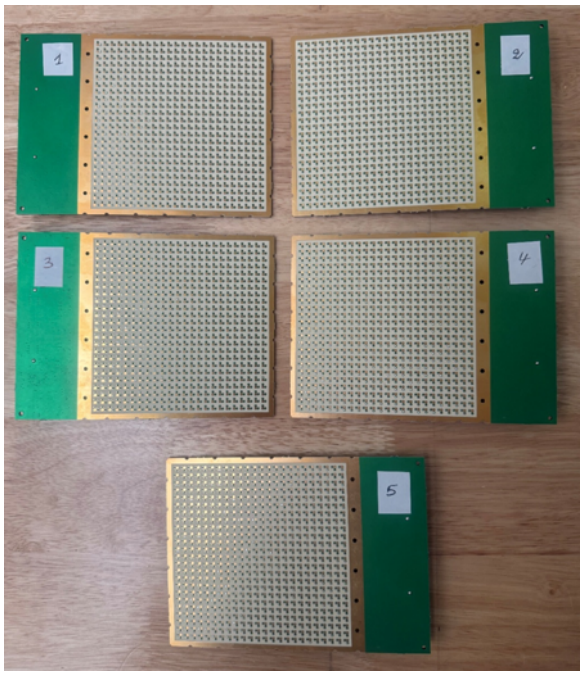

FIGURE 66: THE CHARACTERIZED 5 SAMPLES OF V2 VTX

The used setup elements are presented in the table below:

TABLE 53: SETUP NEEDS FOR MTS BISTATIC CHARACTERIZATION

Item	Description
VNA	Rohde & Schwarz ZNA67
RHA (reference horn antennas)	Reference horn antennas (Rx and Tx)
Control board	To control the Pixel states (Ref: CBFV2.1)
Power supply	12 V: to power the MTS & CB
Cables / transitions	2 coax cables: 0.9 m + ribbon cable

5.3.2 MTS measurements Results

Measurement results are presented in Tables 54, 55, and 56

5.3.2.1 TE polarization

TABLE 54: CO-POLARIZATION (TE) MEASUREMENT RESULTS FOR THE 5 MTSS

MTS	Amplitude	Phase
MTS1	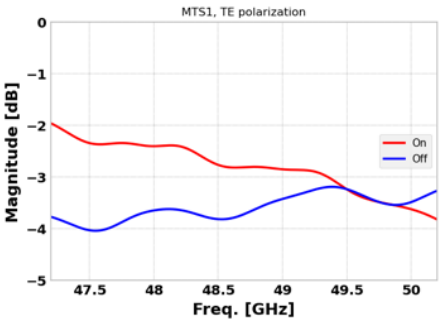	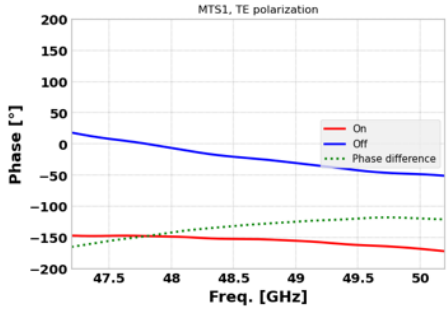
MTS2	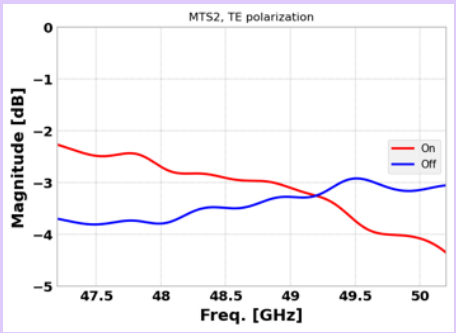	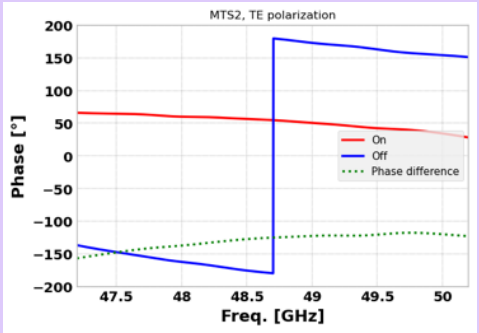
MTS3	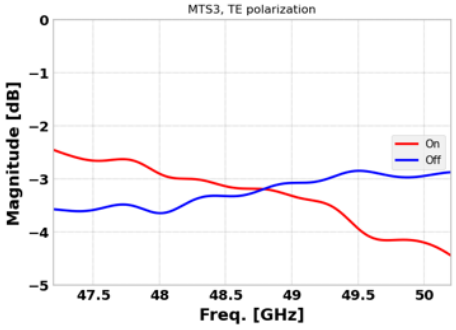	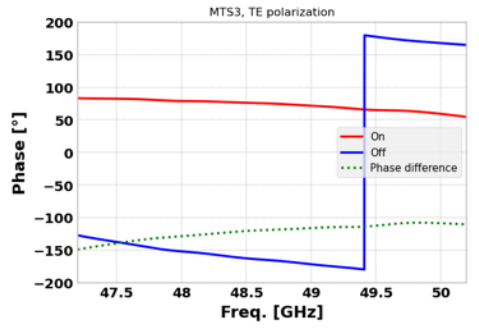

MTS4	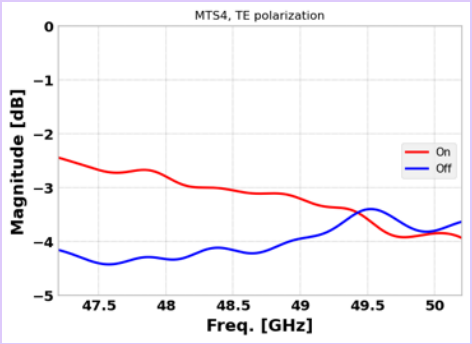	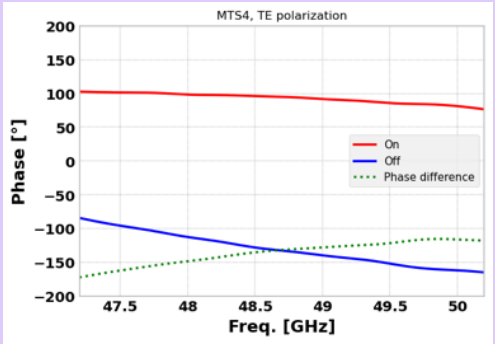
MTS5	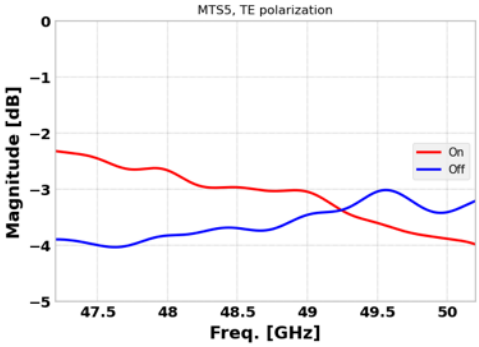	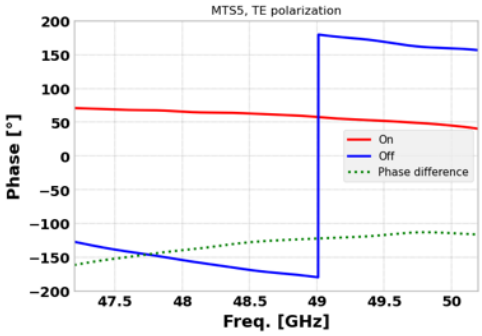

5.3.2.2 TM polarization

TABLE 55: CO-POLARIZATION (TM) MEASUREMENT RESULTS FOR THE 5 MTSS

MTS	Amplitude	Phase
MTS1	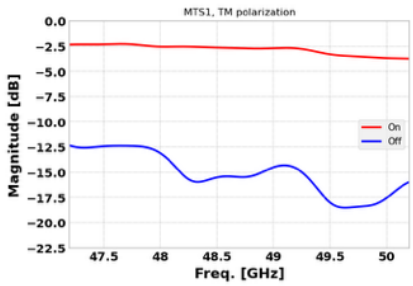	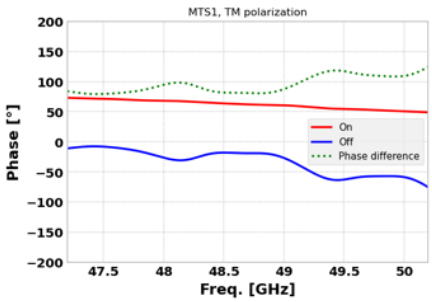
MTS2	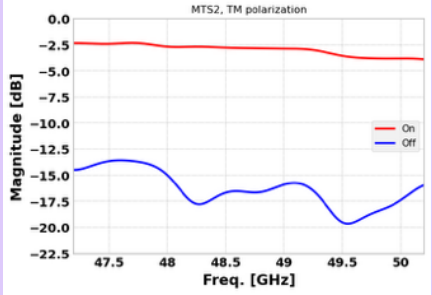	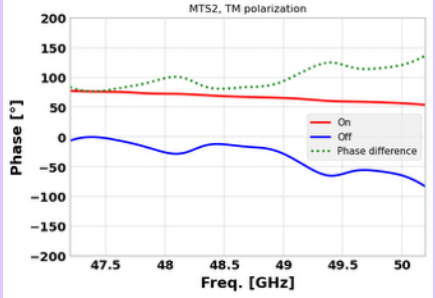

MTS3	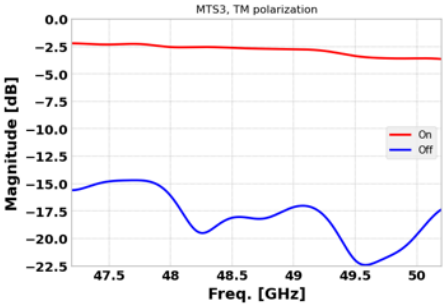	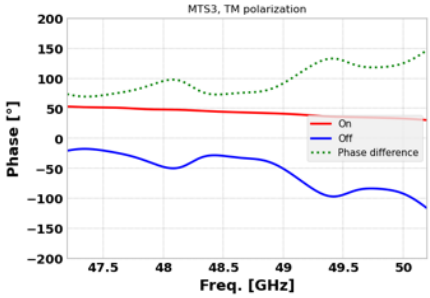
MTS4	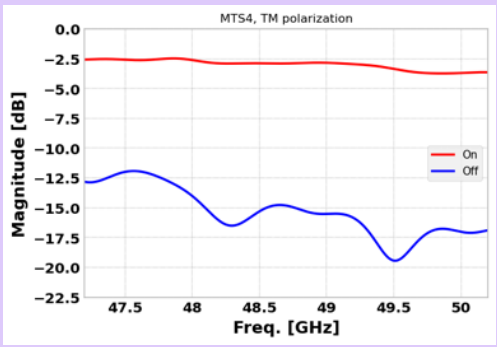	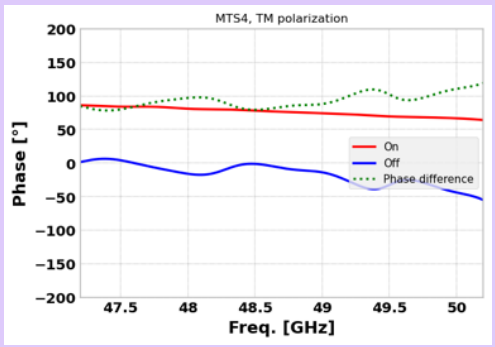
MTS5	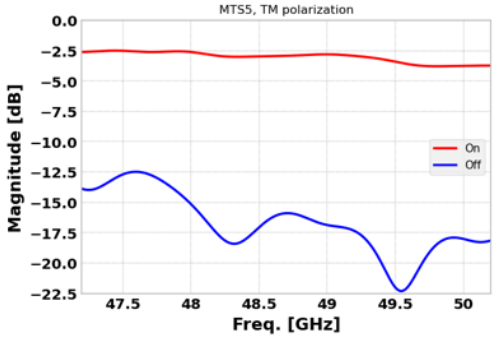	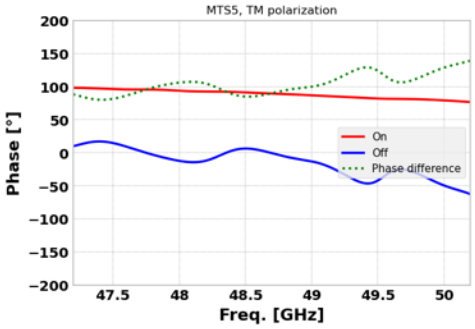

5.3.2.3 Cross polarization

TABLE 56: CROSS-POLARIZATION MEASUREMENT RESULTS FOR THE 5 MTSS

MTS	Amplitude	MTS	Amplitude
MTS1	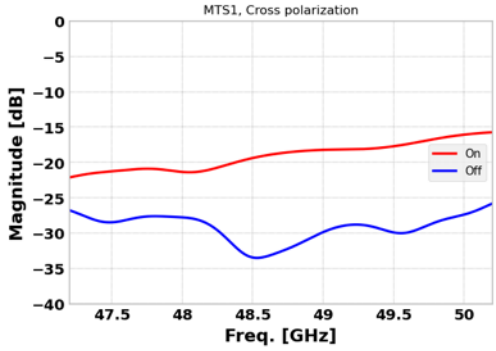	**MTS2**	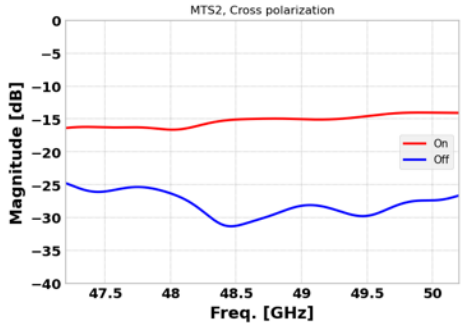

MTS3	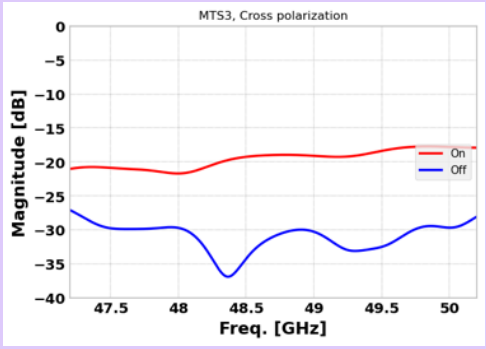	MTS4	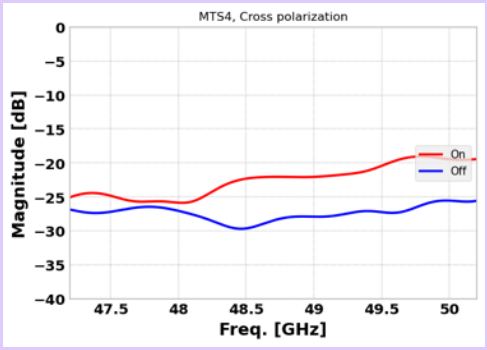
MTS5	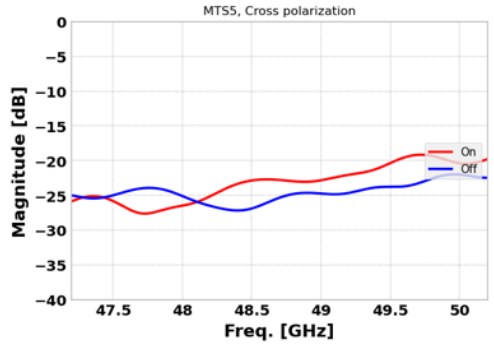		

All the 5 MTS were tested, and most presenting 100% diode detection.

Bistatic measurements results for the 5 MTS samples are quite similar. For each MTS, the RHA should be rotated to have different polarizations (V,H and Xpol). The small differences between all MTSs measurements could be due to the horn positioning on the holder (holder not adapted to fix perfectly the horn horizontally and vertically.

Dissipation in TE mode is between -2 dB and -4 dB for samples 1,2,3 and 5. For sample 4, dissipation is higher than -4 dB in the off state. The phase shift is very similar.

For TM mode, dissipation level is very similar. In the On state, it is between -4 dB and -2.5 dB and in the Off state it is < -12.5 dB for samples 1, 4 and 5 and < -14 samples 2 and 3.

Cross pol is lower than -15 dB for all samples.

5.4 V2 VTX MINI-MTS MEASUREMENT (SAMPLE 2)

In the table below, we compare measurement results for the V2 VTx mini-MTS best sample (sample2) and V2 VTx MTS best sample (sample 1). The best sample represents results of the best prototype selected among multiply tested samples.

TABLE 57: CROSS-POLARIZATION, CROSS POLARIZATION MEASUREMENTS OF BEST MINI MTS AND MTS SAMPLES

	V2 VTx Mini MTS best sample (sample2)		V2 VTx MTS best sample (sample1)	

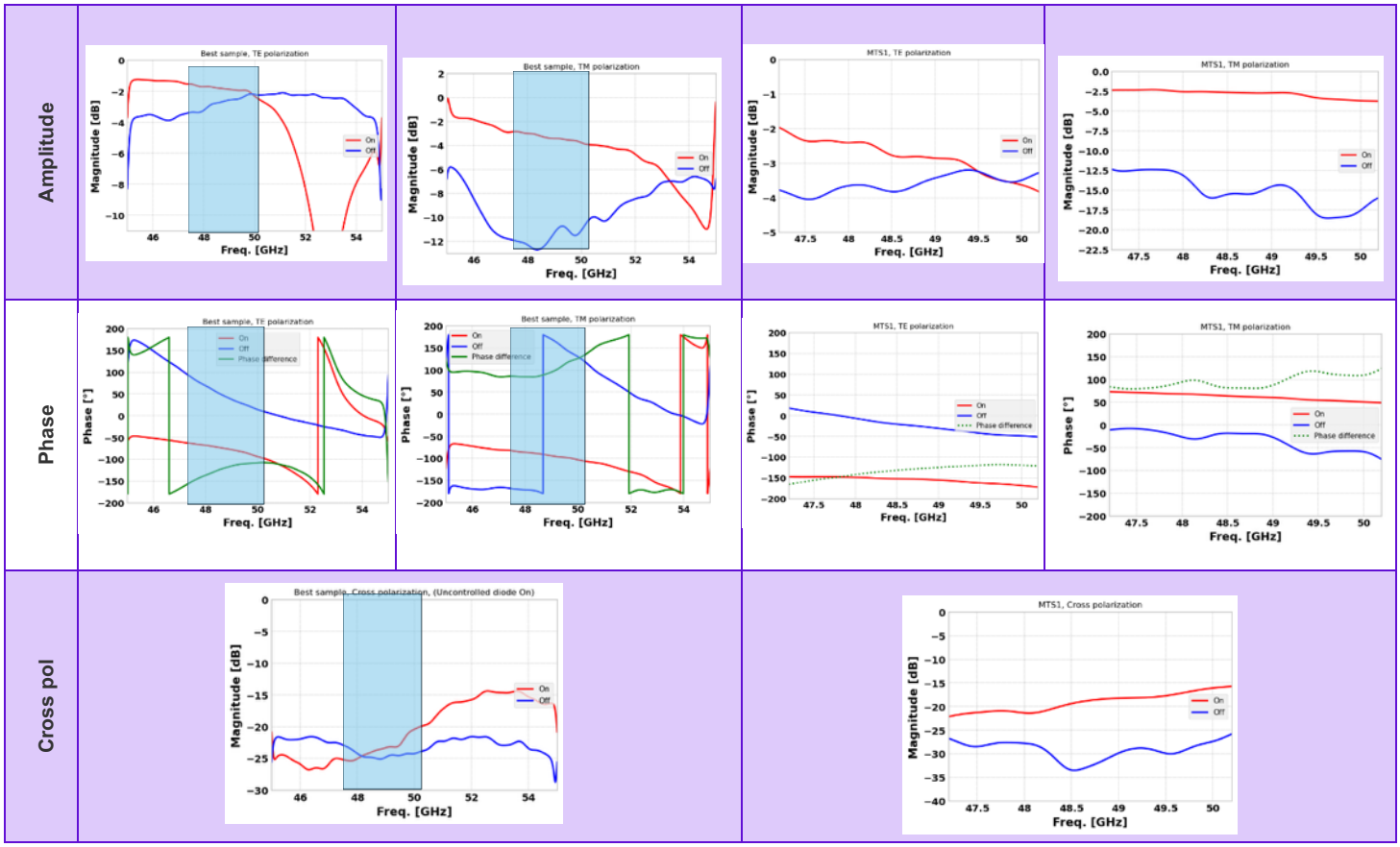

Measurements of V2 VTx MTS best sample are compared with the mini-MTS best sample. Results showed good agreement with the best sample measurements. This validates the performance and the fabrication of the MTS considering the selected design (Sample 2 of VTx mini-MTS). The design was considered due to time constraints that did not allow us to have a second design iteration.

5.4.1 Presentation of the AUT

The antenna under test is: VTx antenna

- Metasurface: V2 VTx
  - **Design:** one layer diode-based MTS (total of 4608 diodes)
  - **Size:** MTS 20cmx20cm composed of four 10cmx10cm MTSs
- **Cavity**: aluminum of 4.37cm height.
- **Antenna Feeder**: aluminum, 16 sources (different from QRx feeder sources) and WR19 input port
- **Mask:** one layer PCB mask with slot pattern (facing the inside of the cavity), uniform with 65% transmittance

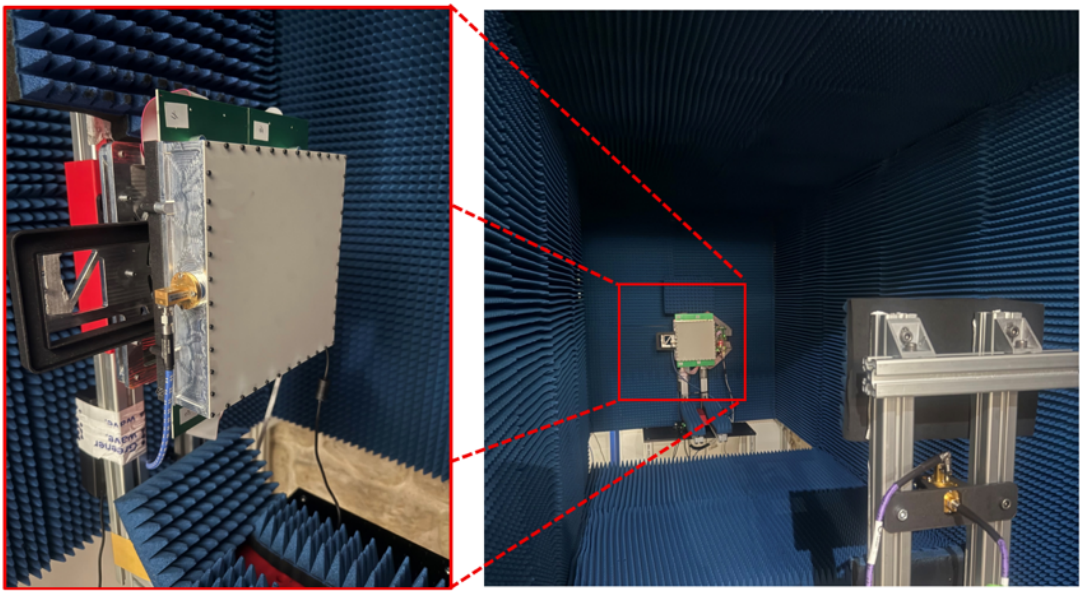

FIGURE 67: AUT ON THE CHARACTERIZATION SETUP

5.4.2 Experimental setup

VTx antenna characterization was conducted in the same setup (Nemo spherical near field setup located in Greenerwave's premises at Paris). For this measurement setup, we needed the following components:

- VNA: Rohde & Schwarz ZNA67
- Reference horn antenna: **LB-19-20-C-1.85F**
- Probe antenna (measurement antenna): Choke Flange horn antenna (inhouse designed antenna)
- Amplification chain:

LNA (2 items): 30 dB gain	SBL-3335033040-2F2F-S1
PA (1 item): 35 dB gain	SBP-3537033520-VFVF-S1
Heatsinks for PA + LNAs	Used to dissipate the heat of PA & LNAs

- OMT: Orthomode transducer (Datasheet OTM)
- Power supply: To power the amplifier
- Motor/ cables/ mechanical holders/ transition

5.4.3 Measurement process

The same measurement process is followed for VTx antenna characterization:

1. Reference horn antenna measurement

2. S11 measurements
3. VTx antenna measurement
   - Boresight measurement
   - Scan loss
   - Radiation pattern

5.4.4 Measurement results

5.4.4.1 Reference horn antenna (RHA) measurement

First, we evaluate the RHA correction. This correction allows us to avoid gain error due to misalignment of the DUT antenna with respect to the setup elements.

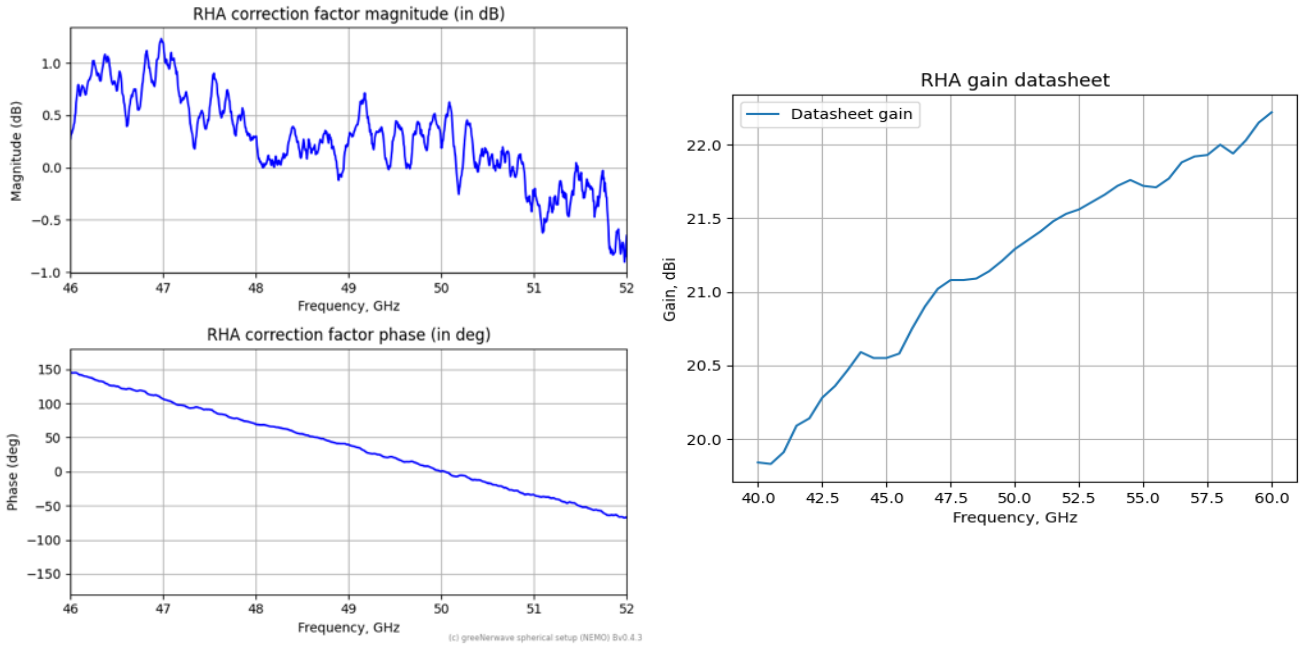

FIGURE 68: GAIN OF THE REFERENCE HORN ANTENNA AND ITS CORRECTION FACTOR

Figure 68 on the right side represents the correction factor of the RHA. On the right, its gain as given in the data sheet is represented.

Co-funded by the European Union

The measured radiation pattern of the antenna is presented in Figure 69.

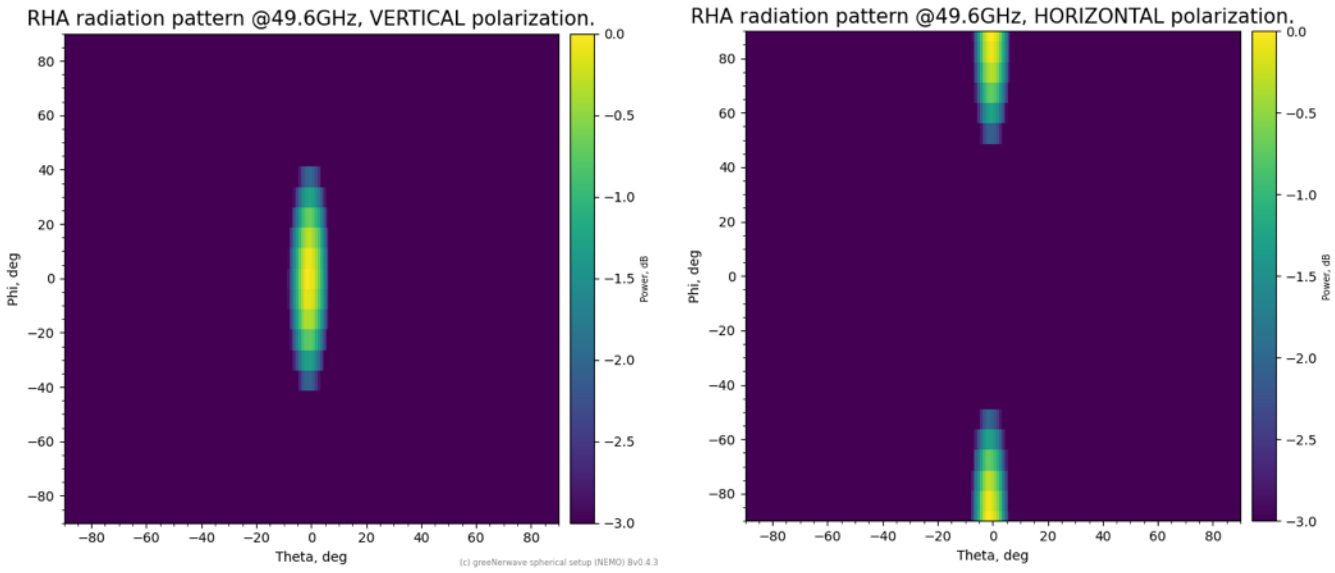

FIGURE 69 RADIATION PATTERN OF RHA

The radiation pattern is plotted as a function of azimuth angle of scan Theta and rotation angle Phi. This explains the elongated shape of the pattern.

For horizontal polarization, the maximum radiation is obtained at Phi = +/- 90°, which explains the split in the plotted radiation pattern.

5.4.4.2 Return loss

For this measurement, the AUT's S11 was calculated indirectly following the same procedure as with QRx antenna.

The RHA S11 extracted from the datasheet is calculated using provided SWR values:

$$|S11| = (SWR - 1)/(SWR + 1)$$

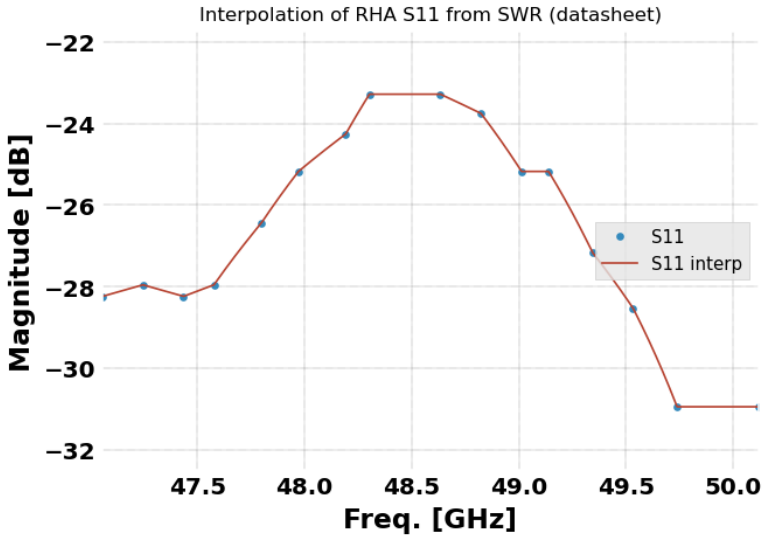

FIGURE 70 RHA S11 EXTRACTED FROM SWR PROVIDED IN DATASHEET

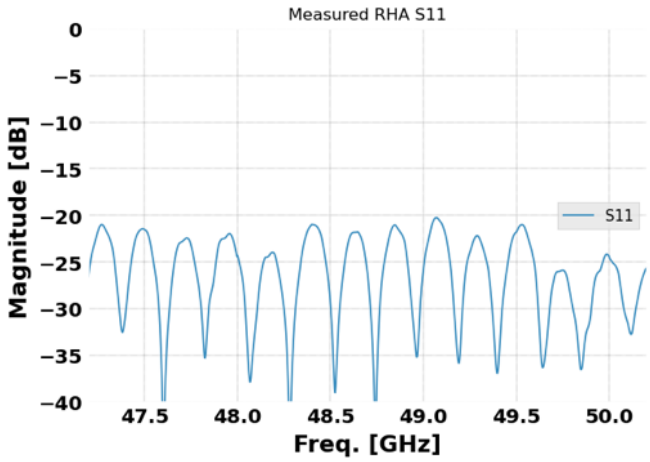

FIGURE 71: MEASURED S11 OF RHA WITH UNCALIBRATED MEASUREMENT SETUP

We perform S11 measurements for both AUT and RHA antennas considering the exact same setup. In the case of the AUT, all off configuration is considered for the MTS.

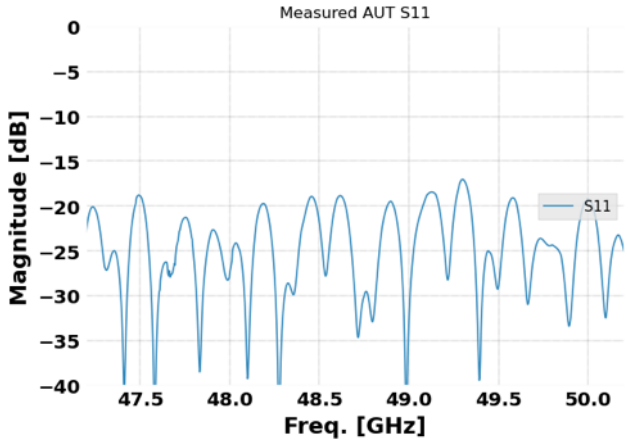

FIGURE 72 MEASURED S11 OF AUT WITH UNCALIBRATED MEASUREMENT SETUP

Using the parameters presented before, we can calculate the AUT's S11:

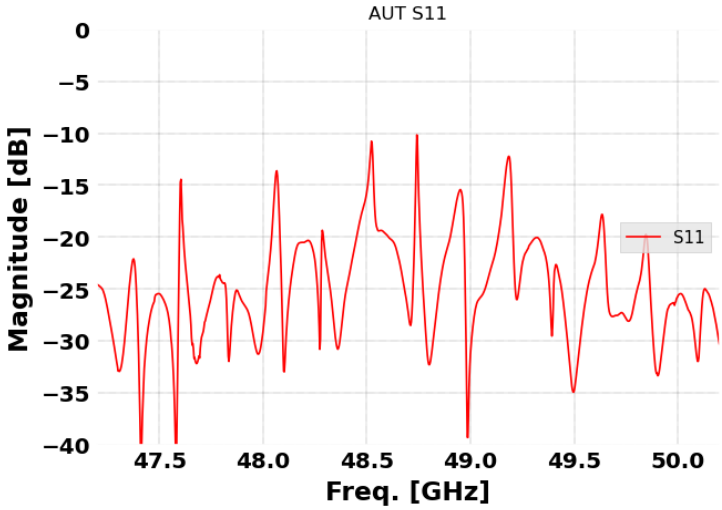

FIGURE 73 RETRIEVED S11 OF VTX ANTENNA

We see that there are some high fluctuations in the resulting AUT S11, this is related to the calculations. However, none of the values is exceeding the -10 dB though.

5.4.4.3 Broadside Gain vs. Frequency

Broadside measurement is done for all 4 polarizations. Antenna calibration was performed with the following settings for RHA measurement.

TABLE 58: BROADSIDE MEASUREMENT PARAMETERS

Parameters	Values
Frequency range	37.2 GHz – 50.2 GHz (21 points) (150 MHz step)
Inst. Bandwidth	100 MHz
Polarization	RHCP, LHCP, HLP, VLP

Optimization procedure	PbP – 10 loops with no kick (as first value)

Results for gain and realized gain are presented in the figures below (Table 59):

TABLE 59: BROADSIDE GAIN MEASUREMENT RESULTS

Linear polarizations	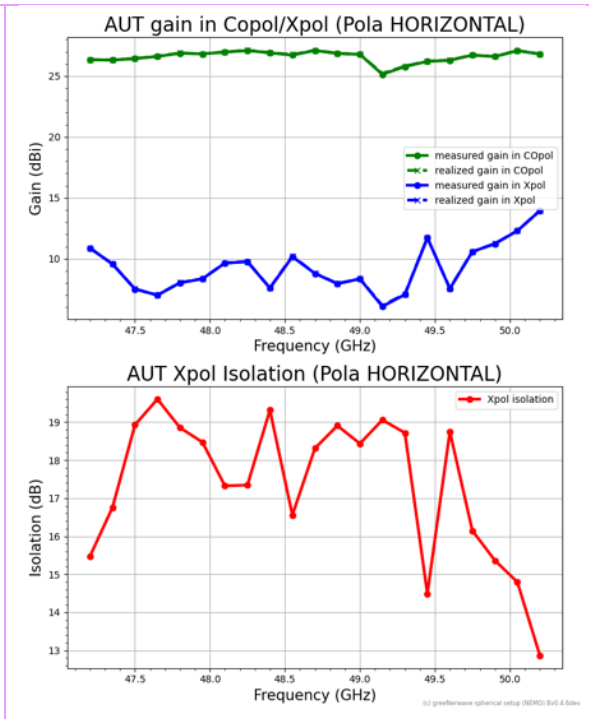	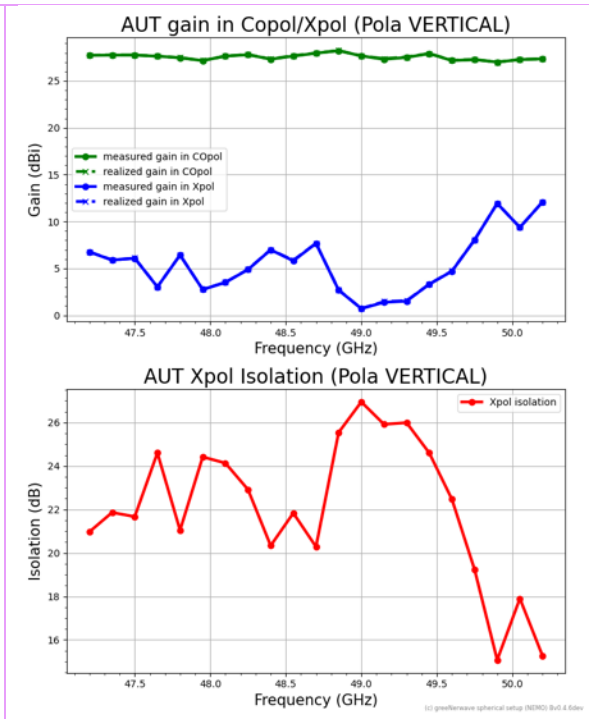
Circular polarizations	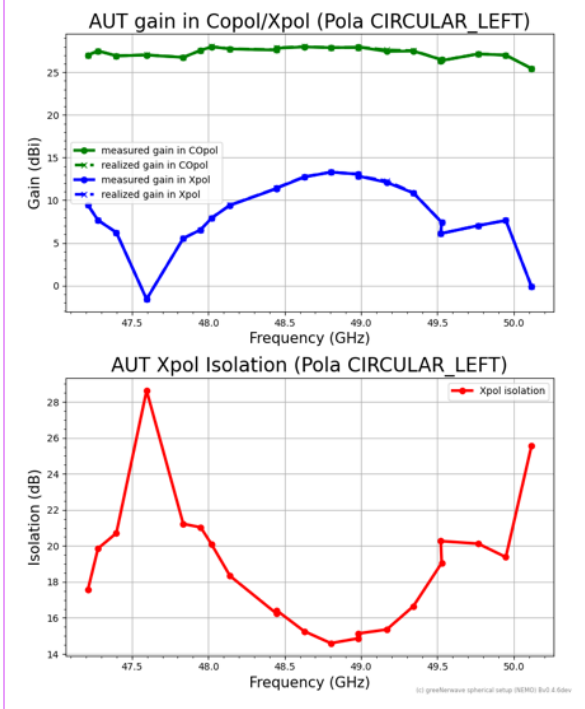	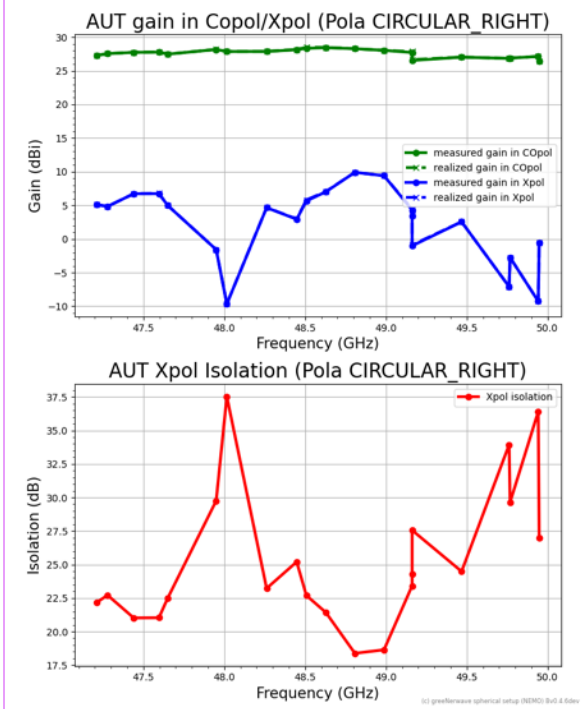

The gain of VTx antenna is in line with the gain values fixed in the specifications (27 dBi) for the four polarizations (H, V, RHCP, LHCP). However, a small drop in the gain is noticed around

49.2 GHz particularly for circular polarizations (LHCP, RHCP) and horizontal polarization (25 dBi).

This could be related to MTS and feeder performance.

For TM polarization, the MTS presents very high dissipation in the Off state (average of |S11|> -15 dB). However, the dissipation level for TE mode is better (average of |S11|> -3.8dB).

TABLE 60: MTS CHARACTERIZATION RESULTS

	Amplitude		Phase	
	TE	TM	TE	TM
MTS1	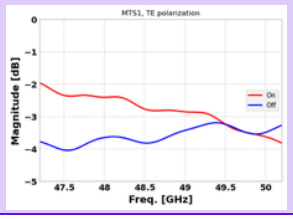	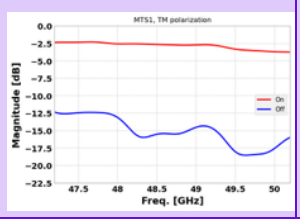	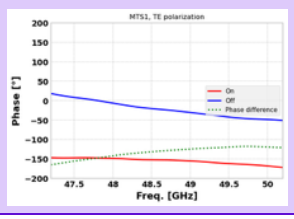	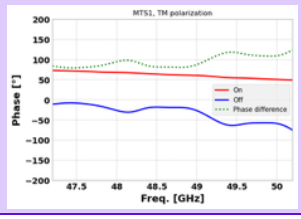

Regarding the feeder around 49.2 GHz, it presents a higher leakage compared to the rest of the frequency band. At the same time, we notice a slight drop in the gain around this frequency.

TABLE 61: AFS CHARACTERIZATION RESULTS

	47.2 GHz	48.2 GHz	49.2 GHz	50.2 GHz
UOF	0.41	0.39	0.39	0.39
Spillover (%)	8.0	8.13	**9.1**	

Despite this drop in the gain, the VTx antenna is still in line with the expected gain in specifications.

5.4.4.4 Scan loss

Scan loss represents the reduction in the gain of the steered beam as compared with the maximum gain. For VTx antenna scan loss measurements, we considered the following measurements parameters.

TABLE 62: SCAN LOSS PARAMETERS

Parameters	Values
Frequency range	47.2 GHz – 50.2 GHz (21 points) (150 MHz step)
Angular beamforming	Theta = -70°-70° /Step of 10° (15 pts) Phi = 0°, 45°, 90°
Inst. Bandwidth	100 MHz
Polarization	V, H
Optimization procedure	PbP – 10 loops with no kick (as first value)

We consider three frequency points (**47.2 GHz**, **48.7 GHz** and **50.2 GHz**) and 5 different values of Phi angles including the broadside. Scan loss is then plotted for a Theta angle rage [-70° 70°] with a step of 10° and linear polarizations (V pol and H pol).

5.4.4.5 Vertical polarization

TABLE 63: SCAN LOSS FOR VERTICAL POLARIZATION

	47.2 GHz	48.7 GHz	50.2 GHz
Phi = 0°	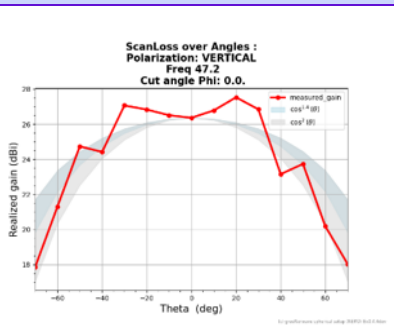	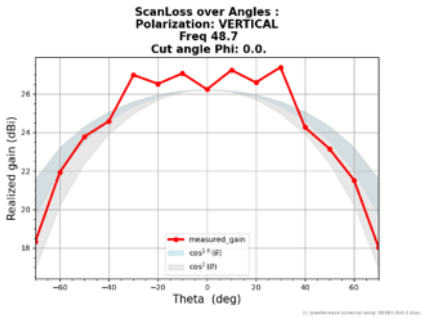	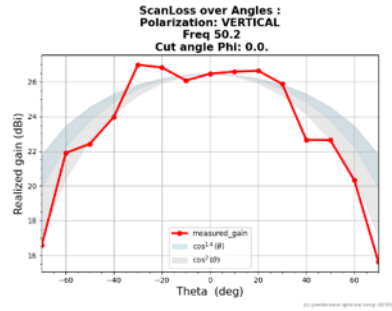
Phi = 45°	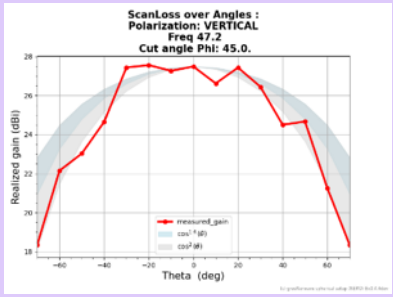	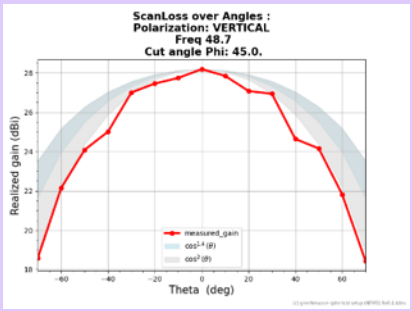	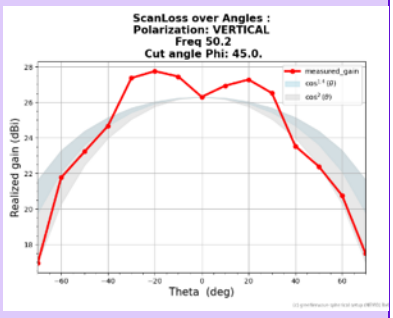
Phi = 90°	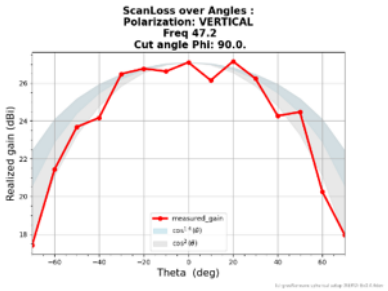	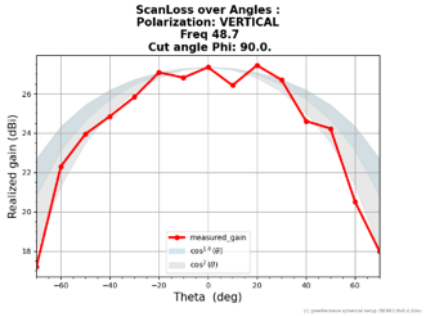	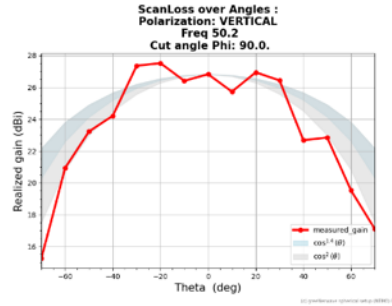

5.4.4.6 Horizontal polarization

TABLE 64: SCAN LOSS FOR HORIZONTAL POLARIZATION

	47.2 GHz	48.7 GHz	50.2 GHz
Phi = 0°	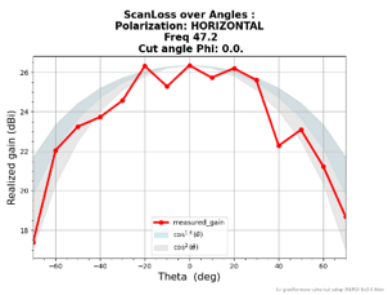	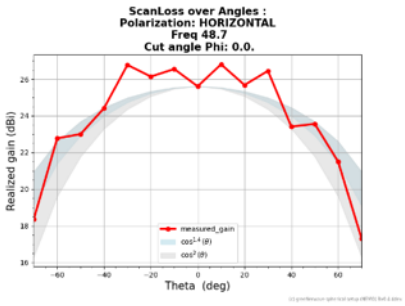	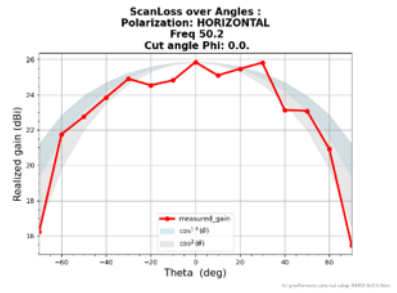
Phi = 45°	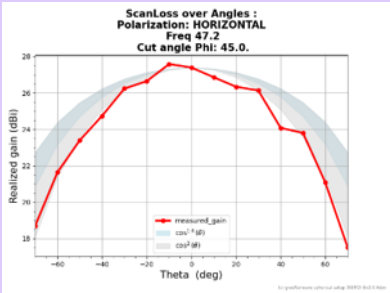	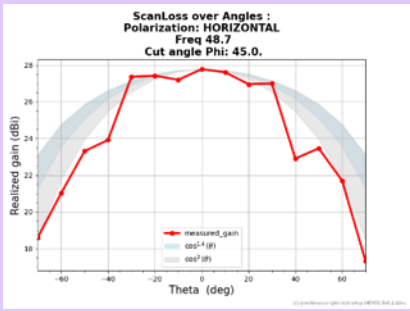	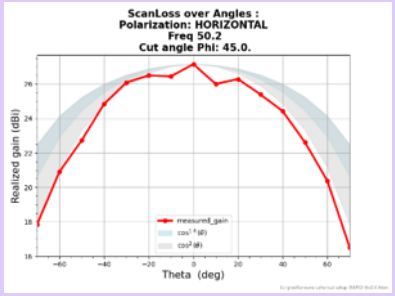
Phi = 90°	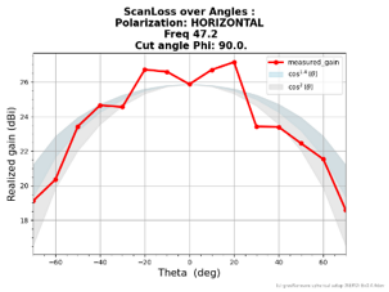	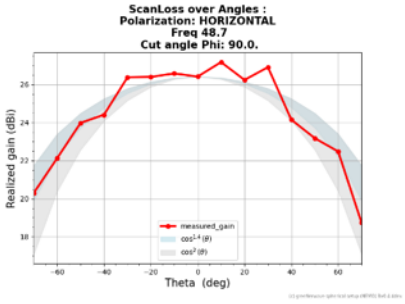	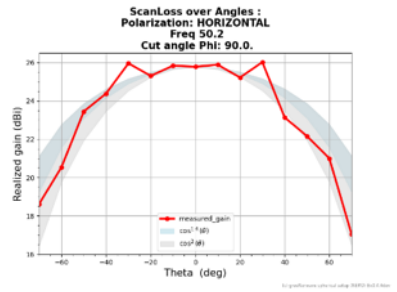

Scan loss follows the cosine law defined in the specifications for most frequency points. However, for a few frequency points, we are far from the specified cosine law. This can be due to the flat mask that did not consider any constraints on the phase as is the case with dome masks.

5.4.4.7 Directivity, aperture, rf and total efficiencies

The directivity was calculated through the combined maximum power radiated in both co-pol and cross-pol (for linear and circular polarizations).

Aperture efficiencies were calculated taking the aperture size as 200x200 mm2.

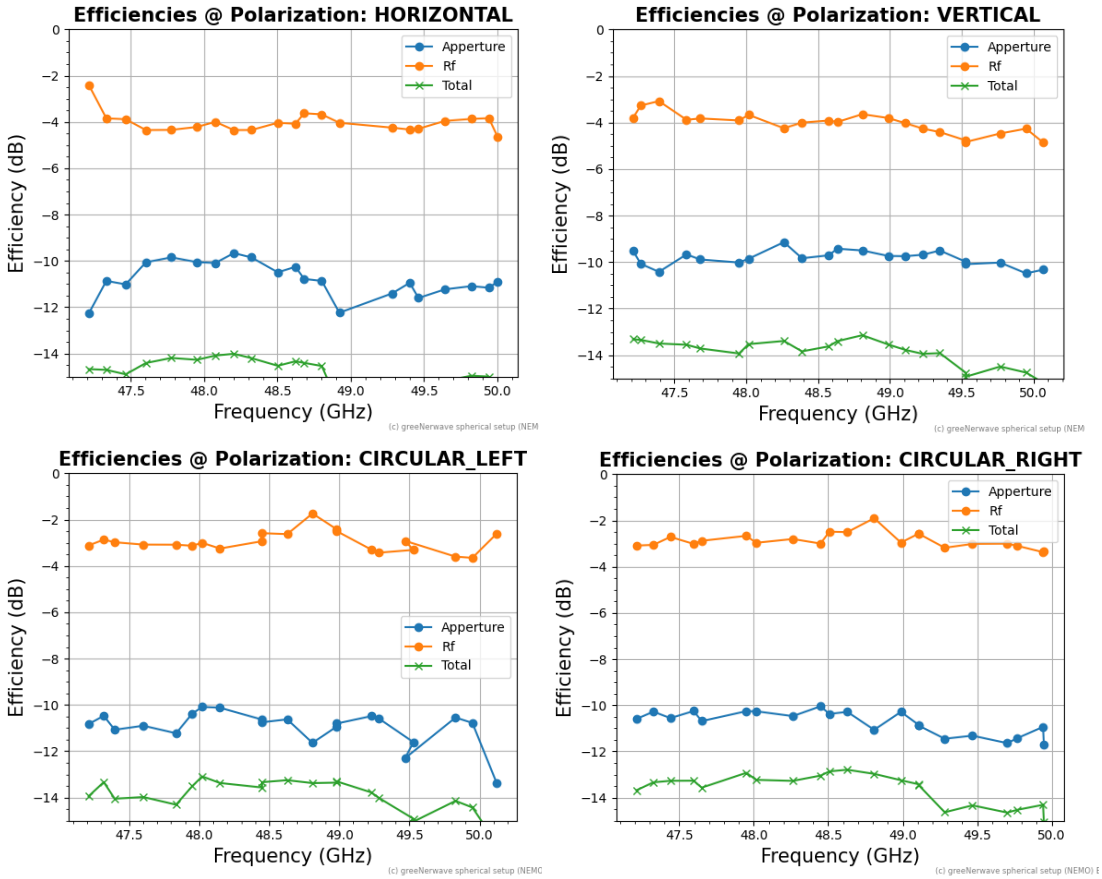

FIGURE 74 EFFICIENCIES VS FREQUENCY FOR DIFFERENT POLARIZATIONS. HERE RF IS RADIOFREQUENCY EFFICIENCY, WHICH REPRESENTS THE LOSS OF ENERGY AND APERTURE EFFICIENCY REPRESENTS THE EFFICIENCY OF THE WAVE CONTROL INSIDE THE CAVITY.

Total efficiency is around -14 dB for most of polarizations, from 39 GHz total efficiency drops bellow -14 dB. These values are coherent with what is specified in the specs.

5.4.4.8 Radiation pattern

Results are presented for three frequency points from the VTx band (47.2 GHz, 48.7 GHz and 50.2 GHz) and for the four polarizations (V, H, RHCP, LHCP)

Radiation pattern measurements were performed considering the following settings

TABLE 65: RADIATION PATTERN PARAMETERS

Parameters	Values
Theta range	-70°: 70° / step of 0.5°
Phi range	0°, 45°, 90°
Frequency range VNA	47.2 GHz – 50.2 GHz (21 points) (150 MHz step)
Polarization	V, H, RHCP or LHCP

5.4.4.8.1 Radiation pattern at 39.5 GHz

TABLE 66: RADIATION PATTERN FOR PHI= 0°,45° AND 90

Vertical @ 47.2 GHz GHz	Horizontal @ 47.2 GHz GHz
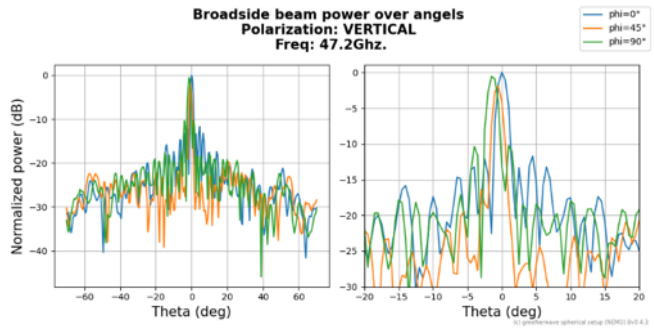	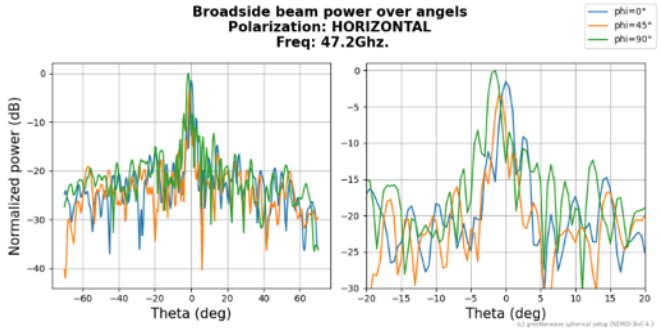
RHCP @ 47.2 GHz GHz	**LHCP @ 47.2 GHz GHz**
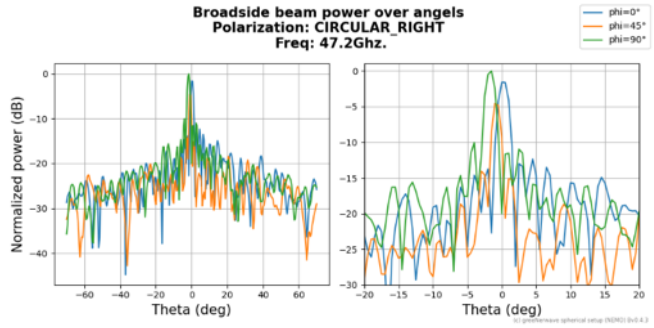	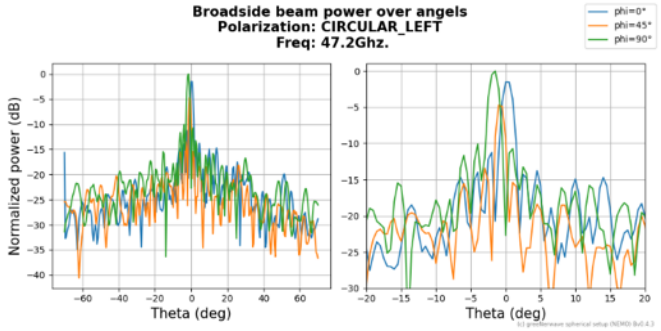

TABLE 67: RADIATION PATTERN FOR DIFFERENT POLARIZATIONS

Phi = 0° @ 47.2 GHz	Phi = 45° @ 47.2 GHz
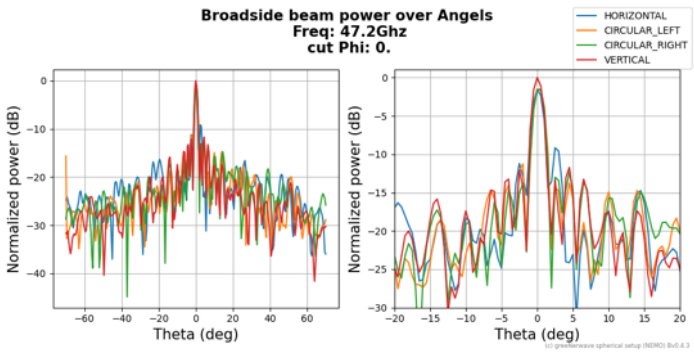	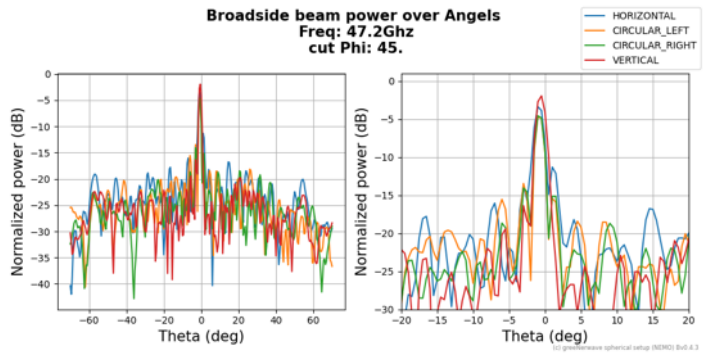

Phi = 90° @ 47.2 GHz
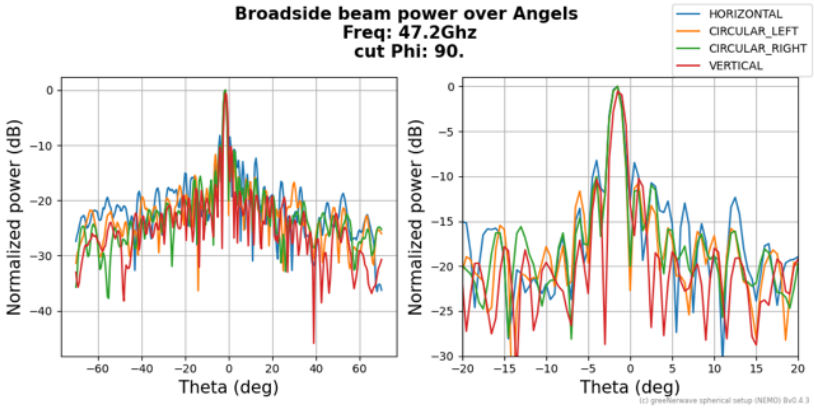

5.4.4.8.2 Radiation pattern at 40.5 GHz

TABLE 67: RADIATION PATTERN FOR PHI= 0°,45° AND 90°

Vertical @ 48.7 GHz	Horizontal @ 48.7 GHz
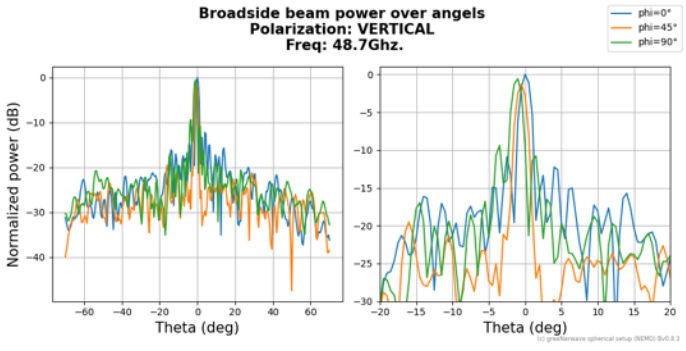	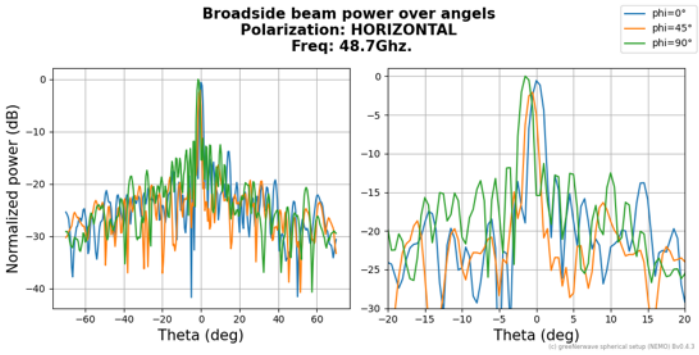
RHCP @ 48.7 GHz	**LHCP @ 48.7 GHz**
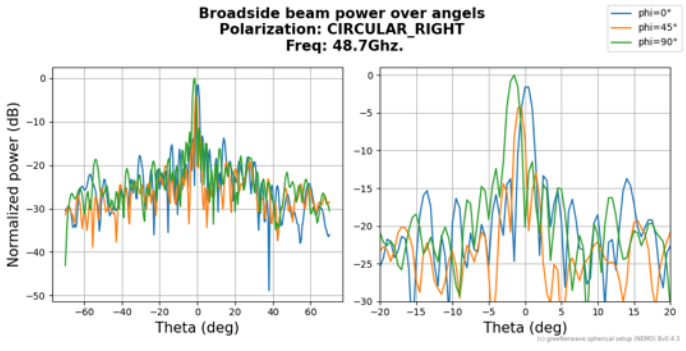	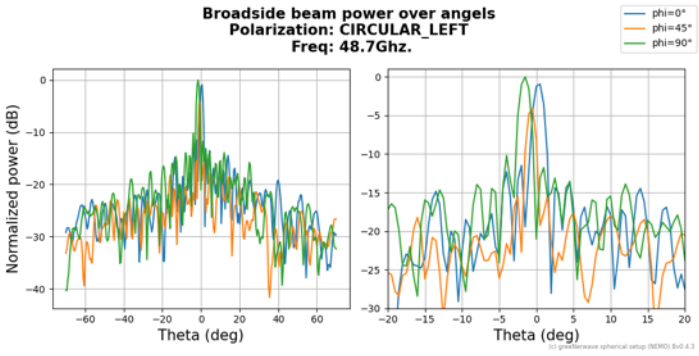

5.4.4.8.3 Radiation pattern at 50.2 GHz

TABLE 68: RADIATION PATTERN FOR PHI= 0°,45° AND 90°

Vertical @ 50.2 GHz	Horizontal @ 50.2 GHz
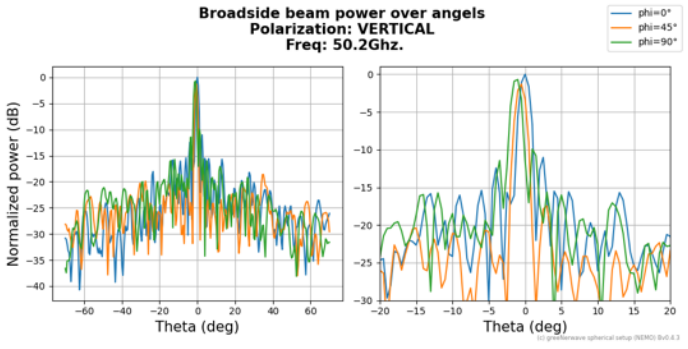	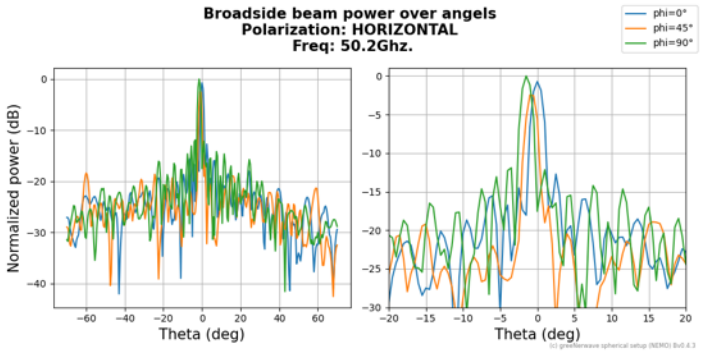
RHCP @ 50.2 GHz	**LHCP @ 50.2 GHz**
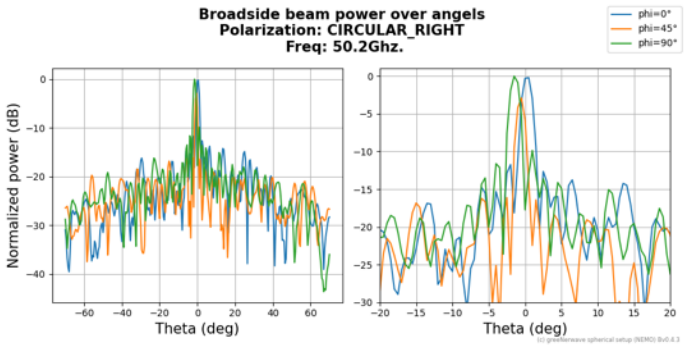	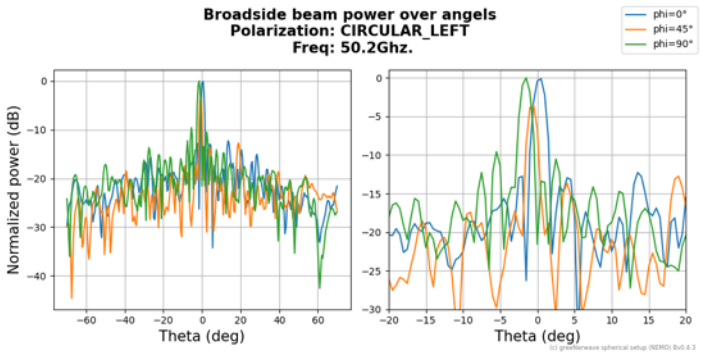

TABLE 70: RADIATION PATTERN FOR DIFFERENT POLARIZATIONS

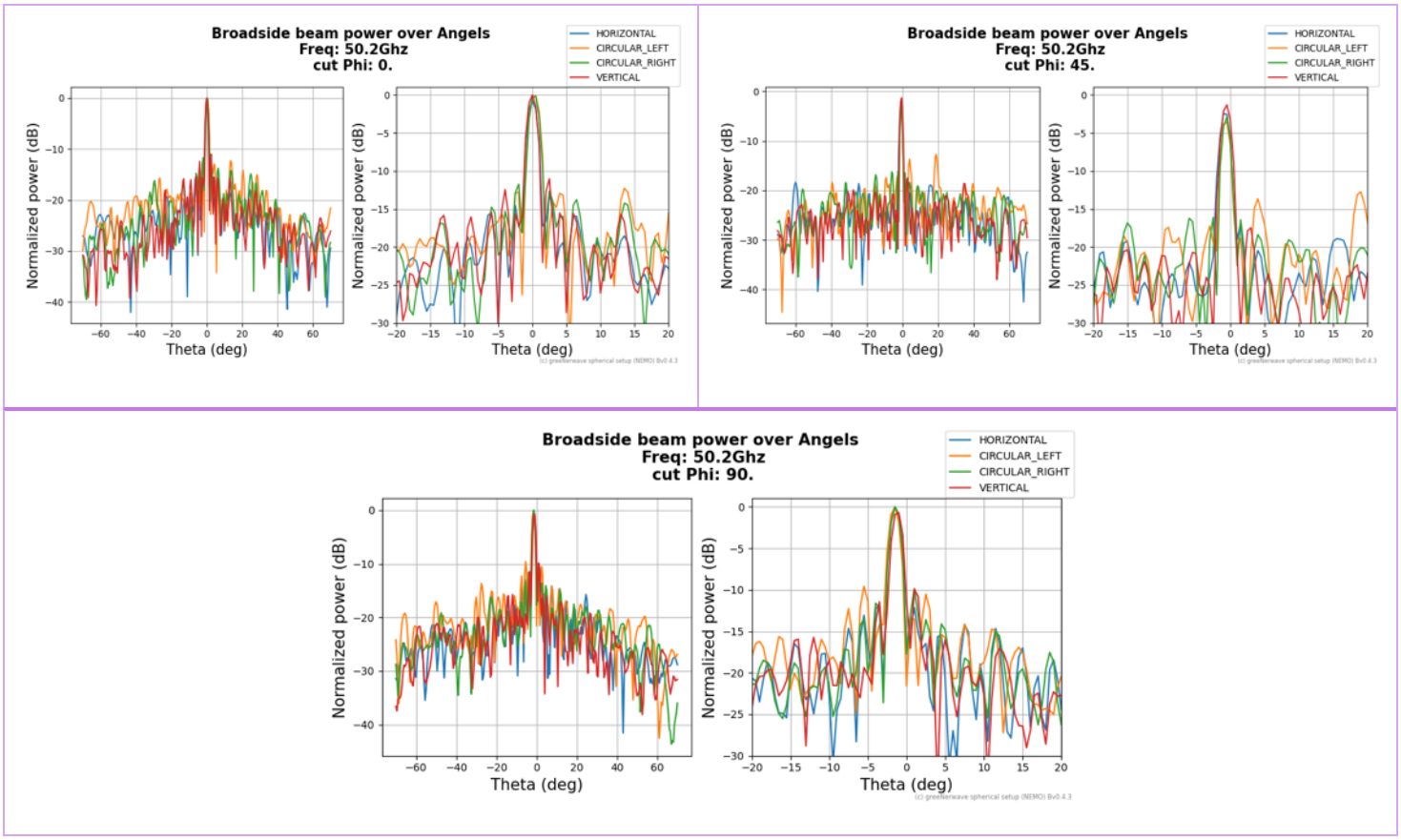

We observe a first side lobe level that fluctuates between -10 dB and -12 dB depending on the polarization and Phi angle value. These values are higher than the SLL mentioned in the specifications (-15 dB).

The shift in the radiation pattern for different Phi angles might be related to a misalignment of the setup between AUT and the probe antenna.

6 SMALL QV ANTENNA 10CM X 10CM

6.1 INTRODUCTION

The first part of the 6G-NTN project deliverables focused on the simulation, design and characterization of a $2 \times (20\text{cm} \times 20\text{cm})$ QV antenna to validate the GW technology and antenna performances at these frequencies.

However, the final specification for the 6GNTN project communicated to GW by the consortium concerns a $2 \times (10\text{cm} \times 10\text{cm})$ QV antenna. For this antenna, only the feeder needs to be redesigned and adapted to the reduced antenna size. Both MTS and mask designs are identical to the previously used versions for the $20\text{cm} \times 20\text{cm}$ antenna.

In this section, we will present simulation results for both QRx and VTx $10\text{cm} \times 10\text{cm}$ $10\text{cm} \times 10\text{cm}$ feeder.

6.2 QV 10CM X 10CM ANTENNA FEEDING SYSTEM (AFS)

6.2.1 QRX feeding system 10 cm x10 cm

Figure 75 shows the QRx 10x10 AFS. The cavity measures (100 mm x 100 mm x 43.78 mm). The Return loss of the feeding system is shown in Figure 76. A reflection coefficient that is lower than -20 dB over the whole band of interest is noticed.

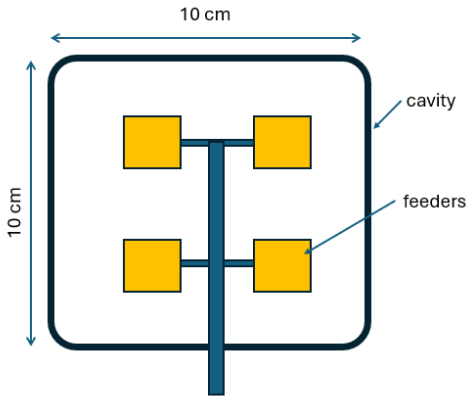

FIGURE 75: SCHEMATIC REPRESENTATION OF THE QRX 10CM X 10CM ANTENNA FEEDING SYSTEM

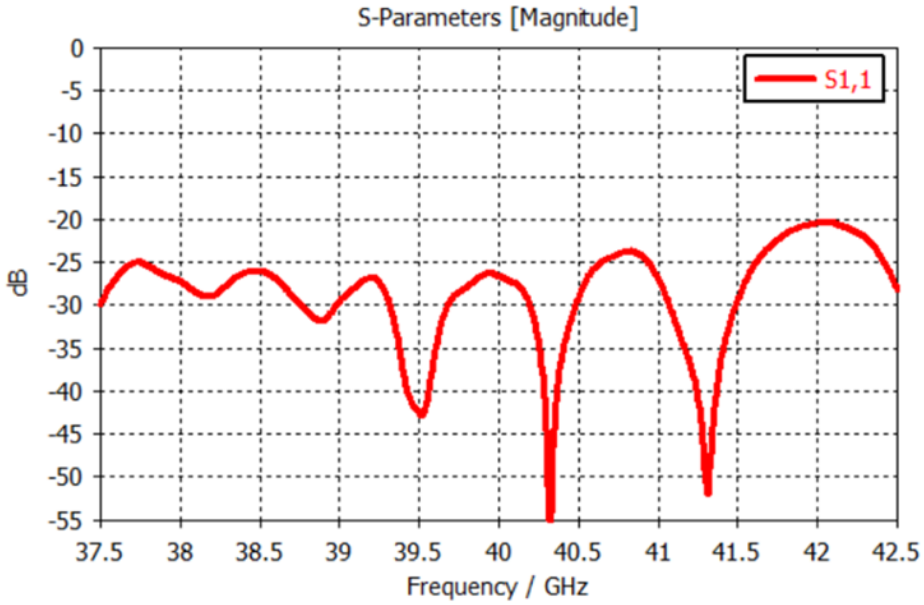

FIGURE 76: SIMULATED REFLECTION COEFFICIENT OF THE QRX 10CM X10CM AFS.

6.2.1.1 QRx feeding system KPIs 10 cm x10 cm

Two KPI's are evaluated for the AFS: the Uniformity of the field (UOF) (Figure 77) and Leakage (Table 69).

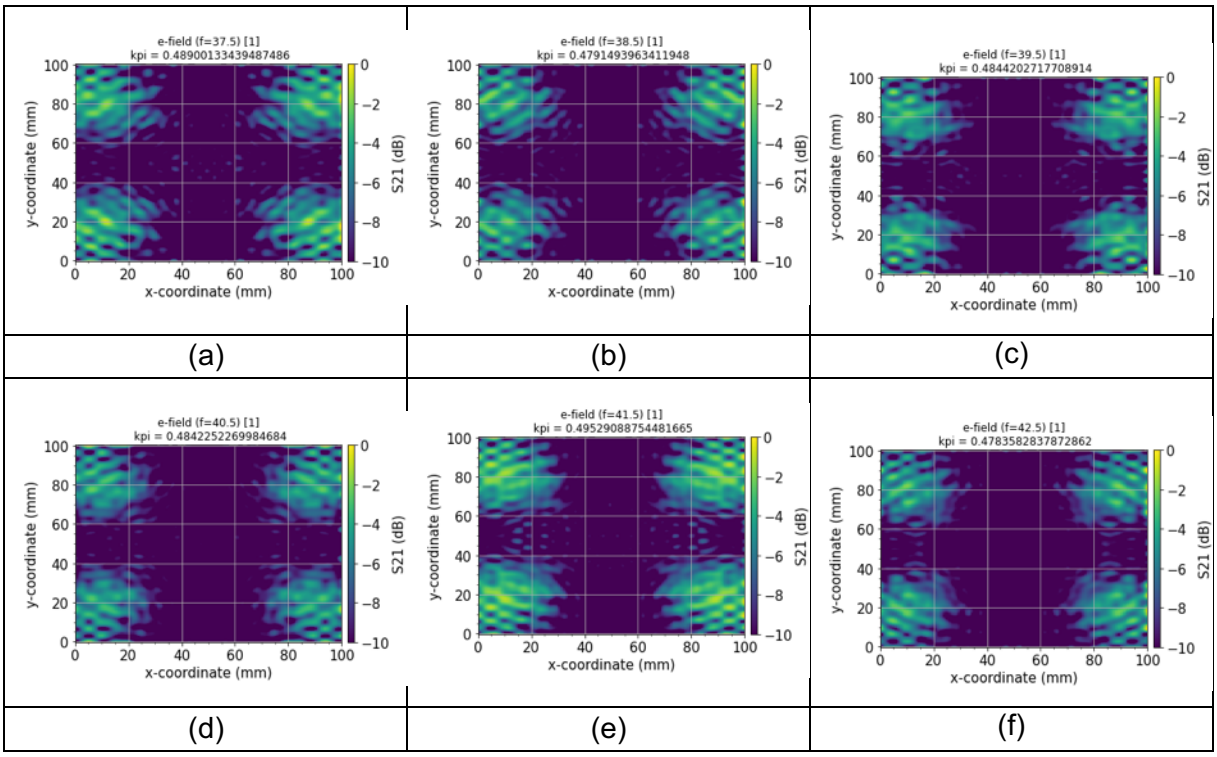

FIGURE 77: QRX 10CM X 10CM UOF FOR 10X10 AT (A) 37.5 GHZ (B) 38.5 GHZ (C) 39.5 GHZ (D) 40.5 GHZ (E) 41.5 GHZ AND (F)42.5 GHZ

TABLE 69: QRX FEEDING SYSTEM 10X10 LEAKAGE KPIS FOR DIFFERENT FREQUENCIES.

Frequency [GHz]	37.5	38.5	39.5	40.5	41.5	42.5
UOF	0.49	0.48	0.48	0.48	0.49	0.48
Leakage KPI [%]	8.92	8.26	9.34	6.88	6.50	5.32

For the QRx AFS best UOF of 0.48 was observed at (38.5 GHz, 39.5 GHz, 40.5 GHz and 42.5). A high value of 9.34 is obtained at 39.5 GHz for leakage.

6.2.2 VTX feeding system 10 cm x10 cm

Figure 78 shows the VTx 10cm x10cm AFS. The cavity measures (100 mm × 100 mm × 43.78 mm). The Return loss of the feeding system is shown in Figure 79. A reflection coefficient that is lower than -20 dB over the whole band of interest is noticed.

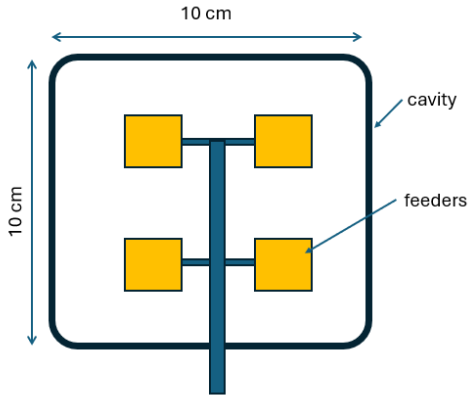

FIGURE 78: SCHEMATIC REPRESENTATION OF THE VTX 10CM X 10CM ANTENNA FEEDING SYSTEM

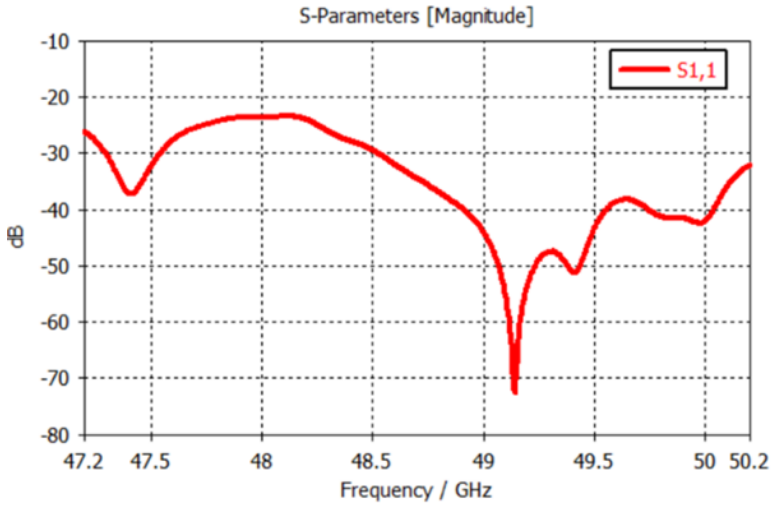

FIGURE 79: SIMULATED REFLECTION COEFFICIENT OF VTX 10CM X 10CM AFS

6.2.2.1 VTx feeding system KPIs 10 cm x 10 cm

The UOF is represented in Figure 80 and Leakage in Table 70.

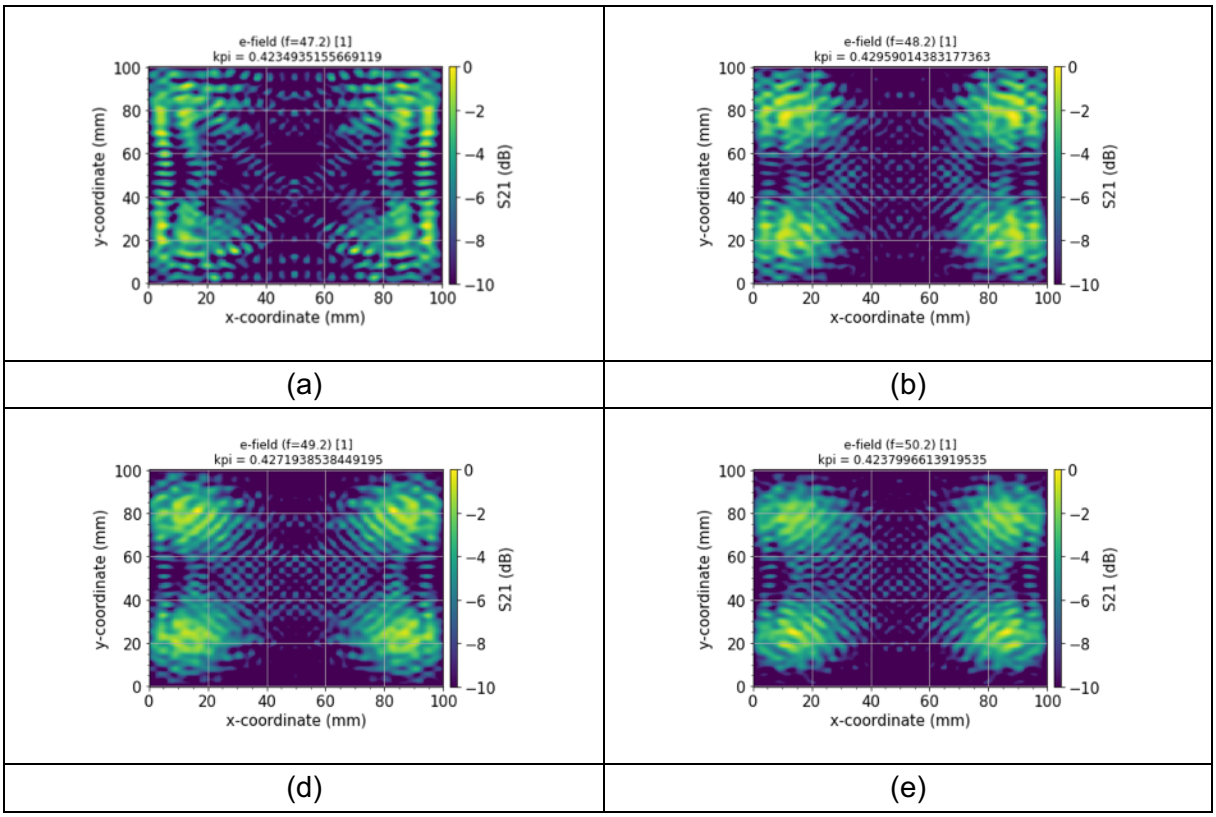

FIGURE 80: VTX 10CM X10CM UOFS AT (A) 47.2 GHZ (B) 48.2 GHZ (C) 49.2 GHZ AND (D) 50.2 GHZ.

TABLE 70: VTX 10X10 FEEDING SYSTEM LEAKAGE KPIS FOR DIFFERENT FREQUENCIES

Frequency [GHz]	**47.2**	**48.2**	**49.2**	**50.2**
UOF	0.42	0.43	0.43	0.42
Leakage KPI [%]	5.64	3.43	3.54	3.73

For the small VTx AFS, values of UOF KPI are even lower than the case of QRx small AFS. Indeed, a UOF KPI < 0.42 is obtained for all measured frequencies (47.2 GHz, 48.2 GHz, 49.2 GHz, and 50.2 GHz). Leakage KPI values are also very low (lower than 3.43 for the same frequencies).

7 FINAL CONSIDERATIONS

Results for QRx (20cm x 20cm) antenna performances are presented in Table 71 and compared with the 6-GNTN project specifications.

The (10cm x 10cm) QRx antenna has the same type of MTS and mask as the (20cm x 20cm) antenna and very similar feeder performances as presented in the previous section. The only difference with the previously characterized antenna is the size which is four times smaller. This can allow us to estimate the performance of the small (10cm x 10cm) antenna (in terms of gain and efficiency), knowing the QRx (20cm x 20cm) characterization results.

TABLE 71: QRX ANTENNA PERFORMANCES COMPARED TO THE SPECIFICATIONS

		Specifications for Q-Rx size 20cm x 20cm	***Measurement results for Q-Rx size 20cm x 20cm***	***Estimations for Q-Rx size 10cm x 10cm***
Frequency Range		37.5-42.5 GHz	37.5-42.5 GHz	37.5-42.5 GHz
Beamformer dimension		20cm x 20cmx 3cm ~27x27λ @ 40 GHz	20cm x 20cmx 4.37cm ~27x27λ @ 40 GHz	10cm x 10cm x 4.37cm ~14x14λ @ 40 GHz
Total Efficiency		-14 dB	Average -10 dB	Estimated -10 dB
Gain (Elev 90°)		25.5 dBi	Average 30 dBi	Estimated 24 dBi
Bandwidth	**Total**	5 GHz	5 GHz	5 GHz
	Instantaneous (from 0°-60°)	150 MHz	100 MHz	150 MHz
Side Lobe Level		First sidelobe -15 dB typical	First sidelobe -11 @ 39.5 GHz First sidelobe -12.5 @ 41.5 GHz	/
Scan Angle		ScanLoss (power cos): target: TBD ±70°, 1.4 ±50°	±50° @ $\cos^{1.4}$ ±70° @ $\cos^{2}$	/

Following the same reasoning we can estimate the performances of the small VTx (10cm x 10cm) antenna (gain, efficiency) knowing the VTx (20cm x 20cm) characterization results (Table 72).

TABLE 72: VTX ANTENNA PERFORMANCES COMPARED TO THE SPECIFICATIONS

	Specifications for V-Tx size 20cm x 20cm	***Measurement results for V-Tx size 20cm x 20cm***	***Estimations for V-Tx size 10cm x 10cm***

Frequency Range		47.2-50.2 GHz	47.2-50.2 GHz	47.2-50.2 GHz
Beamformer dimension		20cm x 20cmx 3cm ~33x33λ @ 50 GHz	20cm x 20cmx 4.37cm ~33x33λ @ 50 GHz	10cm x 10cm x 4.37cm ~16x16λ @ 50 GHz
Total Efficiency		-14 dB	Average -14 dB	Estimated -14 dB
Gain (Elev 90°)		27 dBi	Average 27 dBi	Estimated 21 dBi
Bandwidth	**Total**	3 GHz	3 GHz	3 GHz
	Instantaneous (from 0°-60°)	150 MHz	100 MHz	150 MHz
Side Lobe Level		First sidelobe -15 dB typical	First sidelobe between -10 dB and -12 dB	/
Scan Angle		ScanLoss (power cos): target: TBD ±70°, 1.4 ±50°	±50° @ $\cos^{1.4}$ ±70° @ $\cos^{2}$	/

One can note that the measured side lobe (SLL) of the antenna is higher than the value defined in specifications. It should be noted that the theoretical best SLL value for a square antenna is approximately –13 dB, which is close to the measured value. The defined SLL parameter is achievable for an antenna with a circular aperture (with the best theoretical value ~ -17 dB). For example, the measured SLL in the diagonal direction (when phi angle is equal to +- 45 degrees) was below –15 degrees.

The deviation of the measured SLL can be explained by sub-optimal antenna optimization, which could be further improved especially if targeted goal function was focused on SLL level.

Further improvement of SLL parameters is possible with different methods. First the circular antenna aperture can be used. Also, apodization law can be applied to the semi-transparent antenna mask. For example, Gaussian of Hanning distribution of the aperture transmittance level will reduce the level of side lobes.

8 CONCLUSION

This deliverable focused on a new antenna design in Q/V band.

The in-house designed and fabricated Q/V-band antenna demonstrated performance that aligns closely with the target specifications of the 6G-NTN project. Based on characterization results, the key outcomes are as follows:

1. The antenna exhibits a good operation within the designed Q/V-band frequency range.
2. The measured gain and radiation patterns are in good agreement with the expected values for NTN communication use cases and project specifications.
3. The full integration of the metasurface, feeder, and mask shows strong potential for scalable manufacturing and system-level deployment and validates the efficiency of our cutting-edge technology.

These results confirm the feasibility of the proposed antenna design for high-frequency NTN applications and contribute positively to the technical validation phase of the 6G-NTN project.

9 REFERENCES

[1] https://www.satixfy.com/product_category/antennas/
[2] S. V. Hum and J. Perruisseau-Carrier, "Reconfigurable Reflectarrays and Array Lenses for Dynamic Antenna Beam Control: A Review
[3] 3GPP TS 38.101-5 V18.10.0 (2025-07), "User Equipment (UE) radio transmission and reception; Part 5: Satellite access Radio Frequency (RF) and performance requirements (Release 18)"
[4] ETSI EN 302 217-4 - V2.1.1 (2017-05), "Characteristics and requirements for point-to-point equipment and antennas; Part 4: Antennas"
[5] 3GPP TS 38.101-1 v18.5.0, "User Equipment (UE) radio transmission and reception; Part 1: Range 1 Standalone (Release 18)"
[6] 3GPP TS 38.101-2 V18.5.0, "User Equipment (UE) radio transmission and reception; Part 2: Range 2 Standalone (Release 18)"
[7] 3GPP TS 38.101-3 v18.5.0, "User Equipment (UE) radio transmission and reception; Part 3: Range 1 and Range 2 Interworking operation with other radios (Release 18)"
[8] 3GPP TS 38.101-4 v18.5.0, "User Equipment (UE) radio transmission and reception; Part 4: Performance requirements (Release 18)"
[9] 3GPP TS 38.101-5 v18.5.0, "User Equipment (UE) radio transmission and reception; Part 4: Performance requirements (Release 19)"
[10] 6G-NTN deliverable D4.4 - "Spectrum Regulation Analysis for 6G NTN Scenarios"
[11] 3GPP TS 38.300 V18.1.0, "Technical Specification Group Radio Access Network; NR and NG-RAN Overall Description; Stage 2 (Release 18)"
[12] ITU-R Recommendation SM.329-12, "Unwanted emissions in the spurious domain"
[13] OpenAMIP Standard, online available at https://www.idirect.net/products/openamip/
[14] Variable inclination continuous transverse stub array, US patent number US6919854B2
[15] F. Ahmed, K. Singh and K. P. Esselle, "State-of-the-Art Passive Beam-Steering Antenna Technologies: Challenges and Capabilities," in *IEEE Access*, vol. 11, pp. 69101-69116, 2023, doi: 10.1109/ACCESS.2023.3278570.
[16] Yuanzhi He, Fan Yang, Guodong Han, Yuanyuan Li, High-throughput SatCom-on-the-move antennas: technical overview and state-of-the-art, Digital Communications and Networks, 2023, ISSN 2352-8648, https://doi.org/10.1016/j.dcan.2023.11.005.
[17] G. Amendola *et al.*, "Low-Earth Orbit User Segment in the Ku and Ka-Band: An Overview of Antennas and RF Front-End Technologies," in *IEEE Microwave Magazine*, vol. 24, no. 2, pp. 32-48, Feb. 2023, doi: 10.1109/MMM.2022.3217961.
[18] T. Chaloun *et al.*, "Electronically Steerable Antennas for Future Heterogeneous Communication Networks: Review and Perspectives," in *IEEE Journal of Microwaves*, vol. 2, no. 4, pp. 545-581, Oct. 2022, doi: 10.1109/JMW.2022.3202626.
[19] W. Hong et al., "Multibeam Antenna Technologies for 5G Wireless Communications," in IEEE Transactions on Antennas and Propagation, vol. 65, no. 12, pp. 6231-6249, Dec. 2017.
[20] https://www.microwavejournal.com/articles/36358-thinkom-unveils-new-q-v-band-phased-array-satellite-antennas-for-next-generation-satellite-constellations, retrieved on June 2024
[21] https://www.hanwha-phasor.com/
[22] https://www.satixfy.com/product_category/antennas/
[23] S. V. Hum and J. Perruisseau-Carrier, "Reconfigurable Reflectarrays and Array Lenses for Dynamic Antenna Beam Control: A Review
[24] Liu Shuang , Li Yin , Wong Sai-Wai , Zhang Xiao , Wang Shiyan , Fang Liang , Gao Qiang , A circularly polarized folded reflectarray antenna using a polarization-sensitive linear-to-circular polarization converter, Frontiers in Physics ,VOLUME10, YEAR 2022, DOI:10.3389/fphy.2022.983951
[25] A. Oliner and A. Hessel, “Guided waves on sinusoidally-modulated reactance surfaces,” IRE Trans. Antennas Propag., vol. TAP-7, no. 5, pp. 201–208, Dec. 1959.
[26] https://www.kymetacorp.com/solutions/?utm_medium=adwords&utm_campaign=brand&gad_source=1&gclid=CjwKCAjwmrqzBhAoEiwAXVpgonw47E94QzL_cIBGYfK_nhYr0iVyxKPHThZp78HcMQktey46AsEguxoCgEsQAvD_BwE
[27] P. Commware, “Holographic beam forming technology – Pivotal commware,” Accessed: Mar. 22, 2022.

[28] J. Ruiz-García, C. Bilitos, E. Martini, G. Toso, S. Maci and D. González-Ovejero, "Metal-only Multi-beam Fabry-Perot Antenna," *2022 16th European Conference on Antennas and Propagation (EuCAP)*, Madrid, Spain, 2022, pp. 1-4, doi: 10.23919/EuCAP53622.2022.9769193.

[29] Saeid Karamzadeh, Vahid Rafiei, and Mesut Kartal, "Beam Steering Fabry Perot Array Antenna for mm -Wave Application," *Progress In Electromagnetics Research M*, Vol. 91, 81-89, 2020. doi:10.2528/PIERM20020101

[30] Amirhossein Askarian and Ke Wu, "Aperture-Shared Radiation Surface: A Promising Technique for Multifunctional Antenna Array Development," Electromagnetic Science, vol. 1, no. 3, article no. 0030082, 2023. doi: 10.23919/emsci.2023.0008

[31] X. Artiga, "Effects of Unit Cell Enlargement and 1-Bit Quantization in 5G Linear Metasurface Antennas," *2018 European Conference on Networks and Communications (EuCNC)*, Ljubljana, Slovenia, 2018, pp. 1-9, doi: 10.1109/EuCNC.2018.8442638.

[32] Y. Wang, L. Sun, Z. Du and Z. Zhang, "Review Antenna Design for Modern Mobile Phones: A Review," in Electromagnetic Science, vol. 2, no. 2, pp. 1-36, June 2024, doi: 10.23919/emsci.2023.0052.

[33] P. Li, Y. Zhang, X. Qin, K. Wei, P. Liang and Y. Li, "Wideband Widebeam Circular-Polarized Antenna Using Asymmetrical Tri-Dipoles for Direct Satellite-to-Handset Communications," in *IEEE Transactions on Antennas and Propagation*, vol. 72, no. 8, pp. 6270-6277, Aug. 2024, doi: 10.1109/TAP.2024.3420086.

[34] S. Rao, Y. Wang, F. Xu, J. Wang, Y. Shi and Y. Han, "Dual-Band Circularly Polarized Antenna With Circular Polarization in the Endfire Direction in Metal-Bezel Smartphones for n256-Band Direct Phone-to-Satellite Communication," in *IEEE Transactions on Antennas and Propagation*, vol. 73, no. 4, pp. 2385-2394, April 2025, doi: 10.1109/TAP.2024.3515453.

[35] X. P. Zhang, K. P. Wei, Y. Li, et al., "A polarization reconfigurable antenna for satellite communication in foldable smartphone," IEEE Transactions on Antennas and Propagation, vol. 71, no. 12, pp. 9938–9943, 2023.

[36] X. Zhang, K. Wei, Y. Li and Z. Zhang, "A Circularly Polarized Antenna Based on Narrowed Crossed Dipole for Smartphone Satellite Communication," in *IEEE Antennas and Wireless Propagation Letters*, vol. 23, no. 8, pp. 2511-2515, Aug. 2024

[37] A. Zhao and Z. Ren, "Wideband MIMO Antenna Systems Based on Coupled-Loop Antenna for 5G N77/N78/N79 Applications in Mobile Terminals," in *IEEE Access*, vol. 7, pp. 93761-93771, 2019, doi: 10.1109/ACCESS.2019.2913466.

[38] Khan, A.A.; Wang, Z.; Li, D.; Ahmed, A. A Compact C-Band Multiple-Input Multiple-Output Circular Microstrip Patch Antenna Array with Octagonal Slotted Ground Plane and Neutralization Line for Improved Port Isolation in 5G Handheld Devices. *Electronics* **2024**, *13*, 2196. https://doi.org/10.3390/electronics13112196

[39] L. Sun and H. Wang, "Circularly-Polarized Antenna Design in Mobile Phones by the Combination of Common and Differential Modes," 2024 IEEE MTT-S International Wireless Symposium (IWS), Beijing, China, 2024, pp. 1-3

[40] J. F. Zhang, Y. J. Cheng, Y. R. Ding, et al., "A dual-band sharedaperture antenna with large frequency ratio, high aperture reuse efficiency, and high channel isolation," IEEE Transactions on Antennas and Propagation, vol. 67, no. 2, pp. 853–860, 2019.

[41] Kin-Lu Wong, "Compact and Broadband Microstrip Antennas", John Wiley & Sons, 2002, ISBNs: 0-471-41717-3 (Hardback); 0-471-22111-2 (Electronic)

[42] J. Zhu, Y. Yang, S. Liao, S. Li and Q. Xue, "Dual-Band Aperture-Shared Fabry–Perot Cavity-Integrated Patch Antenna for Millimeter-Wave/Sub-6 GHz Communication Applications," in *IEEE Antennas and Wireless Propagation Letters*, vol. 21, no. 5, pp. 868-872, May 2022, doi: 10.1109/LAWP.2022.3148408.

[43] M. B. Young, K. A. O'Connor and R. D. Curry, "Reducing the size of helical antennas by means of dielectric loading," *2011 IEEE Pulsed Power Conference*, Chicago, IL, USA, 2011, pp. 575-579, doi: 10.1109/PPC.2011.6191490.

[44] Tang, Xihui, Feng, Botao, Long, Yunliang, The Analysis of a Wideband Strip-Helical Antenna with 1.1 Turns, *International Journal of Antennas and Propagation*, 2016, 5950472, 7 pages, 2016. https://doi.org/10.1155/2016/5950472

[45] I. Lim and S. Lim, "Monopole-Like and Boresight Pattern Reconfigurable Antenna," in *IEEE Transactions on Antennas and Propagation*, vol. 61, no. 12, pp. 5854-5859, Dec. 2013, doi: 10.1109/TAP.2013.2283926.

[46] C.-X. Wang, X. You, X. Gao, et al., “On the road to 6g: Visions, requirements, key technologies, and testbeds,” IEEE Communications Surveys Tutorials, vol. 25, no. 2, pp. 905–974, 2023. DOI: 10.1109/ COMST.2023.3249835.
[47] A. Guidotti, A. Vanelli-Coralli, V. Schena, et al., “The path to 5g-advanced and 6g non-terrestrial network systems,” in 2022 11th Advanced Satellite Multimedia Systems Conference and the 17th Signal Processing for Space Communications Workshop (ASMS/SPSC), 2022, pp. 1–8. DOI: 10.1109/ASMS/SPSC55670.2022.9914764.
[48] About 6g-ntn, 6G-NTN, [Online]. Available: https://www.6g- ntn.eu/ about-6g-ntn/, Accessed: March 15, 2024.
[49] Q. Wu, S. Zhang, B. Zheng, C. You, and R. Zhang, “Intelligent reflecting surface aided wireless communications: A tutorial,” Jul. 2020.
[50] M. A. ElMossallamy, H. Zhang, L. Song, K. G. Seddik, Z. Han, and G. Y. Li, “Reconfigurable intelligent surfaces for wireless communications: Principles, challenges, and opportunities,” IEEE Transactions on Cognitive Communications and Networking, vol. 6, no. 3, pp. 990–1002, 2020. DOI: 10.1109/TCCN.2020.2992604.
[51] C. Pan, H. Ren, K. Wang, et al., “Reconfigurable intelligent surfaces for 6g systems: Principles, applications, and research directions,” IEEE Communications Magazine, vol. 59, no. 6, pp. 14–20, 2021. DOI: 10. 1109/MCOM.001.2001076.
[52] M. Jian, G. C. Alexandropoulos, E. Basar, et al., “Reconfigurable intelligent surfaces for wireless communications: Overview of hardware designs, channel models, and estimation techniques,” Intelligent and Converged Networks, vol. 3, no. 1, pp. 1–32, 2022. DOI: 10 . 23919 / ICN.2022.0005.
[53] J.-B. Gros, V. Popov, M. A. Odit, V. Lenets, and G. Lerosey, “A reconfigurable intelligent surface at mmwave based on a binary phase tunable metasurface,” IEEE Open Journal of the Communications Society, vol. 2, pp. 1055–1064, 2021. DOI: 10.1109/OJCOMS.2021. 3076271.
[54] J.-B. Gros, V. Popov, M. Odit, R. Faggiani, and G. Lerosey, “Electronically reconfigurable leaky cavity antennas,” 2021

